

A Reproduced Copy

OF

N65-33140

Reproduced for NASA

by the

NASA Scientific and Technical Information Facility

N 65 - 33 140

FACILITY FORM 602

(ACCESSION NUMBER)

156

(PAGES)

CR 64615

(NASA CR OR TMX OR AD NUMBER)

(THRU)

1

(CODE)

14

(CATEGORY)

GPO PRICE \$

CSFTI PRICE(S) \$

Hard copy (HC)

Microfiche (MF)

5.00

1.00

ff 653 July 65

EVALUATION OF STAR GYRO TORQUING

FINAL REPORT

15 July 1965

Prepared By

W. H. Quick, Staff Specialist
W. C. Wey, Research Engineer
Inertial Instruments Research Department
Navigation Systems Division

Approved By

Earl H. Jacobs

E. D. Jacobs, Assistant Manager
Inertial Instruments Research Department
Navigation Systems Division

This work was performed for the Jet Propulsion Laboratory, California Institute of Technology, sponsored by the National Aeronautics and Space Administration under Contract NAS7-100.

Autonetics A DIVISION OF NORTH AMERICAN AVIATION, INC., ANAHEIM, CALIFORNIA



C5-1277/32

The government has the right to reproduce, use, and disclose this report for governmental purposes in accordance with Contract ~~250862~~----- . Subject to the foregoing, this document contains proprietary information of North American Aviation, Inc.

SYNOPSIS

BACKGROUND

The STAR Gyro is a vibrating-string instrument which is particularly attractive because of its potential high reliability, small size, low weight, and low power requirements. The instrument contains no parts which slide or roll. It has no liquid which can become contaminated and no tight clearances between the parts. Because of the exceptionally low power requirement, the instrument is expected to have quick warmup capability, high reliability after long periods of being inoperative, and high reliability for long continuous operation.

It has been recognized since the inception of the STAR Gyro Program that it is possible to "torque" this instrument. However, other development aspects being more important, torquing has received little study until recently. Previous to this program, some work had been done on electromagnetically torquing the instrument during first mode operation.

PROGRAM GOALS

It was the purpose of this program to develop the theory of STAR Gyro torquing in sufficient detail to permit the accurate prediction of torquing scale factors for any future instrument design, and to determine the effect of all important error sources. It was also the purpose of this program to conduct torquing experimental work to demonstrate the feasibility of torquing at rates from 0 to 2000 degrees per hour, and to make measurements to provide data sufficiently accurate to be used for checking the theoretical results being developed. Other detailed objectives are discussed at appropriate locations in the report.

MAJOR RESULTS

The most important results of this study are discussed below, without attempting to recount all details of this study, or the methods by which these results were obtained:

1. In Section 3 of this report, the general theory for the response of a vibrating string (operating in its n^{th} mode) to an arbitrary

applied lateral force is developed. Although this development follows the lines of previous work (Reference 2), it has been expanded to include the following results:

- a. Response, with string operating in an arbitrary n^{th} mode, has been obtained in Equations 3-14 and 3-15.
 - b. The amount of elliptical, subharmonic, and harmonic motion generated incidentally to the desired torquing precession is obtained in Paragraph 3.4.
 - c. A time function for a torquing pulse has been found which will eliminate all elliptical, subharmonic, and harmonic extraneous string motion, independent of the space function which is used for the torquing (see Paragraph 3.5) while producing the desired torquing response.
 - d. Using this optimum pulse shape, the net pulse sensitivity, including the effect of phase-angle errors in the pulse, is obtained in Equations 3-31 and 3-32. It is also shown that sensitivity to these phase errors can be minimized without adverse effect on other optimization (Paragraph 3.8).
2. In Section 4, the expression is derived for the electrostatic force on a fiber between two parallel plates. The fiber and two plates may be at three different voltages. Although this problem may not appear difficult (the force between a cylinder and a single plate, for example, is well known), the solution could not be found in the literature and seems worth presenting in some detail. The result, of course, has a somewhat more general application than that required here. In Figure 4-8 the expressions required to calculate this force are summarized and the terms are redefined. The expression for C_w , the capacity from the wire to the pair of plates connected in parallel (Equation 4-28), is a subsidiary result which also may find independent application, as it has not been found in the literature.
 3. Reference 1 presents the basic theory of the vibrating string as an angular motion sensor, including (1) the conditions for the desired vibration to start under parametric excitation, (2) the conditions for this oscillation to continue, (3) the amplitude of this oscillation under given drive conditions, (4) the expression for anisoclastic precession rate, (5) the very important condition which brings this precession rate to zero, known as the "critical" condition, and finally (6) the damping bias or precession rate. These expressions in this reference, however, are limited to first mode operation.

In Section 5 these expressions are obtained for the operation of the string in an arbitrary n^{th} mode. Although the results in Section 5 are required for application here to the torquing expression, these results of course have considerably wider application and are important in themselves. Figure 5-2 depicts these results for first and second mode operation and summarizes the important equations, so that the figure is self-contained and convenient for reference.

4. The major result in terms of program objective is contained in the expression for net torquing scale factor (Equation 6-15), along with the expression for string amplitude (Equation 6-21), and the summary of definitions following these equations. The expression for error terms follows directly from these equations and may be expressed as in Equations 6-49, 6-51, 6-59, or in other ways. A typical method of applying these results to a particular error budget is illustrated in the paragraph containing Equation 6-60.

Another useful result contained in Section 6 is the expression for string pickoff sensitivity obtained when a transformer is used to tune the pick-off capacities to resonance, as illustrated in Figure 6-4. This is obtained by using the capacity-variation results in Section 4 and is given in Equations 6-43 and 6-47.

5. The specific program goal of showing torquing feasibility for rates up to 2000 degree per hour was achieved electrostatically with no particular difficulty. Electrostatic torquing rates of one or even two or more orders of magnitude greater than this appear attainable with practical electronic and instrument configurations.
6. Finally, the experimental work has, within the general accuracy of the data, served to substantiate the theoretical expressions. The parameters during tests were, in general, varied over a wider range than would be of interest in normal operation, the purpose being to check the theoretical expressions with a greater degree of resolution. These comparisons are presented and discussed in Section 8.

CONCLUSION

The results of this study indicate that there is no fundamental or practical limitation in the precision torquing of the STAR Gyro. The

preferable means of torquing appears to be electrostatic. This method can obtain high rates of torquing with reasonable voltages, negligible power consumption, and an accuracy which appears to be limited only by the degree of precision which is built into the torquing system in accordance with the error model.

CONTENTS

| | <u>Page</u> |
|----------------------------------------------------------------------------------------------------|-------------|
| 1. Introduction | 1-1 |
| 1.1 Description of the STAR Gyro | 1-1 |
| 1.2 General Concept of STAR Torquing | 1-2 |
| 1.3 Torquing History and the Approach in the Current Study | 1-3 |
| 2. Comparative Study of Electromagnetic and Electrostatic Torquing | 2-1 |
| 2.1 Introduction | 2-1 |
| 2.2 Consideration of the Two Torquing Methods | 2-1 |
| 2.2.1 Temperature Effects | 2-1 |
| 2.2.2 Physical Instrument Considerations | 2-2 |
| 2.2.3 Electronic Considerations | 2-2 |
| 2.2.4 Accuracy | 2-4 |
| 2.3 Conclusion | 2-5 |
| 3. Torquing and Lateral-Force Response of the Vibration-String Gyro in Any Mode | 3-1 |
| 3.1 Summary | 3-1 |
| 3.2 General Lateral-Forcing Response | 3-2 |
| 3.3 Normal "Torquing" Response | 3-6 |
| 3.4 Elliptical, Harmonic and Subharmonic Production | 3-8 |
| 3.5 Harmonic and Subharmonic Elimination | 3-10 |
| 3.5.1 Space Function Only | 3-10 |
| 3.5.2 Time Function Only | 3-11 |
| 3.6 Harmonic Generation by a Single-Sine-Wave Pulse — Second Mode | 3-12 |
| 3.7 Pulse-Interval and Phase Torquing Errors (Independent of any Harmonics Generated) | 3-15 |
| 3.8 Conclusion | 3-18 |
| 4. Electrostatic Force on a Fibre Between Two Plates | 4-1 |
| 4.1 Force Equation | 4-2 |
| 4.2 Wire-to-Parallel-Plate Capacity | 4-9 |
| 4.3 Special Case, One Plate | 4-16 |

CONTENTS (CONT)

| | <u>Page</u> |
|----------------------------------------------------------------------------------------|-------------|
| 4.4 Plots for $(H/r_0) = 10$ | 4-18 |
| 4.5 Special Case, String Centered | 4-18 |
| 4.5.1 Reduced Equation | 4-18 |
| 4.5.2 Maximum Force | 4-24 |
| 4.5.3 Increase of Force Due to Second Plate | 4-24 |
| 4.5.4 Maximum "Drive"—Minimum Pickup | 4-24 |
| 5. General n^{th} Mode String Equations | 5-1 |
| 6. Determination of Detailed Model for STAR Gyro Torquing | 6-1 |
| 6.1 Introduction | 6-1 |
| 6.2 Development | 6-2 |
| 6.2.1 Combined Torquing Expressions | 6-2 |
| 6.2.2 Effect of Plate Width and Curvature | 6-9 |
| 6.2.3 Platform Servo-Error Effect | 6-12 |
| 6.2.4 String Amplitude Pickoff Sensitivity | 6-14 |
| 6.3 Torquing Errors | 6-17 |
| 7. Laboratory Mechanization for Providing STAR Torquing Data | 7-1 |
| 7.1 Introduction | 7-1 |
| 7.2 Detailed Consideration | 7-3 |
| 7.2.1 Circuit Consideration | 7-4 |
| 7.2.2 Laboratory Setup Operation | 7-15 |
| 7.2.3 Data Accumulation Technique | 7-23 |
| 8. Experimental Results and Comparisons to Theoretical Results | 8-1 |
| 8.1 Introduction | 8-1 |
| 8.2 Torquing Results and Comparisons | 8-2 |
| 8.2.1 Absolute Value of Torquing Scale Factor—Experimental vs Theoretical | 8-2 |
| 8.2.2 String Amplitude Pickoff Sensitivity— Experimental vs Theoretical | 8-5 |
| 8.2.3 Torquing Pulse Scale Factor vs Torquing Pulse Rate | 8-6 |

CONTENTS (CONT)

| | <u>Page</u> |
|--------------------------------------------------------------------------------------------------------------------------------------|-------------|
| 8.2.4 Effect of Torque Pulse Magnitude Change on Torquing Pulse Scale Factor | 8-7 |
| 8.2.5 Effect of Torque Pulse Phase Shift Due to Shifts in the String Reference Signal (2-volt peak-to-peak pulses) | 8-9 |
| 8.2.6 Effect of Torquing Pulse Phase Shift Due to Shifts in the String Reference Signal (1-volt peak-to-peak pulses) | 8-12 |
| 8.2.7 Effect of Temperature Variations on Torquing Pulse Scale Factor | 8-16 |
| 8.2.8 Effects of Torque Pulse Phase Shifts in Pulse Turn-On Phase and Pulse Turn-Off Phase | 8-18 |
| 8.2.9 Effect of D-C Torquing Bias | 8-24 |
| 8.2.10 Effect of Harmonics | 8-25 |
| 8.2.11 Torque Pulse Phase and Amplitude Stability | 8-25 |
| 8.3 Conclusions | 8-27 |
| References | R-1 |

ILLUSTRATIONS

| <u>Figure</u> | | <u>Page</u> |
|---------------|--------------------------------------------------------------------------------------------------------------------------------------------------------------------------------------------------------------------------|-------------|
| 3-1 | String Equations, Illustrated for String Vibration in Second Mode, $n = 2$ | 3-2 |
| 3-2 | Two-Cycle Pulse in Second Mode Vibration | 3-3 |
| 3-3 | The Single-Sine-Wave Pulse, $T_{ssp}(t_I)$ | 3-13 |
| 3-4 | Phase Angles θ_r , θ_{sa} , and θ_d , Defining Switching-Time and Torquing-Wave Phases. (Harmonics are Eliminated if $k = n$, But This Development not Restricted to $k = n$.) | 3-16 |
| 4-1 | Cylindrical Fibre and Electrostatic Plates | 4-1 |
| 4-2 | Capacity Model-Three Stray Capacitors to Ground and Three Interelectrode Capacities | 4-2 |
| 4-3 | Relative Voltage Picture and Dimensions. C_w is Capacity From Cylinder to Both Plates Paralleled | 4-4 |
| 4-4 | Interelectrode Capacity in Terms of Geometry. C_w Is Capacity From Cylinder to Both Plates Paralleled | 4-6 |
| 4-5 | Illustration of C_w , a Function of H , a , r_o , L and ϵ | 4-10 |
| 4-6 | Central Portion of Infinite Set of Line Charges Used to Obtain Desired Boundary Conditions at A, B, and f | 4-11 |
| 4-7 | Grouping of Charges in the Individual Terms in Equations (4-26) and (4-24), and Distances to Central Charge. Subscripts of A Correspond to n's in Equation (4-25), etc. | 4-12 |
| 4-8 | Summary--General Equation for Force. Equations (4-22), (4-28), (4-33), (4-32), (4-34) as well as (4-9), (4-2) and (4-18) | 4-15 |
| 4-9 | Capacity Between Cylinder and One or Two Plates, for Ratio $H/r_o = 10$ | 4-19 |
| 4-10 | Force on Cylinder for $\frac{H}{r_o} = 10$, vs u at Various V_s/V_p | 4-20 |

ILLUSTRATIONS (Cont)

| <u>Figure</u> | | <u>Page</u> |
|---------------|------------------------------------------------------------------------------------------------------------------------------------------------------------------------------------|-------------|
| 4-11 | Force Between Fibre (or Cylinder) and Single Plates (a and c) and on Fibre With Two Plates | 4-22 |
| 4-12 | Forces in Figure 4-11, $F_2 - F_1$ and Their Ratio | 4-23 |
| 5-1 | A Vibrating String Operating in the n^{th} Mode | 5-1 |
| 5-2 | Parametrically-Driven Vibrating String Characteristics for the n^{th} Mode | 5-6 |
| 6-1 | Electrostatic Plate Geometry. String is Vibrating in Second Mode in a Vertical Plane. | 6-1 |
| 6-2 | Free-Hand Plots of Fields. (Field Shown in First Quadrant Only) | 6-11 |
| 6-3 | Vibrating String Gyro (STAR) and Platform Response to Torquing | 6-12 |
| 6-4 | String Amplitude Pick-off Circuit | 6-14 |
| 7-1 | Star Gyro Electrostatic Torquing Loop | 7-2 |
| 7-2 | Pick-off Buffer Amplifier | 7-5 |
| 7-3 | Rejection Pulse Forming Network | 7-6 |
| 7-4 | Tuned Transformer Amplifier | 7-7 |
| 7-5 | Pick-off Channel Filters | 7-8 |
| 7-6 | Pulse Forming and Synchronization Circuitry | 7-9 |
| 7-7 | Timing Diagram Depicting Logic Being Performed by Pulse Forming and Synchronization Circuitry | 7-10 |
| 7-8 | Master Signal Flow Schematic for Pulse Forming and Synchronization Circuitry | 7-11 |
| 7-9 | Torque Pulse Forming Logic - Signal Wiring Schematic | 7-12 |
| 7-10 | Analog Gate Schematic | 7-13 |
| 7-11 | Zero-Cross Detector Wiring Schematic | 7-14 |
| 7-12 | Oscillogram 7.1: Normally Monitored Signals Throughout the STAR Gyro Electrostatic Torquing Mechanization | 7-17 |
| 7-13 | Oscillogram 7.2: Pickoff Error Signals at Various TP's in the Servo Channel. Used to Verify Loop Gains (Note Phase Reversal Between Top and Bottom Traces in Photograph) | 7-17 |

ILLUSTRATIONS (Cont)

| <u>Figure</u> | | <u>Page</u> |
|---------------|------------------------------------------------------------------------------------------------------------------------------------------------------------------------------------------------------------------------------|-------------|
| 7-14 | Oscillogram 7.3: Demodulator Phasing With Respect to Disk Drive Voltage. Normally Used for Demodulator Phasing Checks. (Note That the Error Signal Phase has Been Reversed Between the Top and Bottom Traces) | 7-18 |
| 7-15 | Oscillogram 7.4: Pickoff Error Signal Phasing With Respect to Disk Drive Voltage. Normally Used for Error Channel Phasing Checks. (Note That the Error Signal has Been Reversed Between the Top and Bottom Traces) | 7-18 |
| 7-16 | Oscillogram 7.5: String Amplitude Reference Phasing With Respect to the Disk Pickoff Voltage | 7-19 |
| 7-17 | Oscillogram 7.6: Torque Pulse Phasing With Respect to the Disk Drive Voltage | 7-19 |
| 7-18 | Oscillogram 7.7: Representative Signals When Torquing at Maximum Rate in Both Directions | 7-20 |
| 7-19 | Oscillogram 7.8: Representative Signals When Torquing at One-Half of Maximum Torquing Rate in Both Directions | 7-20 |
| 7-20 | Oscillogram 7.9: Error Angle Build-up During Torquing With Platform Servo Loop Opened | 7-21 |
| 7-21 | Oscillogram 7.10: Representative Torquing Pulse With Various Turn-on and Turn-off Times ($\theta_d = 0$, $\theta_d = 90$ Degrees) | 7-21 |
| 7-22 | Oscillogram 7.11: Representative Torquing Pulse With Various Turn-on and Turn-off Times ($\theta_d = -90$ Degrees, $\theta_d = +135$ Degrees) | 7-22 |
| 8-1 | Torquing Pulse Scale Factor vs Pulse Phasing Using 2V Peak-to-Peak Pulses | 8-10 |
| 8-2 | Torquing Pulse Scale Factor vs Pulse Phasing Using 1V Peak-to-Peak Pulses | 8-13 |

ILLUSTRATIONS (Cont)

| <u>Figure</u> | | <u>Page</u> |
|---------------|-----------------------------------------------------------------------------------------------------------------------------------------------------------------------------------------|-------------|
| 8-3 | Equation of Torque Pulse Scale Factor as a Function of Torque Pulse Phasing With a Sketch of Waveform to Define Terms | 8-19 |
| 8-4 | Representative Torque Pulse Waveform for Various Turn-on and Turn-off Times ($\theta_r = 0$). Only the Left Torquing Pulse is Depicted | 8-19 |
| 8-5 | Torque Pulse Scale Factor as a Function of Turn-on and Turn-off Time ($\theta_r = 0$) Experimental Results are Normalized to Unity by the $\theta_d = \theta_{sa} = 0$ Data | 8-20 |
| 8-6 | Runs to Determine Scale Factor as a Function of Various Torquing Pulse Waveforms | 8-26 |

TABLES

| <u>Table</u> | | <u>Page</u> |
|--------------|------------------------------------------------------------------------------------------------------|-------------|
| 8-1 | Torquing Pulse Scale Factor vs Torquing Pulse Rate | 8-6 |
| 8-2 | Torque Pulse Scale Factor vs Torque Pulse Amplitude | 8-8 |
| 8-3 | Torquing Pulse Scale Factor vs Pulse Phasing (2-volt p-p pulses) | 8-11 |
| 8-4 | Torquing Pulse Scale Factor vs Pulse Phasing (1-volt p-p pulses) | 8-14 |
| 8-5 | Comparison of Torquing Data Scale Factor to Predicted Scale Factor with Temperature Change | 8-17 |
| 8-6 | Torque Pulse Scale Factor as a Function of Tension and Turn-off Times | 8-21 |

C5-1277/32

1. INTRODUCTION

1.1 DESCRIPTION OF THE STAR GYRO

The STAR (vibrating-string) Gyro, from an operational point of view, may be referred to as a "position gyro." The string vibrates essentially in a plane, driven by end-fastening longitudinal motion at double the string vibration frequency. This drive does not coerce the plane of string vibration toward any specific orientation. The string, in a manner analogous to the Foucault pendulum, vibrates so that its plane tends to remain angularly fixed in inertial space. (In both, the energy of the stored angular information is periodically interchanged between the potential energy associated with a position vector, and the kinetic energy associated with a momentum vector.) Thus, if the structure supporting the string is allowed to turn about the axis of the string, the plane of string vibration tends to remain fixed in inertial space, although the string itself rotates with the supports. Thus, a sensor attached to the case of the instrument, detecting the angle between the plane of string vibration and the case; will, during normal operation of the instrument, read out the angle in inertial space through which the instrument has turned, in the same manner as a free-gimballed conventional position gyro.

Although the drive itself does not tend to coerce the string plane, there are important effects which do tend to rotate the string plane toward a preferred case-oriented angle of operation. These effects must be considered if operation of the vibrating string is to be attained with sufficient angular stability that we could apply the term "gyro" to the instrument. The dominant effect, by a large margin, is that resulting from elastic asymmetry (anisoeasticity) of the fibre ends and fibre end mountings. Even when care is taken to construct a uniform fibre and mounting, the string plane will be observed to tend strongly toward a preferred plane.

Reference 1 presents an analysis of this anisoeastic behavior and shows the way in which it causes the string plane to precess toward a preferred plane, the rate of precession being proportional to the "angle off" of this plane. Of particular importance in the results of this solution is the fact that, for certain relationships between the frequency and amplitude of the string drive, the precession rate of the string plane, at a given angle off, goes through zero and reverses direction. The

condition at which this precession rate goes through zero has been termed the "critical" condition. Thus, at a given drive amplitude we have a critical drive frequency. At a given drive frequency we have a critical drive amplitude. By maintaining the drive condition as closely as possible to critical, while operating the string as closely as possible to its preferred elastic plane, it is possible to obtain string-plane stability sufficiently good that we may think of the vibrating string as a position gyro.

When the anisoelastic bias is thus controlled by having operation near "critical," the next dominant effect which is seen and which must be eliminated by careful construction of the instrument is a bias which results from asymmetrical loss or damping. This effect also involves a principal axis but unfortunately the elastic and damping axes are not, in general, coincident. The damping effect is basically much smaller than the anisoelastic effect, but its control presents difficulties which are now under intensive investigation.

1.2 GENERAL CONCEPT OF STAR TORQUING

For many applications in which gyroscopes are used, it is desirable to be able to "torque" the gyro. Torquing in this sense means the causing of the stable element to precess in proportion to an applied torquing signal. In the usual application, the gyro pickoff senses the offset angle produced by this torquing and, by means of the platform servo, rotates the platform and gyro case until this sensed offset angle is nulled out.

In the case of the STAR Gyro we find that the precessing of the stable element (the string plane) is produced, not by an actual torque, but by the application of a somewhat different force. This force is distributed along the string and is perpendicular to the string plane. In analysis, it is convenient to think of the torquing force, distributed along the length of the string, as consisting of a series of impulses which may be integrated, over time, to find the response to any particular waveform. The total response of the string to these torquing forces is twofold: First, there is the desired shift in the plane of string vibration. Secondly, there is a concomitant production of an elliptical component in the string vibration — that is, a beginning of a component of string motion which is slightly out of its nominal plane of vibration. If the impulse is applied when the string is at its center point of vibration, there will be no elliptical motion produced and, at the same time, the tendency to precess the string plane will be maximum.

On the other hand, an impulse applied when the string is at its maximum point of vibration will produce maximum elliptical motion while producing no rotation of the string plane. Fortunately, as can be seen in the equations of Section 3, pulse and analog waveforms exist which eliminate the average production of elliptical components, while producing the desired torquing.

Thus, as a matter of interest, we see that when the actual torque on the string (about its neutral axis) is maximum, there is no precessing whatsoever of the string plane. Contrarily, when the tendency of the force to precess the string is maximum, there is no actual torque, as such, generated. However the word "torquing" is used here to describe this precessing of the STAR Gyro plane without apology, because it is supposed that those long familiar with the torquing of more conventional gyros will tend to use the term, whatever technically more correct term might be applied. (In the same way, we do not hesitate to call the vibrating string a "gyro" or "gyroscope," even though it may, semantically, not truly be a gyroscope. It functions as a gyroscope, and the application of the word seems advisable.)

1.3 TORQUING HISTORY AND THE APPROACH IN THE CURRENT STUDY

Since the inception of the STAR gyro, it has been recognized that it would be possible to torque this instrument by the application of suitable forces perpendicular to the string plane. A static or d-c force has no precessing effect on the string because any precessing effect which might occur during one half of a cycle will be exactly cancelled out during the succeeding half cycle. Thus, any force applied to the string to create a torquing effect must vary at string frequency.

Early torquing methods which were considered, included both what was termed "induction torquing" and "direct torquing." With induction torquing, a magnetic field perpendicular to the string plane causes a voltage to be generated in the string as a result of its motion in the magnetic field. The result of this voltage is that current flows through an external resistor, and in conjunction with a second magnetic field, parallel to the string plane, produces a force in phase with the velocity of the string — the phase which produces the maximum torquing effect. An advantage of induction torquing is that the force is automatically in proportion to the string amplitude, because of the

method of force generation. This method is not suitable for pulse torquing because of its inherent nature. This torquing must be controlled by controlling one d-c magnetic field, which eliminates the use of a permanent magnet. Also, the method is limited as to maximum torquing rate because of the rather high resistance of a typical string. In addition, an undesired damping force is produced incidental to torquing.

Direct torquing may take a number of forms. Any method by which force can be applied to the string in a controlled manner is suitable for torquing the string gyro. Electromagnetic generation of this force by use of a steady magnetic field with a controlled current in the string has been studied and tested at least twice in the past (References 3 and 4). Emphasis in the current study has been on the electrostatic force production. Section 2 of this report discusses the reasons for this emphasis.

Sections 3, 4, and 5 cover n^{th} mode torquing, electrostatic force, and general n^{th} mode equations, developments needed for the required detailed torquing expression. Key results are noted in the abstract. These developments are then combined in Section 6 to obtain a detailed equation for the scale factor or torquing sensitivity of the STAR Gyro. This expression is derived on an entirely theoretical basis and thus is useful in finding the effect of various terms on torquing. It is, of course, obviously useful in finding what voltages will be required to torque a STAR Gyro of a new design.

With this detailed expression for STAR Gyro torquing, error expressions are determined in Section 6.3 simply by the use of a series of partial derivatives. Those terms in this expression which are sensitive to temperature in a known way are then combined to obtain an error expression with one temperature term. Thus, errors which are correlated through temperature have been grouped together. The summation of individual uncorrelated error terms is then made on a root sum square basis. A typical error budget for a sample desired rss accuracy is presented.

In Section 7 considerable detail is given on the laboratory mechanization which was used in the tests performed under this contract. The main object of these tests was not to obtain a particular stated accuracy but rather to obtain data to verify the theoretical expressions so that we could apply these expressions with confidence to determine

errors, in terms of known errors of standard components, such as the accuracy with which a d-c bias voltage can be supplied, the accuracy with which an electronic gain can be produced, and so forth.

Finally, in Section 8 comparison is made between experimental and theoretical data. Theoretical torquing scale factor and string-amplitude pickoff sensitivity are calculated in terms of parameters used in the test and the results are compared to experimental data for these. Plots are made to show the effect of shifting the three main phase angles which are important in pulse torquing. These experimental phase angles are shifted extensively, with the idea of proving the general form of the theoretical expressions. These expressions may then be used to calculate errors due to a given phase shift with more accuracy than is presently possible with the experimental setup, or with the STAR Gyro presently available for test. The effects of temperature variation and of torque pulse magnitude change are also compared.

C5-1227/32

2. COMPARATIVE STUDY OF ELECTROMAGNETIC AND ELECTROSTATIC TORQUING

2.1 INTRODUCTION

As evidenced by the contents of this report, primary effort on this contract was directed towards electrostatic torquing of the STAR Gyro. This preponderance of effort came about because of a number of factors. At the contract inception, considerable work had been done on electromagnetic torquing. The STAR Gyro had been torqued electromagnetically (References 3 and 4) and the original basic theory on torquing the vibrating study gyro (Reference 2) had been aimed at electromagnetic torquing. Thus, a body of information existed on this torquing method. By comparison, no electrostatic torquing work had been done. In fact, some doubt existed as to the feasibility of torquing the STAR Gyro electrostatically with reasonable voltage levels. With this in mind, initial experimental effort was directed toward electrostatic torquing while theoretical effort was aimed at general torquing theory, this being applicable to either torquing mechanization. Early in the contract period, it became evident that electrostatic torquing was not only practical but appeared able to satisfy performance requirements. Considerations discussed in Section 2-2 plus the obvious weight and size reduction led to the early conclusion that electrostatic torquing is preferable to electromagnetic torquing.

2.2 CONSIDERATION OF THE TWO TORQUING METHODS

The most important features of electrostatic and electromagnetic torquing of the vibrating string gyro are discussed below.

2.2.1 Temperature Effects

Perhaps the most questionable characteristic regarding satisfactory electromagnetic torquing of the STAR Gyro is the heating caused by the torquing current in the string. Because of the slow dissipation of heat from the vibrating element, small power inputs caused by the I^2R losses may introduce significant heating of the string. Temperature variations, as a function of torquing current and thus torquing rate, are intolerable in available instruments as they cause definite changes in instrument performance. From data available on one instrument which has been torqued electromagnetically, a rough calculation as to probable temperature rise for various torquing rates has been made.

It is estimated that a torquing rate of 2000 degree per hour would cause a string temperature increase of 5 F. This estimate assumes no heat transfer to the vacuum surrounding the string and is made on an Invar STAR Gyro operating in the first mode. Although wide fluctuations could be expected with different instruments, the point to be emphasized is that significant temperature rises for rates of 2000 degree per hour can be expected. To torque at rates this large, it would thus be necessary to modify the electronics to provide a constant I^2R power input to the string regardless of torquing rate. Two methods can be used to accomplish this: (1) A direct current could be provided to the string, interrupted only by a torquing pulse; if the d-c value is made equal to the rms current of the pulse, a constant power input is obtained. (2) the instrument could be consistently torqued either left or right. A zero torque rate would call for alternate left and right torquing pulses. Either of these would hold the temperature of the string stable but the requirement of a constant power input and associated warmup time for stabilization would remain as an undesirable feature. It should be pointed out that no such difficulty exists for electrostatic torquing. Power input to the instrument is insignificant.

It is appropriate to comment here on the peak torquing limitation imposed by the I^2R power loss on electromagnetic torquing. If an increase in torquing rate of ten (20,000 degree per hour) were desired, estimation of temperature rise using a calculation of the type discussed earlier would cause a temperature rise of 500 F. This is obviously a ridiculous figure but it serves to illustrate a very real limitation on the rates which might be achieved electromagnetically. A similar increase of ten electrostatically does not introduce unreasonable voltage requirements and the power requirements remain insignificant.

2.2.2 Physical Instrument Considerations

A considerable reduction in size and weight is obtained by use of electrostatic torquing over electromagnetic torquing because of the size and weight of the magnet and magnetic circuit, as well as the larger case size required. In addition, design and fabrication of an instrument incorporating electromagnetic torquing is necessarily more complicated and expensive. However, no apparent fundamental problems exist for constructing an instrument with either torquing capability.

2.2.3 Electronic Considerations

As derived from laboratory work, the circuitry requirements for either method of torquing are equivalent (neglecting the constant power

input requirements discussed in Paragraph 2.2.1). In fact, essentially the same set of breadboard electronics was used to torque a STAR Gyro both ways. Experimental work has shown that current and voltage levels for either method of torquing are at values easily obtained using miniaturized semiconductor circuits. In both cases, the power required by the electronics in optimized circuitry would be measured in milliwatts.

Electrostatic torquing requires a precision d-c plate excitation which directly affects the torque scale factor. Of course, a similar scale factor dependence is exerted by the electromagnetic fixed field (this will be discussed further in Paragraph 2.2.4). Obtaining d-c excitation with the necessary stability does not appear to be a difficulty. The disc drive oscillator, necessary for driving the string into a stable oscillation, requires plate excitation of comparable magnitude and stability. Also, whether an instrument be torqued electrostatically or electromagnetically, the need for a stable d-c plate excitation in the torquing channel remains. This will be made more apparent in the next paragraph.

Consideration of electronic requirements necessitates some comment on the complete pickoff torquing transducer configuration. This is especially true since any electrical cross-talks within the instrument which will need rejection electronically will be determined by the chosen configuration. In all practical instruments presently envisioned as suitable for torquing, the following three basic signal transducers are required: (1) A pickoff to sense the angle between the string vibration plane and a reference plane defined by a null output from this sensor. This pickoff measures the deviation from the angular reference originally set up by the instrument. (2) A pickoff which measures the amplitude of the string vibration and provides a signal proportional to the amplitude. This signal provides two functions. It is used as a reference to define instantaneous string position (phasing information). It also provides a signal from which torquing pulses can be derived. The pulse can then be made proportionate to the amplitude of the string oscillation which correspondingly makes the torquing scale factor insensitive to string amplitude variation. (3) A torquing pulse transducer (inverse pickoff) which accepts a torquing pulse and provides a proportionate force to act on the string. Having available three electromagnetic and/or electrostatic transducers opens up a large number of combinations for fitting a transducer to a function. However, some of these can rapidly be discarded. An important point must be made here. Because the string carries any current derived from the electromagnetic phenomenon, voltages proportionate to the required pickoff functions will appear at the same physical point. Thus, any use of the magnetic circuit to obtain multiple functions will cause direct

cross-coupling at the string. Because of this cross-coupling, use of an electromagnetic transducer to provide more than one function is unrealistic. If the magnetic circuit were used as both a torquing transducer and a string plane angle pickoff, common currents with a ratio of 10^5 would require separation. This type of rejection is not particularly practical. It should be noted that assuming reasonable physical separation of the plates, a similar cross-coupling does not occur in the electrostatic case. The pickoff is at the plate, not at the string. With this in mind, it appears that only two transducer configurations deserve consideration for use in a practical torquable instrument: (1) An all-electrostatic configuration with three sets of plates to perform the forementioned functions. (2) A combination which utilizes electromagnetic phenomena for torquing and electrostatic pickoffs for the string plane angle and string oscillation amplitude. It is almost ironic to note, however, that if an instrument were constructed with both electromagnetic and electrostatic capability, strong influence would exist for using the magnetic circuit for the string-plane angle pickoff rather than for torquing, because of a more satisfactory signal with respect to signal source impedance. Thus, it turns out that the probability of ever torquing a STAR Gyro electromagnetically is less than the probability of ever constructing a STAR with a magnetic field.

A final minor point should be noted. Whether torquing electrostatically or electromagnetically a precision d-c plate excitation is required. The string oscillation amplitude plate from which the torque pulse is derived always requires it and the torquing transducer may require it.

2.2.4 Accuracy

To date, no fundamental accuracy advantages of either electrostatic or electromagnetic torquing have been uncovered. The actual physical torquing of the string is a function of the force acting on the string with no direct connection to the mechanism causing the force. Thus, any general theory relating to the response of the vibrating string gyro in any mode is identically applicable to either torquing mechanization. Thus, the fact that second-mode operation is being used does not influence the choice between electromagnetic and electrostatic torquing. Any basic accuracy difference then must relate to the ability of each method to control the force acting on the STAR Gyro. In the case of electromagnetic torquing, the force is a function of the permanent field and the torquing pulse current. Electrostatically the force

is a function of the electrostatic field set up by the d-c plate excitation and the torquing pulse voltage. In both cases the torquing pulses come from comparable circuitry and can be considered equivalent in accuracy and controlability. As far as the respective electromagnetic and electrostatic fields are concerned, studies indicate that state-of-the-art technology can provide sufficient linearity and stability for envisioned requirements in either case. It does appear that a great deal of care and effort would be needed to obtain an adequately stable electromagnetic field.

2.3 CONCLUSION

As a result of these investigations and experimental work done to date, it is felt that electrostatic torquing of the STAR Gyro is both feasible and preferable to electromagnetic torquing. This does not say that the latter would yield unsatisfactory results. Given two simultaneous programs to develop each method to a practical working system, both would probably achieve the development goals. However, the electrostatic version would be lighter and the instrument less complex. It should be pointed out that present STAR instrument research and anticipated future efforts are toward an all-electrostatic instrument.

C5-1227/32

3. TORQUING AND LATERAL - FORCE RESPONSE OF THE VIBRATING - STRING GYRO IN ANY MODE

3.1 SUMMARY

This study is an extension of the work on precision torquing (and general vibrating-string lateral-force response) described in References 2 and 5.

The two major areas of extension are (1) the specific response for the case of the string in any higher vibration mode, and (2) the harmonic and subharmonic response of the string to torquing forces. All information given in References 2 and 5 (some of which is not repeated here) remains valid for the conditions specified there.

The general torquing response, in differential form, for the n^{th} string mode, is described by Equation 3-14. This expression reduces to the expression given by Equations 108 and 115 or Equation 130 in Reference 2, when $n = 1$. Also the method of calculating higher-mode torquing effects by taking the value given by the single-mode equation on the torqued loop and dividing by the number of loops, is verified by the $1/n$ multiplier in Equation 3-14.

It is shown in Paragraphs 3.4 and 3.5 that all elliptical, harmonic, and subharmonic motion of the string can be eliminated by proper choice of the time function of the torquing pulse. This pulse shape is a sine-wave pulse, at string frequency, in phase with string velocity, and of as many full cycles in time as the order of the space-mode vibration. For example, with second-mode vibration as in Figure 3-1, the optimum torquing pulse is as trace (c) in Figure 3-2. Although the above condition is satisfied by any pair of start and stop times which are spaced by the interval specified, the requirement of least sensitivity to timing errors is shown in Paragraph 3.7 to govern the selection of switching phase to be as indicated in Figure 3-2 (start and stop times at zero values of torquing voltage and string velocity). The conditions for no harmonic generation are shown to be completely compatible with the conditions required to obtain minimum error for a given pulse phase error.

Error components resulting from reference-signal amplitude and phase deviation from desired value, zero-cross-detector phase errors, and switching-difference phase errors are given in Paragraph 3.7.

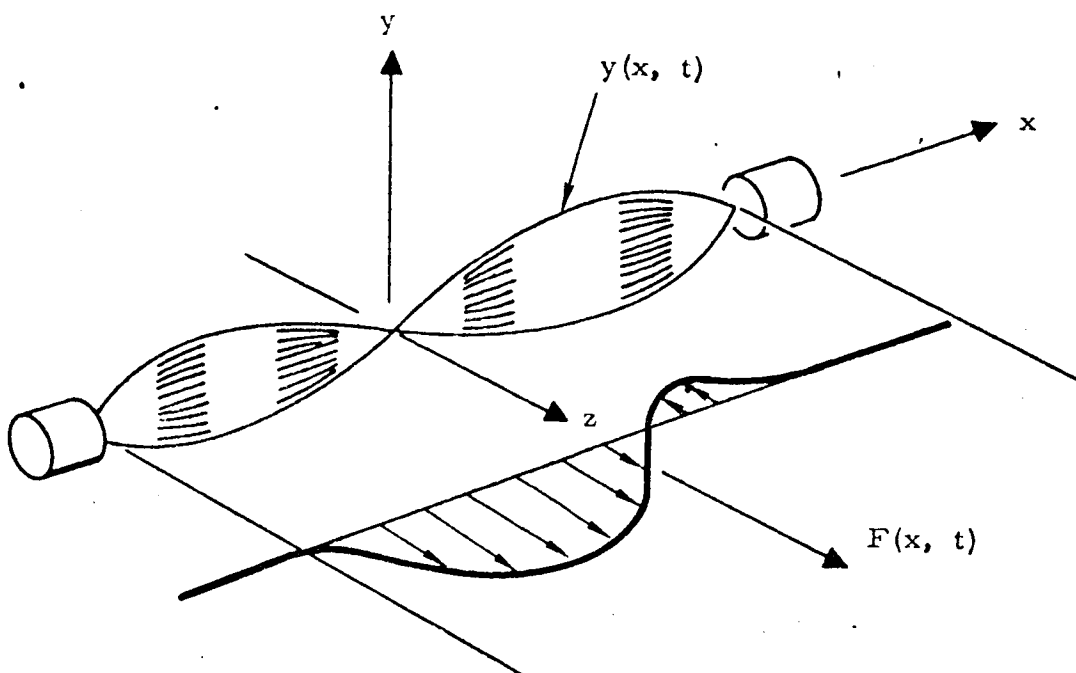


Figure 3-1. String Equations, Illustrated for String Vibration in Second Mode, $n = 2$

3.2 GENERAL LATERAL-FORCING RESPONSE

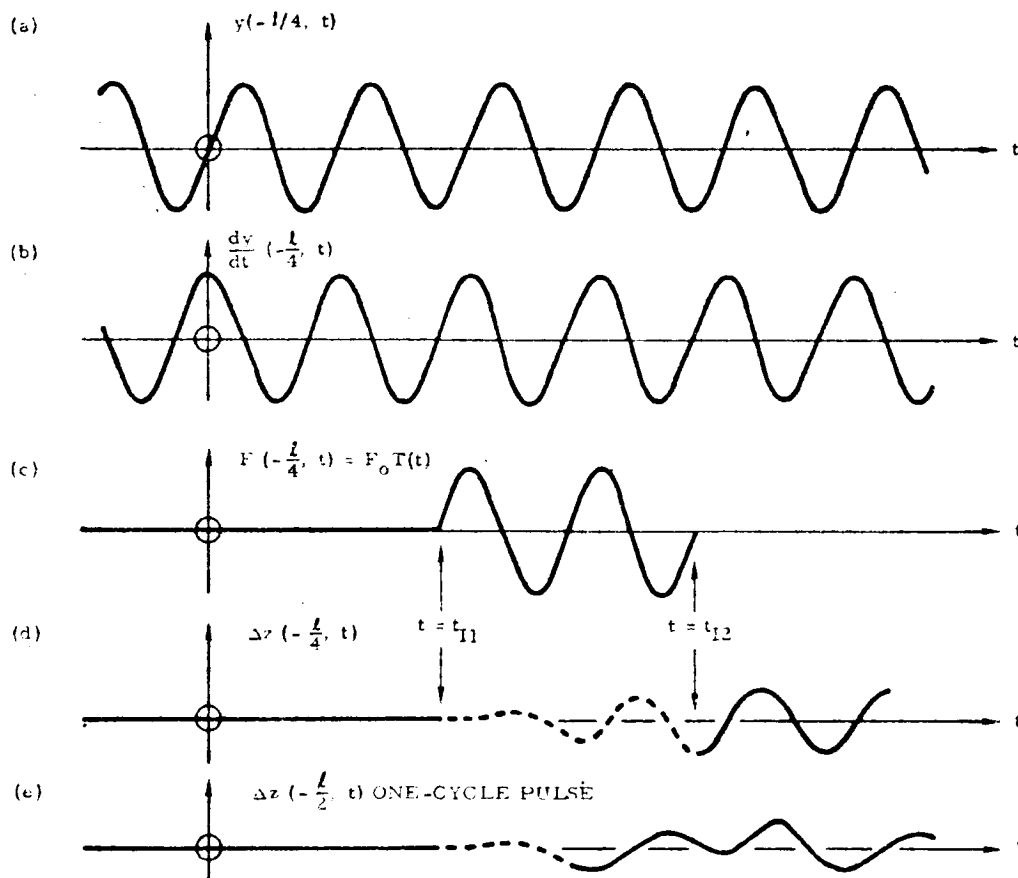
A vibrating string gyro, operating in the n^{th} natural mode, will have normal transverse vibratory motion, y , of the form,

$$y(x, t) = Y_{1n} \sin \left[\frac{n\pi}{l} \left(x + \frac{l}{2} \right) \right] \sin \omega t \quad (3-1)$$

where ω is the frequency at which the string is vibrating. Figure 3-1 illustrates this motion for $n = 2$.*

We now assume that a force in the z direction (perpendicular to the plane of string motion) is applied to the string. The function $F(x, t)$, Figure 3-1, represents the force x -distribution and time variation in a general form.

*In detail, there will be remanent higher time harmonics, Y_{3n} , Y_{5n} , etc, but it is shown in Reference 3 that, when operating as a string gyro near "critical," these higher harmonics are essentially zero, so are not of interest here. The subscript 1 in Y_{1n} is carried in order to be consistent with Reference 3.



NOTE: Δz IS PLOTTED TO A MUCH LARGER SCALE THAN y ($\Delta z \gg y$). TRACE (e) IS A FREE-HAND SKETCH OF THE TYPE OF RESPONSE WHICH MAY BE EXPECTED FROM A ONE-CYCLE PULSE. AS t BECOMES LARGE, THE HARMONICS ON TRACE (e) WILL DECAY UNTIL TRACES (d) AND (e) ARE THE SAME.

Figure 3-2. Two-Cycle Pulse in Second Mode Vibration

The technique employed here to obtain an expression for the response to this arbitrary input, is essentially that of the convolution-integral, * although the terminology used is entirely different. The response of the string to a time impulse is first obtained; then the total response is obtained by an integration (the "convolution") of the responses due to all incremental impulses, which impulses comprise the total finite pulse. The linearity which must be assumed to justify the validity of the superposition involved in this integral is argued on the basis of two facts: (1) The amplitude of the z-motion is extremely small compared to the orthogonal string y-motion, and even smaller compared to the standing wave length. (2) When the string is operating as a gyro, the tension in the string is constant to a high degree of precision (see Reference 1). Hence, the lateral motion of the string has a highly linear force-deflection characteristic.

First consider the response of the string to a force impulse which is applied from t_I to $(t_I + dt_I)$. This impulse on the element dx has the magnitude $F(x, t_I) dt_I dx$. The resulting velocity change in the z direction may be obtained by equating this impulse to the momentum change from time t_I to $t_I + dt_I$, $d\dot{z}(x, t_I) \rho a dx$,

$$d\dot{z}(x, t_I) = \frac{F(x, t_I)}{\rho a} dt_I \quad (3-2)$$

The term $d\dot{z}(x, t_I)$ represents the change in z velocity from the time t_I to the time $t_I + dt_I$, only. It is convenient to express this velocity change as a Fourier series in x over $\pm l/2$. **

$$d\dot{z}(x, t_I) = \sum_{m=1}^{\infty} d\dot{Z}_m \sin \frac{m\pi}{l} (x + l/2) \quad (3-3)$$

$$d\dot{Z}_m = \frac{2}{l} \int_{l/2}^{l/2} \frac{F(x, t_I) dt_I}{\rho a} \sin \frac{m\pi}{l} (x + l/2) dx \quad (3-4)$$

*See, for example, Reference 1, Page 35.

**We use the sine series over the interval π (as opposed to the complete Fourier Series which requires the interval 2π). See, for example, Reference 7, pp. 236, 237.

We now make use of the theory of normal modes. The components in the series of Equation 3-3 are all normal space-modes of the string. This means that each term in Equation 3-3 represents a modal shape which, when excited, will vibrate at a single frequency. (As mentioned above, string tension may be considered constant.) This frequency is $\frac{m\omega}{n}$. Thus, the impulse, $F(x, t_I) dx dt_I$ applied at t_I , specifies the initial condition, $d\dot{z}(x, t_I)$, of a complex string velocity function, $d\dot{z}(x, t)$. The m^{th} term of this expansion contributes a component of velocity to the total motion, which is the value of the m^{th} term in Equation 3-3, multiplied by a cosine function, which starts at t_I and vibrates at the frequency of that mode, $\cos \frac{m\omega}{n}(t - t_I)$. Thus, the value of $d\dot{z}$ for all time after t_I can be written directly from Equation 3-3 as

$$d\dot{z}(x, t) = \sum_{m=1}^{\infty} d\dot{z}_m(x, t_I) \sin \frac{m\pi}{\ell} \left(x + \frac{\ell}{2}\right) \cos \frac{m\omega}{n}(t - t_I) \quad \text{for } t > t_I \quad (3-5)$$

This expression gives, for all $t > t_I$, the component of \dot{z} resulting from that force, $F(x, t) dx$, which occurs between $t = t_I$ and $t_I + dt_I$. Because the expression is valid for all time after $t = t_I$, an integration, in real time, t , can now be performed to obtain an expression for the displacement, rather than velocity,

$$dz(x, t) = \int_{t_I}^t d\dot{z}(x, t) dt \quad (3-6)$$

$$dz(x, t) = \begin{cases} \sum_{m=1}^{\infty} \frac{nd\dot{z}_m(x, t_I)}{m\omega} \sin \left[\frac{m\pi}{\ell} \left(x + \frac{\ell}{2}\right) \right] \sin \frac{m\omega}{n}(t - t_I), & \text{for } t > t_I \\ 0, & \text{for } t < t_I \end{cases} \quad (3-7)$$

*Reference 1 goes into considerable detail to show that at critical operation, which is required to obtain satisfactory angular-reference operation, the tension is constant as mentioned above. That constant value is not the initial tension, but, as shown in Reference 1, is the tension for which the string is resonant at the drive frequency, ω . Thus, in the lateral (z) direction, the resonant frequencies while the string is "at critical" are the m/n multiples of ω and not of ω_0 .

This expression, together with Equation 3-4 for $d\dot{Z}_m$, gives the change in z motion resulting from the application of the force $F(x, t_I) dx$ from t_I to $t_I + dt_I$. Combining Equations 3-4 and 3-7, and performing the dt_I integration results in an equation that is rather complex. Simplification results from separating the time and space variables in the expression for force per unit length,

$$F(x, t_I) = F_0 S(x) T(t_I) \quad (3-8)$$

This requires that the spatial distribution of the force, $S(x)$, along the string, is the same at all times, a fact which is generally true in systems of interest. We will assume that $S(x)$ and $T(t_I)$ each have maximum values of unity. With this substitution, the expression for dz (assuming that ρ , a , and m are independent of x) can be reduced to

$$dz(x, t) = \sum_{m=1}^{\infty} \frac{2F_0 n \sin \left[\frac{m\pi}{l} \left(x + \frac{l}{2} \right) \right]}{\rho a m \omega l} S_m \left[dT_{ms} \sin \frac{m\omega t}{n} - dT_{mc} \cos \frac{m\omega t}{n} \right], \text{ for } t > t_I \quad (3-9)$$

where

$$dT_{ms} = T(t_I) \cos \frac{m\omega t}{n} I dt_I \quad (3-10)$$

$$dT_{mc} = T(t_I) \sin \frac{m\omega t}{n} I dt_I \quad (3-11)$$

$$S_m = \int_{-l/2}^{l/2} S(x) \sin \left[\frac{m\pi}{l} \left(x + \frac{l}{2} \right) \right] dx \quad (3-12)$$

The time function has been broken into its sine and cosine components, although the expression is somewhat more complicated in this form, because this adapts more directly to the desired results.

3.3 NORMAL "TORQUING" RESPONSE

The basic y -motion of the string has been given in Equation 3-1. This motion is maintained by a parametric drive consisting of a longitudinal motion imposed on the string end fastening, as described

in Reference 1. When a torquing force adds a z-motion in phase with this y-motion (and at y-motion frequency), the resultant comprises a new motion of the string in a new plane through the neutral string axis, at some small angle $d\theta$ from the y axis. The basic string drive maintains this resultant motion. On the other hand, the quadrature component of z-motion at string frequency (representing the ellipticity of string-element motion) and the z-motion components at all other frequencies are undriven, and hence are damped out and decay in time. For this reason, it is the sine term of frequency ω only, in Equation 3-9, which is of interest in the torquing solution. This term, divided by y in Equation 3-1 gives the net shift in string plane, $d\theta$, resulting from the applied force.

$$d\theta = \frac{dz(x,t) \Big|_{\sin \omega t \text{ component}}}{y(x,t)} \quad (3-13)$$

$$d\theta = \frac{2F_o S_n}{\rho a \omega l Y_I} T(t_I) \cos \omega t_I dt_I \quad (3-14)$$

where

$$S_n = \int_{-l/2}^{l/2} S(x) \sin \left[\frac{n\pi}{l} \left(x + \frac{l}{2} \right) \right] dx$$

Note that the $\sin \left[\frac{n\pi}{l} \left(x + \frac{l}{2} \right) \right]$ and $\sin \omega t$ factors both cancel out when the substitution is made.

This equation is basic to the vibrating string gyro response to a torquing force or any other lateral force which can be expressed as in Equation 3-8.

To obtain the response to a finite pulse, Equation 3-14 is simply integrated,

$$\Delta \theta = \frac{2 F_o S_n}{\rho a \omega l Y_m} \int_{t_{I1}}^{t_{I2}} T(t_I) \cos \omega t_I dt_I \quad (3-15)$$

The small-angle approximation implied here is not the limitation it might seem. Individual pulses are typically very small (seconds or fractions of a second of arc), while the larger angles resulting from longer torquing periods normally involve a follow-up servo which restores the original orientation between the string and torquing mechanism.

Pulses with an infinite variety of space shapes, $S(x)$, as well as an infinite variety of time shapes $T(t_I)$, will operate satisfactorily to produce torqued steps, $\Delta\theta$. The basic requirement is that they be such that they can be accurately reproduced in the magnitude and timing required.

It seems logical, then, to look first for shapes that cause the least disturbance to the string through the other components of dz in Equation 3-9.

3.4 ELLIPTICAL, HARMONIC AND SUBHARMONIC PRODUCTION

In practice, as well as in theory, non-string-frequency components have been found to have either no effect or a second-order, as-yet-undetected, effect. Elliptical-motion components (at normal string frequency) can cause drift in the presence of noncritical operation. However, because torquing waveforms exist which eliminate these at-least-unneeded components, without sacrificing other features desired of the torquing, we now consider the conditions for eliminating them and later consider the torquing response to such pulses which have no subsidiary effects.

Equations 3-14 and 3-15 are in the most convenient form for obtaining the normal response of the string to torquing forces. However, to find the harmonic and elliptical z -motion, produced, incidental to torquing, we return to Equation 3-9. Performing the dt_I integration

$$\Delta z(x, t) = \sum_{m=1}^{\infty} \frac{2F_0 \sin \left[\frac{m\pi}{l} \left(x + \frac{l}{2} \right) \right]}{\rho a m \omega l} S_m \left[\Delta T_{ms} \sin \frac{m\omega}{n} t - \Delta T_{mc} \cos m\omega t \right], t > t_{I2}$$

(3-16)

$$\Delta T_{ms} = \int_{t_{I1}}^{t_{I2}} T(t_I) \cos \frac{m\omega}{n} t_I dt_I \quad (3-17)$$

$$\Delta T_{mc} = \int_{t_{I1}}^{t_{I2}} T(t_I) \sin \frac{m\omega}{n} t_I dt_I \quad (3-18)$$

$$S_m = \int_{-\ell/2}^{\ell/2} S(x) \sin \frac{m\pi}{\ell} \left(x + \frac{\ell}{2} \right) dx \quad (3-12) \text{ repeated}$$

The expression for $\Delta \emptyset$, Equation 3-15, can also be obtained from Equations 3-16 and 3-1. Thus the $\sin \omega t$ component of $\Delta z(x, t)$, Equation 3-16, may be divided by $y(x, t)$, Equation 3-1, to obtain the same expression for $\Delta \emptyset$ as was obtained in Equation 3-15 by integrating Equation 3-14.

An expression for the change in the ellipse thickness ratio, produced by one full pulse, may be obtained in a manner similar to that described in the paragraph above for obtaining $\Delta \emptyset$. This ratio change is the change in the minor-to-major-axis ratio (which ratio we will call B/A of the ellipse at normal string frequency, ω , and is given by

$$\Delta \left(\frac{B}{A} \right) = \frac{\Delta z(x, t) \big|_{\cos \omega t \text{ component}}}{y(x, t)} \quad (3-19)$$

$$\Delta \left(\frac{B}{A} \right) = \frac{2F_o S_n}{\rho a \omega \ell Y_{ln}} \int_{t_{I1}}^{t_{I2}} T(t_I) \sin \omega t_I dt_I \quad (3-20)$$

Because this elliptical motion is undriven, it begins to decay immediately, so that the expression, to be applicable for all time after t_{I2} , would be multiplied by the factor

$$\exp \left\{ -\frac{\omega}{2Q} \left(t - \frac{t_{I1} + t_{I2}}{2} \right) \right\},$$

where Q is the conventional mechanical resonance factor. The elliptical-motion component appears on the main string pickoff signal as a quadrature signal (at 90-degree phase shift) which is normally rejected by the demodulator. For this discussion, however, we are mainly interested in the possibility of selecting a torquing pulse $T(t_I)$ which will not produce any ellipticity, while still producing a relatively large value for $\Delta\theta$, Equation 3-15. Considering well-known orthogonal functions, we see that $\Delta(B/A)$ of Equation 3-20 is zero if we choose the function

$$T(t_I) = \cos \omega t_I \quad (3-21)$$

provided the proper torquing interval is selected. This interval can be, for example $-\pi/2$ to $+\pi/2$ for ωt_I , or any interval of length $k(2\pi)$ (for k an integer).

We also note that if we include a phase error, θ_r , in the expression, Equation 3-21, so that $T(t_I) = \cos(n\omega t_I + \theta_r)$, then the desired torqued response, $\Delta\theta$, Equation 3-15, is maximized for $\theta_r = 0$, the same value of θ_r which makes the elliptical component zero.

3.5 HARMONIC AND SUBHARMONIC ELIMINATION

We now look for torquing functions, $F(x, t_I)$, for the interval t_{I1} to t_{I2} , which will not generate the unwanted harmonics in $\Delta z(x, t)$, Equation 3-16. That is to say, we would like to select $F(x, t_I)$ and the interval t_{I1} to t_{I2} so that all Δz terms for which $m \neq n$ are zero.

3.5.1 Space Function Only

It is possible to accomplish this for all functions, $F(t_I)$, by choosing $S(x)$ to be

$$\sin \frac{n\pi}{l} \left(x + \frac{l}{2} \right),$$

in which case, from Equation 3-12, $S_m = 0$ for all values of $m \neq n$.

Practically speaking, however, it would be extremely inconvenient to produce a torquing force with this space mode: First, to produce the sine shape in-space, with harmonics limited to a fairly low level would be difficult (especially in view of the simultaneous y -motion of

the string). Secondly, it is highly preferable to introduce torquing forces at one end only, so as to minimize electrical interference of the relatively high torquing voltages on the low-signal-level string-angle and string-reference pickoffs.

3.5.2 Time Function Only

Fortunately, there is a much easier way to substantially eliminate these unwanted terms. Proper choice of the forcing time function $T(t_I)$ will eliminate all unwanted harmonics in the string response to the torquing force for all space functions, $S(x)$. Consider the terms ΔT_{ms} and ΔT_{mc} ; we look for a pulse shape, $T(t_I)$, which will make these zero except for ΔT_{ns} (the coefficient of $\sin \omega t$), which latter term is required for the precessing effect, Equation 3-13. This can be accomplished by choosing

$$T(t_I)_n = \begin{cases} \cos \omega t_I, & \left[-\gamma_0 < (\omega t_I) < (2n\pi - \gamma_0) \right] \\ 0, & \text{elsewhere} \end{cases} \quad (3-22)$$

for all values of the arbitrary phase angle γ_0 . The $\cos \omega t_I$ form clearly gives the type of orthogonal function we require. The pulse width of $2n\pi$ (in place of simply 2π) is required to obtain an interval over which $\cos \omega t_I$ and \cos or $\sin \frac{m\omega}{n} t_I$ are orthogonal, even when m is not an integral multiple of n (as, $m = 1, 3, 5 \dots$ for $n = 2$ — or $m = 1, 2, 4, 5, 7 \dots$ for $n = 3$, etc).

We note now that Equation 3-22 gives an expression for $T(t_I)$ which also satisfies the requirements for eliminating the string-frequency, ellipse-producing z -motion component,* while at the same time being at the phase which maximizes the torquing effect. Thus, Equation 3-22 gives an expression for a highly desirable torquing pulse from the standpoint of its not introducing extraneous string motion while producing maximum torque for a sinusoidal-wave type torquing pulse. The pulse start phase, as determined by γ_0 is free for later choice.**

*See Equation 3-21 and the statement concerning pulse interval which follows that equation.

**Combination cases also exist for eliminating harmonics, where requirements, though less stringent, are placed on both $S(x)$ and $T(t_I)$. The only ones of this type known require force on all string loops and are hence of no more practical value than the "Space Function Only" method described above.

In summary, if a string gyro is torqued with a sinusoidal force at string frequency and in phase with string velocity and of a duration equal to n full cycles (where n is the mode of string vibration), then neither elliptical motion nor harmonic (including sub- and fractional-harmonic) motion is generated incidental to the torquing, no matter what space distribution is used for the force.

As an example, with the string in the second mode, $n = 2$, as pictured in Figure 3-1, a double-sine-wave torquing pulse should be chosen, trace (c), Figure 3-2, in order to prevent the torquing pulse from producing any unwanted string-motion harmonics. Note that by using this pulse, all harmonics are cancelled out, for any space forcing function, $S(x)$, Equation 3-8.

3.6 HARMONIC GENERATION BY A SINGLE-SINE-WAVE PULSE—SECOND MODE

Because testing has been done using the single-sine-wave torquing pulse (Figure 3-3) with the string operating in its second mode, it is desirable to ask what harmonics this produces. For this pulse, with $n = 2$, we define the single-sine-pulse value of $T(t_I)$ as

$$T_{ssp}(t_I) = \begin{cases} \cos \omega t_I, & -Y_o < (\omega t_I) < (2\pi - Y_o) \\ 0, & \text{elsewhere} \end{cases} \quad (3-23)$$

which differs from Equation 3-22 only in that 2π replaces $2n\pi$ in the limits. Combining this pulse with Equations 3-17 and 3-18, we obtain for the coefficients in Equation 3-16,

$$\Delta T_{ms} = \begin{cases} 0, & \text{for } m \text{ even and } \neq 2 \\ \frac{\pi}{\omega}, & \text{for } m = 2 \text{ (the desired torquing effect)} \\ \frac{2}{\omega} \left[\frac{\sin \left[\left(\frac{n}{2} - 1 \right) Y_o \right]}{m - 2} + \frac{\sin \left[\left(\frac{m}{2} + 1 \right) Y_o \right]}{m + 2} \right], & \text{for } m \text{ odd} \end{cases} \quad (3-24)$$

$$\Delta T_{mc} = \begin{cases} 0, & \text{for } m \text{ even} \\ \frac{2}{\omega} \left[\frac{\cos \left[\left(\frac{m}{2} - 1 \right) Y_o \right]}{m - 2} + \frac{\cos \left[\left(\frac{m}{2} + 1 \right) Y_o \right]}{m + 2} \right], & \text{for } m \text{ odd} \end{cases} \quad (3-25)$$

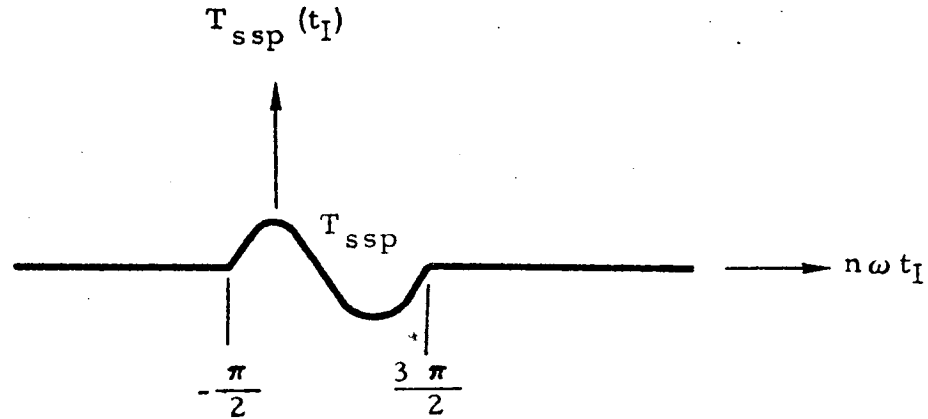


Figure 3-3. The Single-Sine-Wave Pulse, $T_{ssp}(t_I)$

A value for γ_0 can be chosen to eliminate either ΔT_{ms} or ΔT_{mc} , but there is no way of eliminating both. For the purpose of minimizing the effect of timing errors in the pulse-generating circuitry, it is desirable to switch at times when the effect of the actual value of the pulse is minimum. The optimum switching time can be seen in Equation 3-14 to be when $\cos \omega t_I = 0$, or when γ_0 is $-\pi/2$. This is the value of γ_0 being used, as depicted in Figure 3-3. With this selection for γ_0 , Equations 3-24 and 3-25 become

$$\Delta T_{ms} = \left\{ \begin{array}{l} 0, \text{ for } m \text{ even and } \neq 2 \\ \frac{\pi}{\omega} \text{ for } m = 2 \text{ (the desired torquing effect)} \\ \frac{2}{\omega} \left[\frac{\cos \frac{m\pi}{2}}{m-2} - \frac{\cos \frac{m\pi}{4}}{m+2} \right], \text{ for } m \text{ odd} \end{array} \right\} \quad (3-26)$$

$$\Delta T_{mc} = \left\{ \begin{array}{l} 0, \text{ for } m \text{ even} \\ \frac{2}{\omega} \left[\frac{\sin \frac{m\pi}{2}}{m-2} - \frac{\sin \frac{m\pi}{4}}{m+2} \right], \text{ for } m \text{ odd} \end{array} \right\} \quad (3-27)$$

Actually, the magnitude of interest is the vector sum, *

$$\Delta T_m = + \left[\Delta T_{ms}^2 + \Delta T_{mc}^2 \right]^{1/2} \quad (3-28)$$

which can be shown to be

$$\Delta T_m = \left\{ \begin{array}{l} 0, \text{ } m \text{ even} \\ \frac{\pi}{\omega}, \text{ } m = 2 \left[\begin{array}{l} \text{the angle,} \\ \arctan \left(\frac{\Delta T_{2c}}{\Delta T_{2s}} \right) = 0 \end{array} \right] \\ \frac{2}{\omega} \left[\frac{1}{m-2} - \frac{1}{m+2} \right], \text{ } m \text{ odd} \end{array} \right\} \quad (3-29)$$

Thus, we see that, with second-mode string operation, the $1/2$, $1-1/2$, $2-1/2$, $3-1/2$, etc, harmonics of the string frequency (ω) are excited by a single-wave torquing pulse, as opposed to the double-wave pulse, which, as mentioned, excites no harmonics. For example, compared to the precessing term ΔT_{2s} , which in this case is

$$\frac{\pi}{\omega} = \frac{3.14}{\omega},$$

the $1/2$ harmonic ($m = 1$) gives

$$\Delta T_1 = \frac{8}{3\omega} = \frac{2.67}{\omega}$$

and the $1-1/2$ harmonic ($m = 3$) gives

$$\Delta T_3 = \frac{8}{5\omega} = \frac{1.6}{\omega}.$$

These terms decay and certainly do not show any first-order effect on the torqued string gyro.

*Using suitable identities, Equation 3-16 can be rewritten in terms of ΔT_m , as just defined, to give

$$\Delta z(x, t) = \sum_{m=1}^{\infty} \frac{2F_0}{\rho a m \omega l} \sin \left[\frac{m\pi}{l} \left(x + \frac{l}{2} \right) \right] S_m \Delta T_m \sin \left(m\omega t - \arctan \frac{\Delta T_{mc}}{\Delta T_{ms}} \right)$$

3.7 PULSE-INTERVAL AND PHASE TORQUING ERRORS (INDEPENDENT OF ANY HARMONICS GENERATED)

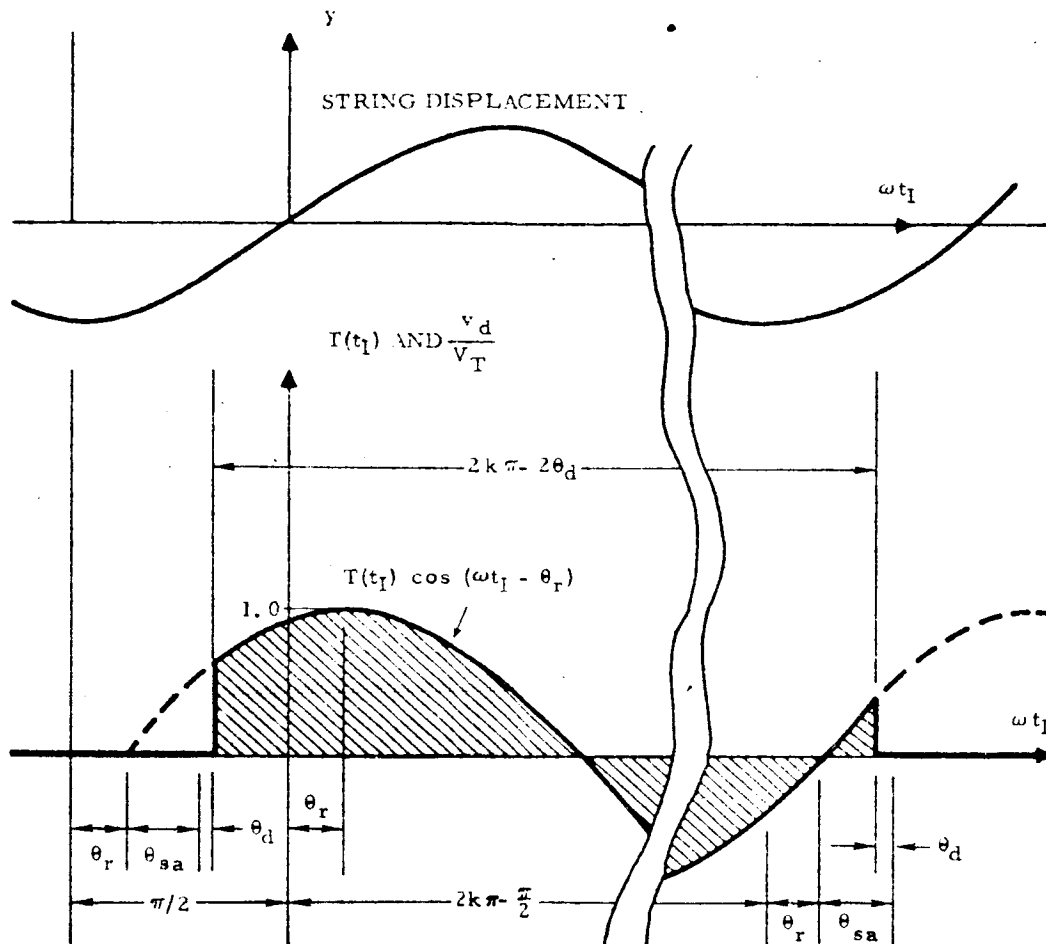
We now examine the torquing response of a time wave, $T(t_i)$, of the sinusoidal form just discussed. In a given instrumentation, there will be deviations from the ideal wave. The timing errors result from three main sources in the circuitry. These are (1) phase shift of the entire string reference signal, (2) phase error in the zero-cross detector, and (3) phase errors due to switching time.

In Figure 3-4 the torquing signal is depicted with significant phase terms. The angle, θ_r , is the shift in phase of the string reference signal. In all mechanizations visualized to date, switching is controlled by a zero-cross detector which operates on the actual string reference signal so that a shift in string-reference-signal phase causes the switching time phase to shift with it. Thus, θ_r adds to the switching-time phase, as seen in Figure 3-4.

The next component of switching phase is θ_{sa} , the average switching-time phase shift. In practice, this phase will result mainly from errors in the zero-cross detector which determines both turn-on and turn-off time. Thus a phase shift in the pulse supplied by the zero-cross detector will shift the turn-on and turn-off times equally. (The use of only full-cycle torquing waves (no half-cycle waves) avoids possible differences between plus-going and minus-going zero-cross detectors.)

In addition to the average switching-time phase, there will be a difference term, θ_d , which adds to the turn-on phase, while subtracting from the turn-off phase. It is this component that changes the total length of the pulse from an even multiple of 2π , to $2k\pi - 2\theta_d$, as indicated in Figure 3-4.

In any case, three phase terms are required to define the pulse, time-wise. The particular definitions picked here were chosen to be as consistent as possible with a typical mechanization. For example, it is convenient to think of one changing while the others remain constant. It also turns out that, with these definitions, the expression for the torquing response turns out in a convenient form.



θ_r = REFERENCE WAVE PHASE SHIFT
 θ_{sa} = AVERAGE SWITCHING TIME PHASE SHIFT
 θ_d = DIFFERENCE MODE OF SWITCHING TIME PHASE SHIFT

Figure 3-4. Phase Angles θ_r , θ_{sa} , and θ_d , Defining Switching-Time and Torquing-Wave Phases. (Harmonics are Eliminated if $k = n$, but This Development not Restricted to $k = n$.)

To obtain the total torquing response to the wave form of Figure 3-4, we integrate Equation 3-14 over the limits defined in Figure 3-4.

$$\Delta \phi = \frac{2 F_o S_n}{\rho a \omega l Y_1} \int_{\frac{-\pi}{2} + \theta_r + \theta_{sa} + \theta_d}^{\frac{-\pi}{2} + 2k\pi + \theta_r + \theta_{sa} - \theta_d} \cos(\omega t_I - \theta_r) \cos \omega t_I dt_I \quad (3-30)$$

This rather imposing-looking integral works out to a rather convenient form.

$$\Delta \phi = K \left[\cos \theta_r - \frac{\theta_d}{k\pi} \cos \theta_r + \frac{1}{2k\pi} \sin 2\theta_d \cos(\theta_r + 2\theta_{sa}) \right] \quad (3-31)$$

where

$$K = \frac{2k\pi F_o S_n}{\rho a \omega^2 l Y_1} \quad (3-32)$$

and S_n is as given in Equation 3-14.

To this point, no small-angle approximations have been made. We would like to maintain the primary torquing term $K \cos \theta_r$ and at the same time be as insensitive to individual changes in other phase shifts as possible. The term θ_d (which is half the deviation from a full-cycle pulse) is particularly troublesome in this regard, but we notice that it is possible to arrange to have the θ_d and $\sin 2\theta_d$ terms cancel. First, assume that θ_d is small so $\sin 2\theta_d \rightarrow 2\theta_d$. Then,

$$\Delta \phi = K \left[\cos \theta_r + \frac{\theta_d}{k\pi} \left[\cos(\theta_r + 2\theta_{sa}) - \cos \theta_r \right] - \frac{2}{3k\pi} \theta_d^3 \cos(\theta_r + 2\theta_{sa}) \right], \text{ for } \theta_d \ll 1 \quad (3-33)$$

In this form we see clearly that by picking θ_r and θ_{sa} both to be approximately zero, the two cosine terms in the brackets nearly cancel, and leave $\Delta\theta$ with but small sensitivity to θ_d .

Thus we wish θ_r , θ_d , and θ_{sa} all to be near zero. Allowing for slight deviations only, we may expand to obtain

$$\Delta\theta = K \left\{ 1 - \frac{1}{2} \theta_r^2 - \frac{2}{k\pi} \theta_d \left[\theta_{sa} (\theta_r + \theta_{sa}) + \frac{1}{3} \theta_d^2 \right] \right\} \quad (3-34)$$

for θ_d , θ_r and θ_{sa} all $\ll 1$

Equation 3-34, together with other defining equations in previous sections gives the response to a torquing pulse with time shape as defined in Figure 3-4. Note that the condition for least sensitivity of torquing response to switching-time phase shifts (the condition $\theta_r = 0$) is also the condition for no elliptical motion, as derived earlier. This is not surprising, upon examining the differential expressions, Equations 3-14 and 3-20.

Also, we would normally expect to pick $k = n$ to eliminate all harmonic z-motion excitation. Note that it is possible to select $k = n$ without having any adverse effect on the rejection of torquing errors due to torque-pulse phasing deviations, so that optimum pulse shape for both harmonic rejection and minimum sensitivity to phase errors can be realized simultaneously.

3.8 CONCLUSION

It has been shown that, by properly choosing the time-form of the torquing force, it is possible to "torque" a string gyro without inducing any subsidiary harmonic, sub-harmonics, or elliptical-component motion, and that this can be accomplished with complete independence of the choice of the space distribution of the force, and without adding any difficulty to the pulse-generating circuitry. Further, an optimum pulse shape required to obtain least torquing-scale-factor error resulting from residual torque-pulse phasing errors, has been found, and shown to be completely compatible with pulse choice for no harmonic generation. Thus, no compromise between these objectives is necessary.

4. ELECTROSTATIC FORCE ON A FIBRE BETWEEN TWO PLATES

This section presents a derivation of the expression for the electrostatic force exerted on a cylindrical bar or string when it is parallel to and between two parallel plates, as depicted in Figure 4-1. The string or fibre and both plates may all three be at different voltages. Although the problem may not appear difficult (the force between a cylinder and a single plate, for example, is well known; see Reference 8), the solution required more effort than had been anticipated and it seems worth presenting in some detail.

Paragraph 4.1 contains the complete derivation of the force expression in terms of the geometry plus the capacity, C_w . C_w represents the capacity between the wire, or cylinder, and the paralleled set of plates. Because the derivation for C_w is rather lengthy, it is set apart in Paragraph 4.2. Finally, in Paragraphs 4.3, 4.4, and 4.5

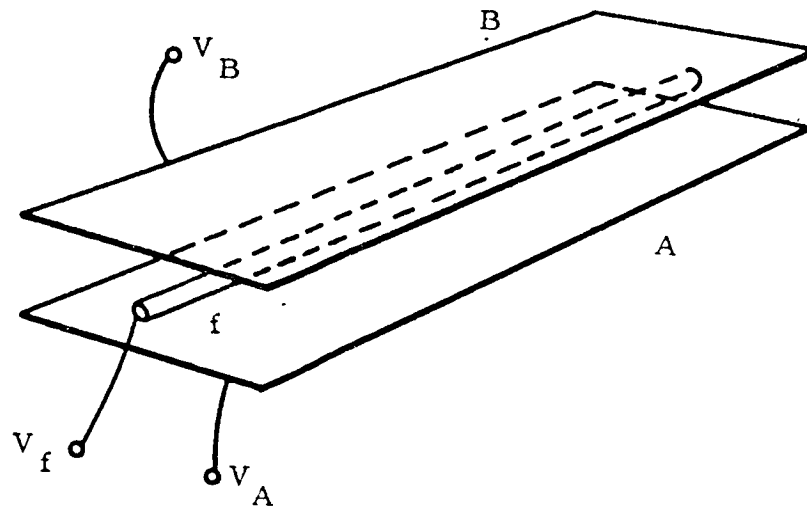


Figure 4-1. Cylindrical Fibre and Electrostatic Plates

the results are examined. For example, special cases are compared to exact solutions for an indication of accuracy; optimum conditions for maximum force are examined; the amount by which the force on a fibre can be increased by using two plates, instead of one, is analysed.

4.1 FORCE EQUATION

The basic method used here, for finding the force is to obtain an expression for the stored energy in the system and differentiate this with respect to displacement in the direction of the required force. To write an expression for the energy, we first obtain the values of the six equivalent capacitors shown in Figure 4-2. These include three capacities directly to ground which would normally be referred to as "stray" capacities. The other three are those which interconnect the three electrodes.

We may intuitively feel that the voltage differences, $(V_B - V_A)$ and $(V_f - V_A)$, are sufficient to express the forces, the absolute level

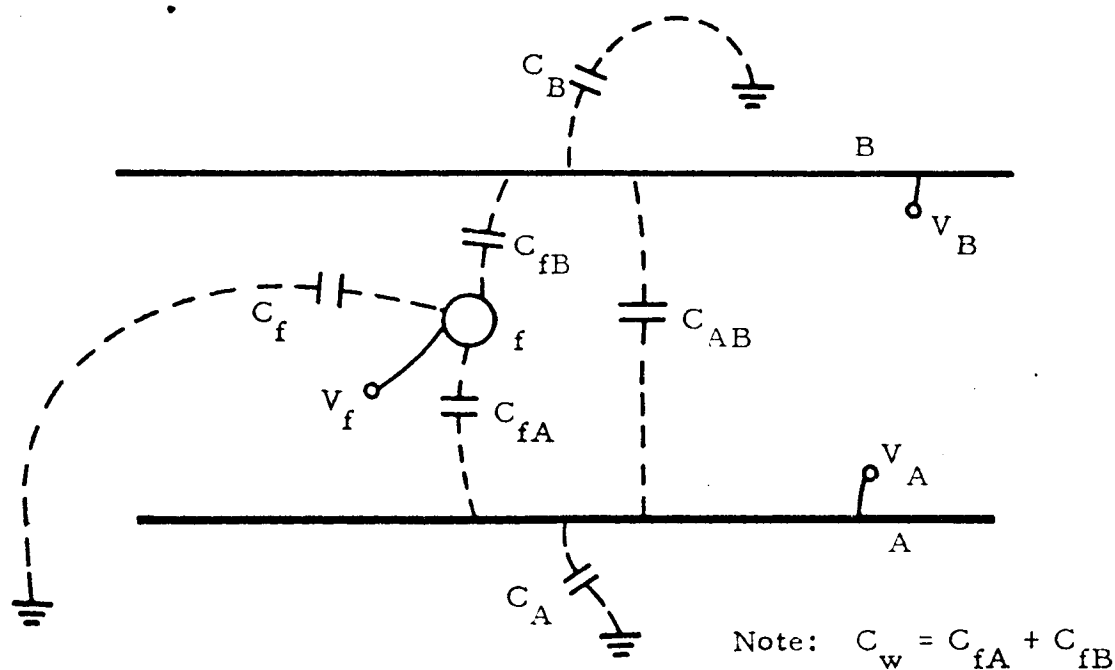


Figure 4-2. Capacity Model-Three Stray Capacitors to Ground and Three Interelectrode Capacities

of voltage not being important. We can verify this intuition by first writing the charge-versus-voltage matrix in the form

$$\begin{bmatrix} Q_A \\ Q_B \\ Q_f \end{bmatrix} = \begin{bmatrix} C_A + C_{AB} + C_{fA} & -C_{AB} & -C_{fA} \\ -C_{AB} & C_B + C_{AB} + C_{fB} & -C_{fB} \\ -C_{fA} & -C_{fB} & C_f + C_{fA} + C_{fB} \end{bmatrix} \begin{bmatrix} V_A \\ -V_B \\ V_f \end{bmatrix} \quad (4-1)$$

The elements of the square matrix have been written in relation to the capacitors of Figure 4-2, by inspection, by considering, for example, that the first term in Q_A is the charge at A when V_B and V_f are both 0, and so forth for other terms. * Note the negative values when the charge component under consideration is on a grounded element.

We shall assume that the plates and cylindrical fibre (of length L) are of sufficient length that end effects may be neglected and the problem is reduced to a two-dimensional problem. If we further assume that the plates A and B are very wide, then the fibre f will be shielded from ground by these plates and C_f is essentially zero. If we also neglect the "stray" capacities to ground C_A and C_B , ** then C_A , C_B and C_f may all be considered to be zero. In this case we expect

*Equation 4-1 can be checked by writing $Q_A = V_A C_A + (V_A - V_f) C_{fA} + (V_A - V_B) C_{AB}$, etc.

**The expressions found in the literature for the force between two parallel plates and for the force between a wire and plate customarily tacitly neglect the effect of "stray" capacity from the elements to ground. Thus if the standard expression for the force between parallel plates is applied to a case where there is a high common-mode voltage [in extreme, for example, the voltages on the two plates could be, say 10^6 and $(10^6 + 1)$ volts], the calculated force could be incorrect, even in direction, because the standard expression depends only on the square of the voltage difference. With high common-mode voltage, thin plates, etc., the stray capacity to ground could be sufficient to allow the charge to be the same on both plates, resulting in a net repulsive, not attractive, force. Neglecting C_A and C_B here is the same type of assumption as this. Only in a rather extreme case would there be sufficiently high capacity (here, or in the other expressions mentioned) to ground and common-mode voltage for this effect to affect the results.

that the resulting expressions will turn out to be independent of the common voltage level; therefore, let us define the relative voltages

$$\begin{aligned} V_s &= V_f - V_A \\ V_p &= V_B - V_A \end{aligned} \quad (4-2)$$

The problem, stated in these terms, appears in Figure 4-3. Making the above substitutions in Equation 4-1, we obtain

$$\begin{bmatrix} Q_A \\ Q_B \\ Q_f \end{bmatrix} = \begin{bmatrix} C_{AB} + C_{fA} & -C_{AB} & -C_{fA} \\ -C_{AB} & C_{AB} + C_{fB} & -C_{fB} \\ -C_{fA} & -C_{fB} & C_{fA} + C_{fB} \end{bmatrix} \begin{bmatrix} V_A \\ V_p + V_A \\ V_s + V_A \end{bmatrix} \quad (4-3)$$

Using the notation change $Q_s \equiv Q_f$ and $Q_p \equiv Q_B$, this reduces to

$$\begin{bmatrix} Q_A \\ Q_p \\ Q_s \end{bmatrix} = \begin{bmatrix} 0 & -C_{AB} & -C_{fA} \\ 0 & C_{AB} + C_{fB} & -C_{fB} \\ 0 & -C_{fB} & C_{fA} + C_{fB} \end{bmatrix} \begin{bmatrix} V_A \\ V_p \\ V_s \end{bmatrix} \quad (4-4)$$

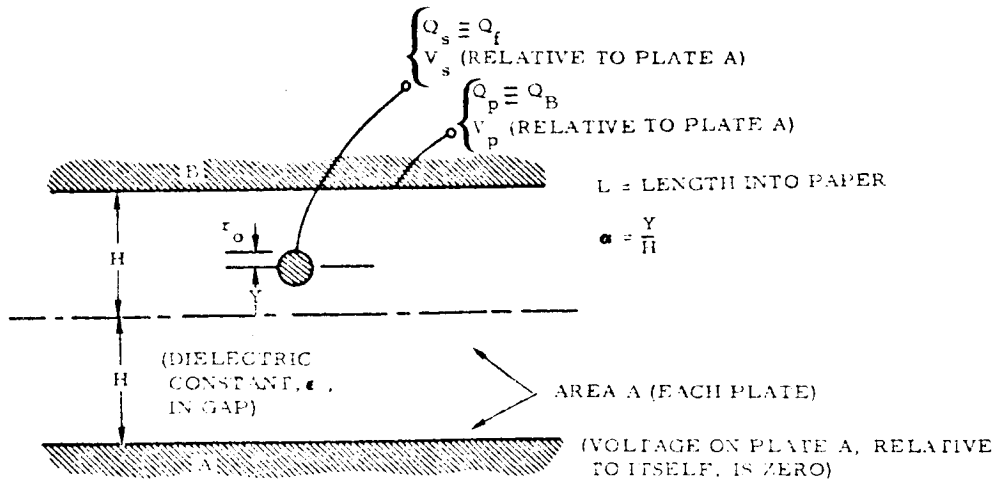


Figure 4-3. Relative Voltage Picture and Dimensions. C_w is Capacity From Cylinder to Both Plates Paralleled

Thus, as expected, it turns out that all charges are independent of the common voltage level V_A . An expression for Q_A is not needed because it is simply $-(Q_B + Q_S)$. We thus can express the entire charge-voltage picture by the expression

$$\begin{bmatrix} Q_P \\ Q_S \end{bmatrix} = \begin{bmatrix} C_{AB} + C_{fB} & -C_{fB} \\ -C_{fB} & C_{fA} + C_{fB} \end{bmatrix} \begin{bmatrix} V_P \\ V_S \end{bmatrix} \quad (4-5)$$

While using this expression we may think of V_A as being grounded, with V_S and V_P being the voltages on the string and on the ungrounded plate. At the end of the solution, however, it will be convenient to return and express the final force in terms of all three voltages.

All of which must seem a rather devious method of demonstrating what must, at least by now, seem obvious to the reader. We have merely shown that a 2×2 matrix is sufficient to express the electrostatic energy picture, and that the condition for this simplification is that C_f , C_A and C_B all are negligible. While there may be some small value of the "stray" capacities, C_A and C_B , the "stray" capacity C_f is far less, and in fact, in the "infinite-plate" case, is identically zero.

It was originally thought that, by using an infinite series of line images, it would be possible to obtain the entire voltage-charge picture on the three electrodes directly. It was discovered, however, that this is not practical. The infinite series of line charge images proved only suitable for determining C_w , the capacity between the cylindrical wire, and the pair of plates connected in parallel (Figure 4-4).

The following three assumptions are important in relating the three elements of the capacity matrix, Equation 4-5, to the geometry involved.

- A. Because the fibre is parallel to the plates, and if the fibre diameter is small compared to the plate gap, then the fibre lies in a plane which would be an equipotential plane in the absence of the fibre. In this case, with $Q_S = 0$ (that is, with the string electrically "floating," i. e., with no initial charge, and not connected to any voltage source which could conduct any charge to it), the capacity between plates A and B is unaffected by the presence of the fibre; this is because the

fibre simply assumes the potential which would be in that plane in its absence, and thus has no effect on the field or inter-plate capacity. Thus we write (the terms being defined in Figure 4-3)

$$\text{For } Q_s = 0$$

(4-6)

$$V_p = \frac{2H}{\epsilon A} Q_p$$

for any consistent set of units. The practical question is: how accurate is the small-diameter solution for larger diameters? This is considered in Paragraph 4.3 by comparison to exact solutions in known special cases. The results prove to be surprisingly good at values of r_o/H as high as $1/3$ to $1/2$.

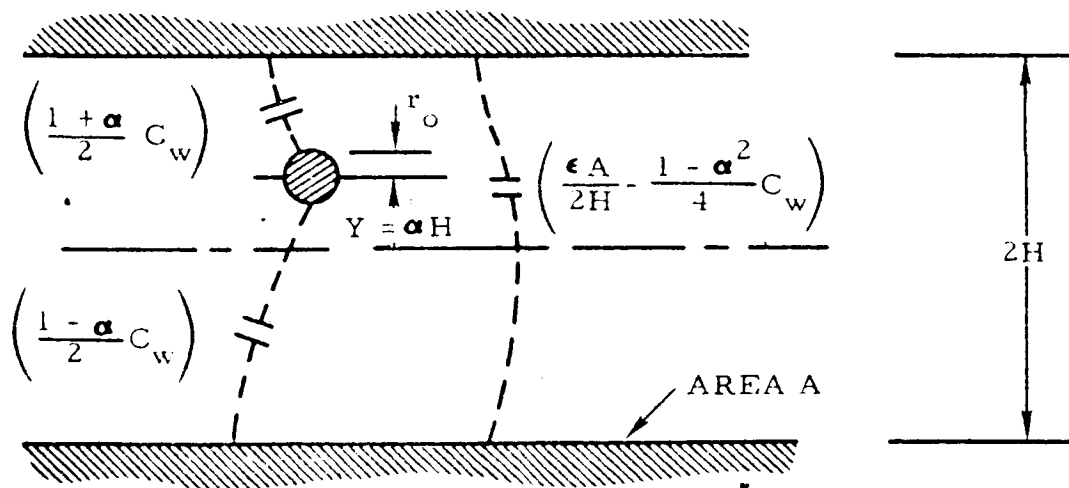


Figure 4-4. Interelectrode Capacity in Terms of Geometry. C_w is Capacity from Cylinder to Both Plates Paralleled (See Figure 4-2 and Equations 4-12, 4-14, and 4-15.)

- B. The second assumption is essentially a restatement of a portion of A, now put in equation form. For $Q_s = 0$, the fibre takes on the potential which would obtain in its plane, were it not present. Thus we write

$$\text{for } Q_s = 0, \quad V_s = \frac{H + Y}{2H} V_p \quad (4-7)$$

$$= \frac{1 + \alpha}{2} V_p \quad (4-8)$$

where we have defined

$$\alpha = \frac{Y}{H} \quad (4-9)$$

- C. Finally we state

$$\text{for } V_p = 0 \quad Q_s = C_w V_s \quad (4-10)$$

This is not really an assumption, other than in assuming that C_w is a value which we can obtain. Because of the complexity in solving for C_w , that exercise is deferred for Paragraph 4.2.

Using, first, assumption C, with Equation 4-5 for Q_s

$$Q_s = (C_{fA} + C_{fB}) V_s \quad \text{for } V_p = 0 \quad (4-11)$$

$$\boxed{(C_{fA} + C_{fB}) = C_w} \quad (4-12)$$

Now, using assumption B, and Equations 4-5 and 4-12

$$0 = -C_{fB} V_p + (C_{fA} + C_{fB}) V_s \quad (4-13)$$

$$\boxed{C_{fB} = C_w \frac{1 + \alpha}{2}} \quad (4-14)$$

Finally, using assumption A, we combine Equations 4-5, 4-12 and 4-14 with $Q_s = 0$. Then, eliminating V_s and substituting V_p from Equation 4-6, we obtain

$$\boxed{C_{AB} + C_{fB} = \frac{\epsilon A}{2H} + C_w \left(\frac{1 + \alpha}{2} \right)^2} \quad (4-15)$$

Thus the entire charge picture can now be written, substituting Equations 4-12, 4-14, and 4-15 in 4-5, as

$$\begin{bmatrix} Q_p \\ Q_s \end{bmatrix} = \begin{bmatrix} \frac{\epsilon A}{2H} + C_w \frac{1+\alpha^2}{2} & -C_w \frac{1+\alpha}{2} \\ -C_w \frac{1+\alpha}{2} & C_w \end{bmatrix} \begin{bmatrix} V_p \\ V_s \end{bmatrix} \quad (4-16)$$

With reference to Figure 4-2, Equations 4-12, 4-14 and 4-15 may also be solved for C_{AB} , C_{fB} and C_{fA} . Thus all the individual capacities (excluding "strays") are known in terms of C_w and the geometry. They are shown in Figure 4-4.

The stored electrostatic energy in the system may now be written as the sum of the energy in the three capacitors of Figure 4-4, or, equivalently, from Equation 4-16 (using Equation 3, page 39, of Smythe, Reference 3),

$$U = \frac{1}{2} \left(\frac{\epsilon A}{2H} + \frac{(1+\alpha)^2}{4} C_w \right) V_p^2 + \frac{1}{2} C_w V_s^2 - C_w \frac{1+\alpha}{2} V_p V_s \quad (4-17)$$

This expression becomes very complex and unwieldy when differentiated to obtain the force. Manageable expressions were not obtained until the following substitution occurred to the writer: From assumption B, we know that charge on the string, Q_s , becomes zero when $V_s = \frac{1}{2} (1+\alpha) V_p$. Force on the string must therefore also be zero for this value of V_s -- hence it may be guessed that the expression for force might be simplified by writing the expressions in terms of the deviation of V_s from $\frac{1}{2} (1+\alpha) V_p$. Thus, we define this deviation,

$$v_s = V_s - \frac{1}{2} (1+\alpha) V_p = (V_f - V_A) - \frac{1}{2} (1+\alpha) (V_B - V_A) \quad (4-18)$$

Upon substituting this in Equation 4-17,

$$U = \frac{1}{2} \frac{\epsilon A}{2H} V_p^2 + \frac{1}{2} C_w v_s^2 \quad (4-19)$$

which proves considerably more manageable.

From Smythe (Reference 8, page 40), the electrostatic force tending to increase a displacement-variable, η_s , is

$$F = - \frac{\partial U(V)}{\partial \eta_s} \quad \left| \begin{array}{l} Q's \text{ constant} \end{array} \right. \quad (4-20)$$

$$= + \frac{\partial U(Q)}{\partial \eta_s} \quad \left| \begin{array}{l} V's \text{ constant} \end{array} \right. \quad (4-21)$$

where $U(Q)$ and $U(V)$ represent the stored electrostatic energy in terms of charge and voltage, respectively.* The electrostatic force in the +Y or + α direction is therefore, using Equation 4-21, 4-19, and 4-18

$$F = + \frac{\partial U}{\partial (\partial H)} \quad \left| \begin{array}{l} V \text{ constant} \end{array} \right.$$

$$F = \frac{1}{2H} \left[\frac{\partial C}{\partial \alpha} v_s^2 - C_w v_s V_p \right] \quad (4-22)$$

Regarding units, F and C_w are both total values, or both on a per unit length basis. The force solution is now complete except for obtaining expressions for C_w and $\partial C_w / \partial \alpha$.

4.2 WIRE - TO - PARALLEL - PLATE CAPACITY

Expressions for C_w and $\partial C_w / \partial \alpha$ are obtained below. In Figure 4-5, the pertinent dimension and the location of the lumped-parameter equivalent of C_w are shown. Figure 4-6 shows the cross-section of the central portion of an infinite set of line charges of values $+q$ and $-q$ (charge per unit length). Without going into the rather devious trial and error process which motivated the selection of this array, we can verify that they comprise a set of images which gives the desired set of surfaces of constant potential.

First: Surfaces A and B are both at zero potential, because, for any point on either surface the $+q$'s and $-q$'s are symmetrically arrayed. Thus, at any point, the component of potential caused by each $+q$ is exactly cancelled by a corresponding line charge of $-q$.

*The change of sign involves the fact that, for a given movement, $d\eta_s$, the energy in terms of voltage is not constant, but changes due to currents which flow from the source maintaining these voltages. While Equation 4-20 is rather "obvious," Equation 4-21 is not nearly so obvious.

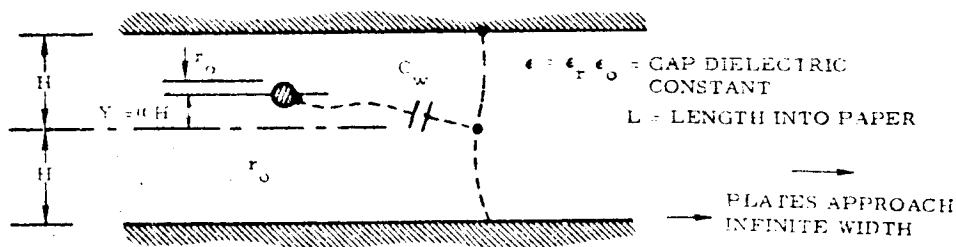


Figure 4-5. Illustration of C_w , a Function of H , a , r_o , L and ϵ

Second: With the assumption that $r_o \ll H$, it is valid to assume that at radius r_o there lies a small equipotential cylinder which is substantially circular and concentric with the central charge. For $r_o \ll H$ it may also be assumed that the distance from any element of this substantially-circular cylinder to all line charges (except the central one) is approximately equal to the center-to-center distances ($2H + 2Y$, etc., Figure 4-6).^{*} The use of center-to-center distances as an approximation allows for partial cancellation of errors on opposing sides of the cylinder. That the accuracy of the results under

^{*}That the small equipotential cylinder is not exactly circular can be seen from the fact that it is a member of a set of cylindrical (non-circular) equipotentials, the outermost of which are squeezed between the plates A and B on the sides, yet extend to infinity above and below. The innermost of the set become more and more circular as they approach the central line charge. Lack of exact concentricity (except for $Y = 0$, an important special case) can be seen by comparing the special case of one plate removed (H and $Y \rightarrow \infty$ as $H - Y = h = \text{constant}$), to the exact solution for that case, Reference 8, where such non-concentricity is observed.

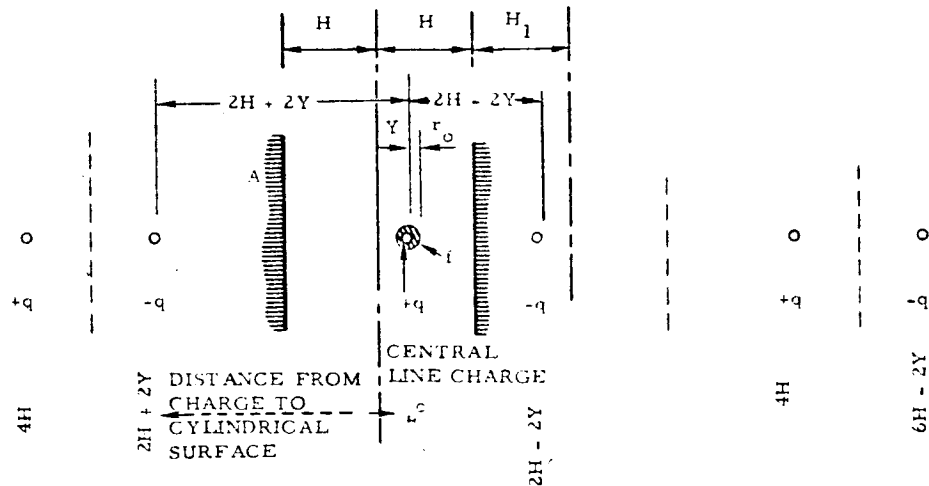


Figure 4-6. Central Portion of Infinite Set of Line Charges Used to Obtain Desired Boundary Conditions at A, B, and f

these assumptions is quite good, is indicated in Paragraph 4.3, where special cases are compared to known exact solutions. In particular, good correspondence is obtained with values of r_o/H as large as $1/3$ to $1/2$.

The field potential, V , a distance r from a line charge of value $+q$ (charge per unit length), is given in Smythe (see Reference 8, page 63) as

$$V = -\frac{q}{2\pi\epsilon} \ln r + C \quad (4-23)$$

Starting with some point on f, thus, the potential component, due to the central charge, is $-(q/2\pi\epsilon) \ln r_0 + C$. The potential due to the nearest charge on the right is $+(q/2\pi\epsilon) \ln (2H - 2Y) + C$; due to the nearest charge on the left, $+(q/2\pi\epsilon) \ln (2H + 2Y) + C$; due to the

next charge on the right - $(q/2\pi\epsilon) \ln 4H + C$; etc. Combining these components in groups of four, we obtain

$$V = \frac{q}{2\pi\epsilon} \left[\ln \frac{2H - 2Y}{r_o} \frac{2H + 2Y}{4H} + \ln \frac{6H - 2Y}{4H} \frac{6H + 2Y}{8H} + \ln \frac{10H - 2Y}{8H} \frac{10H + 2Y}{12H} + \dots \right] \quad (4-24)$$

The grouping used, which resulted in a solution in the most convenient form, is depicted in Figure 4-7.

Using $\alpha = Y/H$ (Equation 4-9), Equation 4-24, after some manipulation, becomes

$$V = \frac{q}{2\pi\epsilon} \left\{ \ln \frac{H}{r_o} (1 - \alpha^2) + \sum_{n=1}^{\infty} \ln \frac{(2n+1)^2}{(2n+1)^2 - 1} \left[1 - \frac{\alpha^2}{(2n+1)^2} \right] \right\} \quad (4-25)$$

$$= \frac{q}{2\pi\epsilon} \left\{ \ln \frac{H}{r_o} (1 - \alpha^2) + \sum_{n=1}^{\infty} \ln \left[1 + \frac{1 - \alpha^2}{4n(n+1)} \right] \right\} \quad (4-26)$$

Testing for convergence, the "ratio test" fails to indicate whether the series is convergent or divergent ($A_{n+1}/A_n \rightarrow 1$). Raabe's Test as given in Reference 7 shows convergence, as does the integral test.

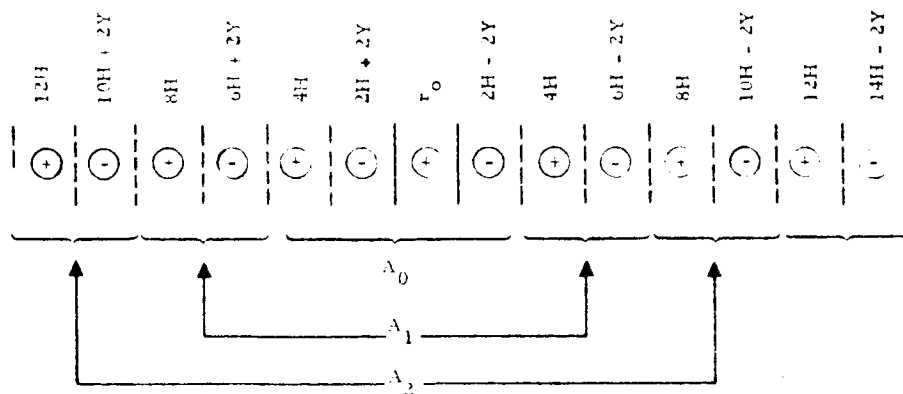


Figure 4-7. Grouping of Charges in the Individual Terms in Equations (4-26) and (4-24), and Distances to Central Charge. Subscripts of A Correspond to n's in Equation (4-25), etc.

Because the plates A and B (Figure 4-6) are at zero potential, the desired capacity from the wire to both plates is

$$C_w = \frac{Q}{V} = \frac{qL}{V} \quad (4-27)$$

$$C_w = \frac{2\pi\epsilon L}{\ln \left[\frac{H}{r_o} (1 - \alpha^2) \right] + \frac{1 - \alpha^2}{4} S} \quad (4-28)$$

where

$$S = \frac{4}{1 - \alpha^2} \sum_{n=1}^{\infty} \ln \left[1 + \frac{1 - \alpha^2}{4n(n+1)} \right] \quad (4-29)$$

The definition of S anticipates a simplified expression for S, which can be obtained by first expanding the log in a series. This permits the summation over n to be made once and for all, leaving only a series in α , the variable. Using the conventional expansion

$$S = \frac{4}{1 - \alpha^2} \sum_{n=1}^{\infty} \left\{ \frac{1 - \alpha^2}{4n(n+1)} - \frac{1}{2} \left[\frac{1 - \alpha^2}{4n(n+1)} \right]^2 + \frac{1}{3} \left[\frac{1 - \alpha^2}{4n(n+1)} \right]^3 + \dots \right\} \quad (4-30)$$

If we now regroup these, collecting powers of $(1 - \alpha^2)$,

$$\begin{aligned} S &= \sum_{n=1}^{\infty} \frac{1}{n(n+1)} - (1 - \alpha^2) \sum_{n=1}^{\infty} \frac{2}{[4n(n+1)]^2} \\ &\quad + (1 - \alpha^2)^2 \sum_{n=1}^{\infty} \frac{4}{3[4n(n+1)]^3} \\ &\quad + (1 - \alpha^2)^3 \sum_{n=1}^{\infty} \frac{1}{[4n(n+1)]^4} + \dots \end{aligned} \quad (4-31)$$

The summations over n can be put in closed form (see Reference 9, page 336); for example the first two summations in S are 1.0 (exactly) and $(\pi^2 - 9)/24$. At higher values of n , the closed form becomes more difficult to evaluate, and the series expression converges more rapidly, hence use of the closed form is not practical above the first or second term. The resultant expression for S is

$$S = 1 - .036233(1 - \alpha^2) + .002712(1 - \alpha^2)^2 - .000248(1 - \alpha^2)^3 + .000024(1 - \alpha^2)^4 + \dots \quad (4-32)$$

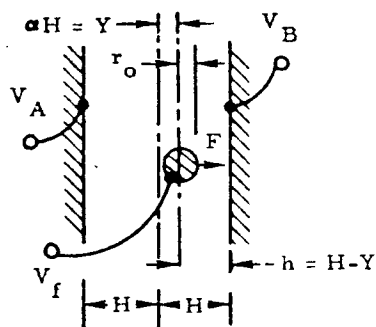
The derivative required for Equation 4-22 can be obtained, directly, in the form

$$\frac{\partial C_w}{\partial \alpha} = \frac{C_w}{2 \left[\ln \left\{ \frac{H}{r_o} (1 - \alpha^2) \right\} + \frac{1 - \alpha^2}{4} S \right]} \left[\frac{4}{1 - \alpha^2} + S^* \right] \quad (4-33)$$

where $S^* = -\frac{1}{2\alpha} \frac{d}{d\alpha} \left[(1 - \alpha^2) S \right]$ is given by

$$S^* = 1 - .072466(1 - \alpha^2) + .008136(1 - \alpha^2)^2 - .000992(1 - \alpha^2)^3 + .000120(1 - \alpha^2)^4 + \dots \quad (4-34)$$

The final result is contained in Equations 4-22, 4-28, 4-32, 4-33, and 4-34. Simplification is not possible after these equations are combined into one expression; hence, as an alternative, the results and definitions are summarized in Figure 4.8. The definitions for the infinite series S and S^* have been chosen so that they are approximately unity.



FIBRE LENGTH (INTO PAPER) = L

$$\alpha = Y/H \quad (4-9)$$

$$V_s = V_f - V_A \quad (4-2)$$

$$V_p = V_B - V_A$$

$$v_s = V_s - (1/2)(1 + \alpha) V_p \quad (4-18)$$

F = ELECTROSTATIC FORCE ON THE FIBRE
(OR CYLINDER) IN DIRECTION SHOWN.

$$F = \frac{1}{2H} \left[\frac{\partial C_w}{\partial \alpha} v_s^2 - C_w v_s V_p \right] \quad (4-22)$$

WHERE

$$C_w = \frac{2\pi\epsilon L}{\ln \left[\frac{H}{r_o} (1 - \alpha^2) \right] + \frac{1 - \alpha^2}{4} S} \quad (4-28)$$

$$\frac{\partial C_w}{\partial \alpha} = \frac{\alpha C_w}{2 \left[\ln \left[\frac{H}{r_o} (1 - \alpha^2) \right] + \frac{1 - \alpha^2}{4} S \right]} \left[\frac{4}{1 - \alpha^2} + S^* \right] \quad (4-33)$$

$$S = 1 - 0.03623 (1 - \alpha^2) + 0.00271 (1 - \alpha^2)^2 - 0.00025 (1 - \alpha^2)^3 + 0.00002 (1 - \alpha^2)^4 + \dots \quad (4-32)$$

$$S^* = 1 - 0.07247 (1 - \alpha^2) + 0.00814 (1 - \alpha^2)^2 - 0.00099 (1 - \alpha^2)^3 + 0.00012 (1 - \alpha^2)^4 + \dots \quad (4-34)$$

$$S(0) = 0.9662$$

$$S^*(0) = 0.9348$$

Figure 4-8. Summary--General Equation for Force. Equations 4-22, 4-28, 4-33, 4-32, 4-34 as well as 4-9, 4-2 and 4-18

4.3 SPECIAL CASE, ONE PLATE

An indication of the accuracy of the result can be obtained by comparing the single-plate special case with known exact solutions. To do this, let H and $Y \rightarrow \infty$ while holding constant the distance from plate B to the fibre,

$$h = H - Y \quad (4-35)$$

$$= H(1 - \alpha) \quad (4-36)$$

$$\alpha = 1 - \frac{h}{H} \quad (4-37)$$

Thus, with $V_A = 0$, as $H \rightarrow \infty$, $\alpha \rightarrow 1$, $1 - \alpha$ and $1 - \alpha^2 \rightarrow 0$, $S \rightarrow 1$, $S^* \rightarrow 1$, and

$$H(1 - \alpha^2) = 2h - \frac{h^2}{H} \quad (4-38)$$

$$\rightarrow 2h$$

Thus

$$C_w \Big|_{H \rightarrow \infty} \rightarrow \frac{2 \pi \epsilon L}{\ln \frac{2h}{r_o}} \begin{pmatrix} \text{one} \\ \text{plate} \end{pmatrix} \quad (4-39)$$

By comparison, the exact solution for one plate only is (Reference 8),

$$C_x = \frac{2 \pi \epsilon L}{\cosh^{-1} \left(\frac{h}{r_o} \right)} \quad (4-40)$$

$$= \frac{2 \pi \epsilon L}{\ln \left\{ \frac{h}{r_o} \left[1 + \sqrt{1 - \left(\frac{r_o}{h} \right)^2} \right] \right\}} \begin{pmatrix} \text{exact,} \\ \text{one} \\ \text{plate} \end{pmatrix} \quad (4-41)$$

The term in brackets, for $r_o \ll h$ is approximately 2, as in Equation 4-39. Even for h/r_o as small as 2, Equation 4-39 gives a value for C which is only 5% lower than the exact solution! This is surprisingly good, especially considering the fact that this is the worst case from the standpoint of cancellation of errors, as discussed before Equation 4-23. We obtain the force, as plate A moves to ∞ , by letting $H \rightarrow \infty$. Then,

$$\frac{C_w}{H} \rightarrow 0,$$

and

$$\frac{1}{H(1 - \alpha^2)} \rightarrow \frac{1}{2h}$$

$$F = \frac{1}{2H} \frac{\partial C_w}{\partial \alpha} v_s^2 \quad (4-42)$$

$$= \frac{\pi \epsilon L}{h \left(\ln \frac{2h}{r_o} \right)^2} (V_f - V_B)^2 \quad \left(\begin{array}{c} \text{one} \\ \text{plate} \end{array} \right) \quad (4-43)$$

compared to the exact value, obtained from Equation 4-40,

$$F_x = \frac{\pi \epsilon L}{h \left[1 - \left(\frac{r_o}{h} \right)^2 \right]^{1/2} \left[\cosh^{-1} \left(\frac{h}{r_o} \right) \right]^2} (V_f - V_B)^2 \quad (4-44)$$

(exact
one plate)

Here, for $h = 3r_o$ the approximation is 9 percent low (about 4-1/2 percent at $h = 4r_o$, and 22 percent at $h = 2r_o$). It is felt that the approximations made in the solution are shown up especially strongly in this highly unbalanced case, so that the errors under other circumstances may well be bounded by these values, in which case the solution, as summarized in Figure 4-8, is believed to be valid for H/r_o as low as 4, that is, the fibre diameter as large as 1/4 of the entire plate-to-plate gap (more or less depending on accuracy required).

4.4 PLOTS FOR $(H/r_0) = 10$

The capacity and force, for a fibre between two plates, are plotted vs α in Figures 4-9 and 4-10 for $H/r_0 = 10$ and (force curve only) for V_s from $+V_p$ to $-V_p$. The curves are more or less self-explanatory. The ordinate units are picofarads/inch and pounds/volt².

The two-plate capacity equation reaches about $2\mu\text{f/inch}$ at $\alpha = 0.9$. At this point the electrodes touch and the capacity actually approaches ∞ . For α between 0.7 and 0.9 the single-plate exact solution is a better approximation for the two-plate capacity. The correct value tends to follow the upper of the two curves with some smoothing around $\alpha = 0.7$, where they cross.

Expressing the force curves in terms of the difference voltages V_p and V_s reduces the parameters needed for the plot to one, V_s/V_p . The "exact force for no left plate" (A), by comparison to the $V_s = 0V_p$ curve, shows the effect of the presence or absence of plate A, when it is at fibre voltage. For $\alpha > 0.7$ these two curves cross, showing that the two-plate solution is beyond its range of accuracy. At these values of α (between about 0.7 and 0.9) the exact single-plate solution is the better approximation.

4.5 SPECIAL CASE, STRING CENTERED

4.5.1 Reduced Equation

A special case of interest is the force on the string when the string is centered, that is, when $\alpha = Y/H = 0$. Considerable simplification is possible in this case. To begin with, $\partial C_w / \partial \alpha$ becomes zero, as is expected from symmetry. The force then reduces to

$$F = -\frac{C_{w0}}{2H} v_s V_p \quad (4-45)$$

where

$$\begin{aligned} C_{w0} &= C_w \Big|_{\alpha=0} \\ &= \frac{2\pi\epsilon L}{\ln \frac{H}{r_0} + 0.24156} \end{aligned} \quad (4-46)$$

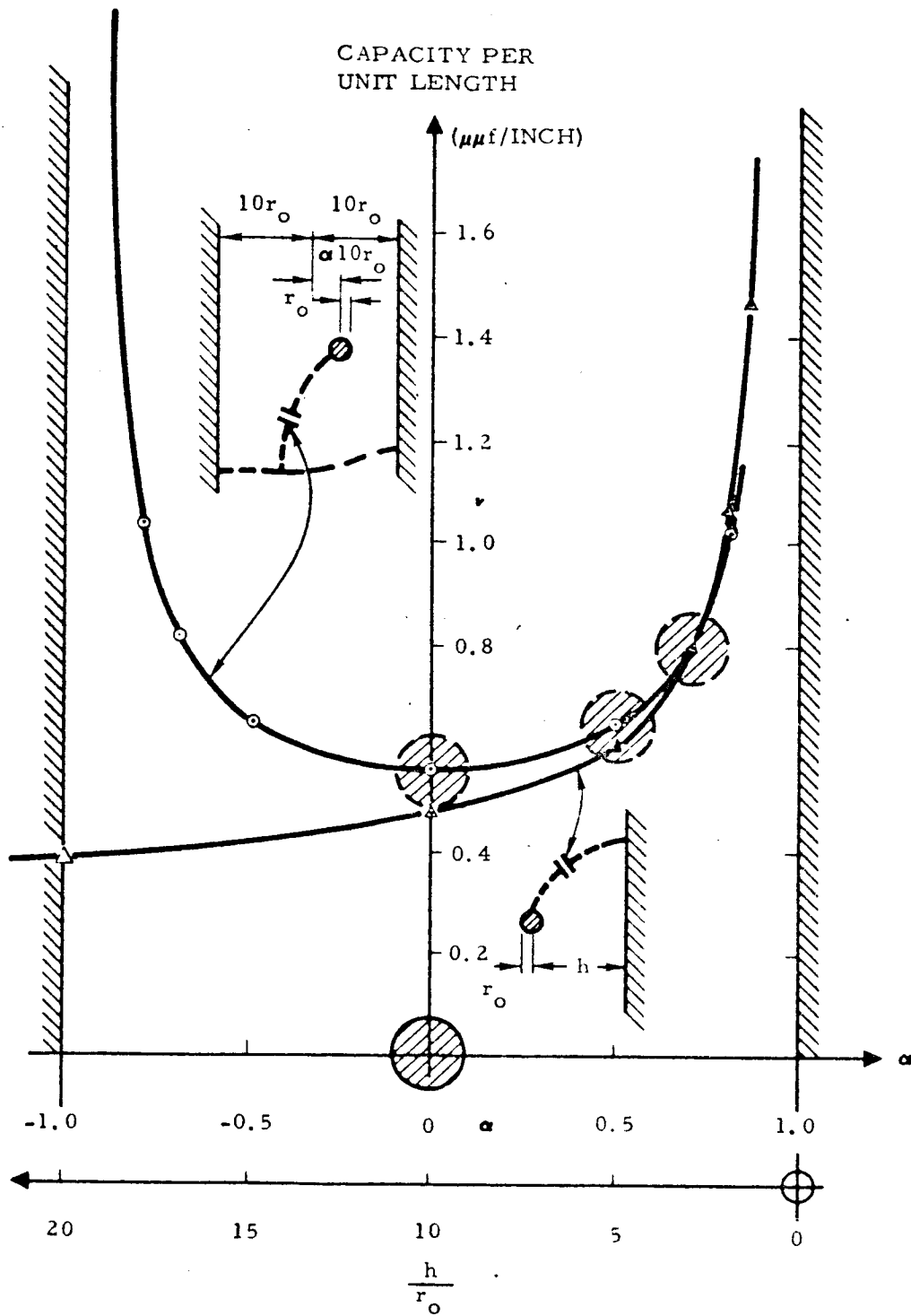


Figure 4-9. Capacity Between Cylinder and One or Two Plates, for Ratio $H/r_o = 10$

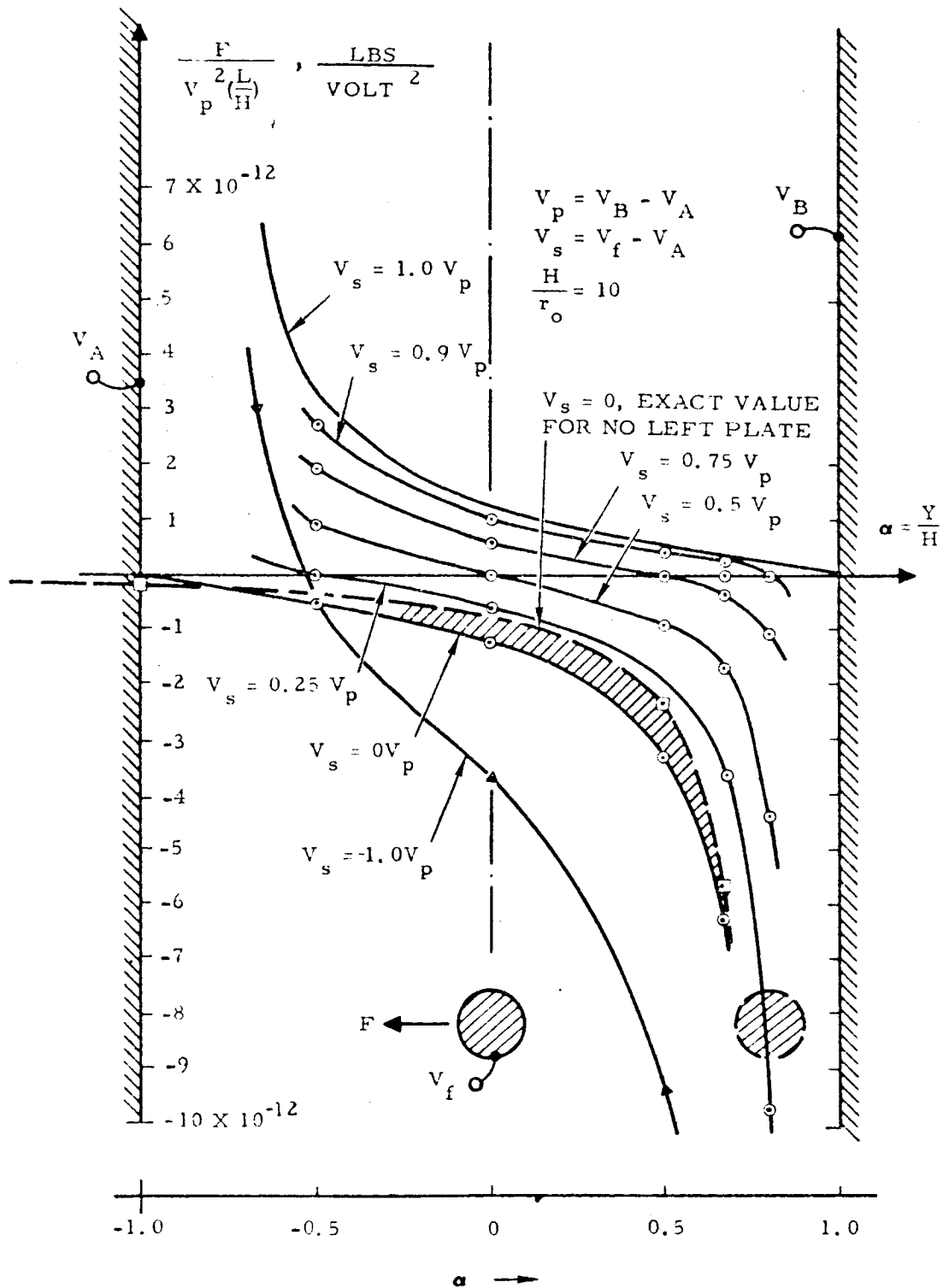


Figure 4-10. Force on Cylinder for $\frac{H}{r_o} = 10$, vs α at Various V_s/V_p

$$C_{wo} = \frac{2\pi\epsilon L}{\ln(1.273 H/r_o)} \quad (4-47)$$

A useful form may be obtained by substituting for v_s and V_p in Equation 4-45. With some manipulation, the following somewhat surprising result is obtained.

$$F = \frac{C_{wo}}{4H} \left[(V_f - V_B)^2 - (V_f - V_A)^2 \right] \quad (4-48)$$

This equation has the same form as the expression for the difference between the forces (Figure 4-11) to each plate individually, each in the absence of the other plate, that is K^* in Figure 4-12. From Equations 4-44 or 4-41, we may obtain the exact solutions for F_1 and F_2 (Figure 4-12),

$$F_1 = K^* (V_f - V_A)^2 L/H \quad (4-49)$$

$$F_2 = K^* (V_f - V_B)^2 L/H$$

where

$$K^* = \frac{\pi\epsilon}{\sqrt{1 - \left(\frac{r_o}{H}\right)^2} \left[\ln \left\{ \left(\frac{H}{r_o}\right) \left(1 + \sqrt{1 - \left(\frac{r_o}{H}\right)^2}\right) \right\} \right]^2} \quad (4-50)$$

The difference, $F_2 - F_1$, having the same form as F , can be plotted in Figure 4-12 to the same ordinate as F ,

$$\text{Force} / \left\{ \left[(V_f - V_B)^2 - (V_f - V_A)^2 \right] \frac{L}{H} \right\},$$

the symbols K^* and F^* being used for this ratio. Units are lbs/volt^2 .

$$F^* = \frac{C_{wo}}{4L} = \frac{\pi\epsilon}{2 \ln \frac{1.273H}{r_o}} \quad (4-51)$$

$$\frac{\pi\epsilon}{2} = 3.13 \times 10^{-12} \text{ lb/volt}^2$$

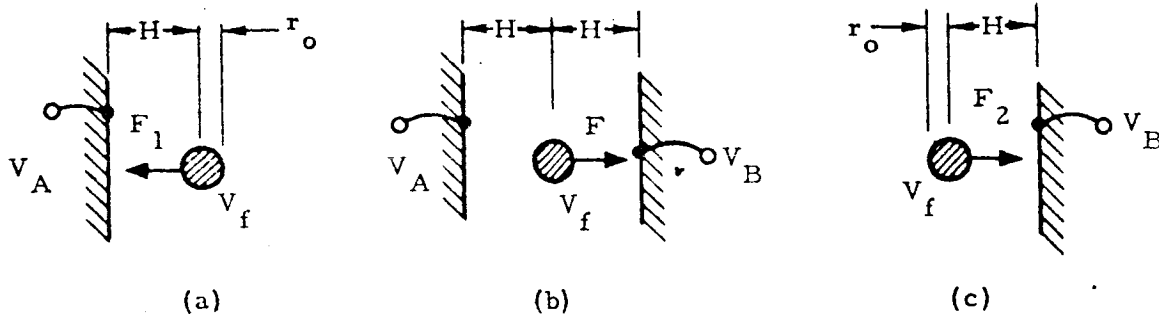


Figure 4-11. Force Between Fibre (or Cylinder) and Single Plates (a and c) and on Fibre With Two Plates

Figure 4-12 is useful in obtaining numerical values for F and F_2 . A comparison of F against $(F_2 - F_1)$, or equivalently F^* against K^* , shows the error which would be made if the force on a wire between two plates were approximated by the difference in the forces to each plate individually. For H/r_o from 5 to 10, the error is relatively small. For high values of H/r_o the difference increases and is more easily seen in the ratio plot, Figure 4-12,

$$\frac{F}{F_2 - F_1} = \frac{C_{wo}}{4HK} \quad (4-52)$$

The force on the fibre may be expressed as the field at the fibre times the charge on the fibre. As r_o/H decreases far below unity, the force on a fibre between two plates decreases mainly because of the reduced charge on the fibre, while the force between a fibre and a single plate decreases because of both the reduced charge and the reduced self-field of the fibre.

On the other hand, as the diameter of the fibre approaches that of the gap ($r_o \rightarrow H$), it seems clear that all significant effects between

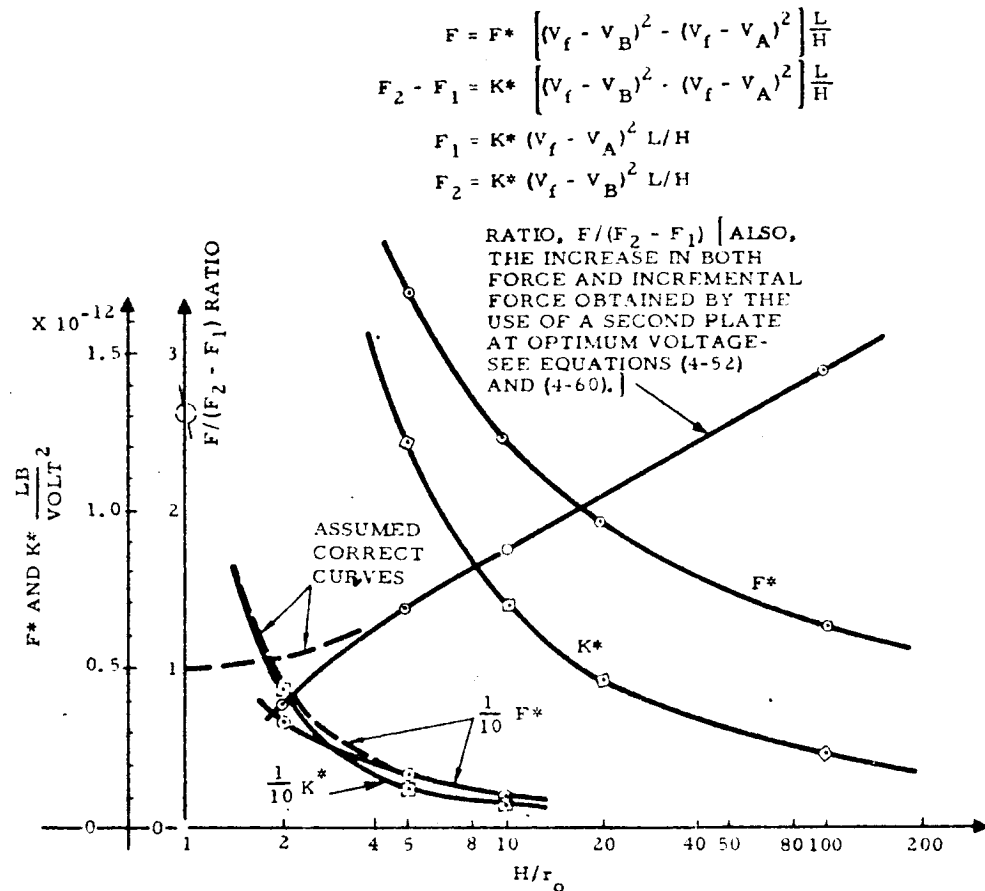


Figure 4-12. Forces in Figure 4-11, F , $(F_2 - F_1)$ and Their Ratio

the cylinder and the plates will be concentrated in the areas where they are nearly touching. As a result, interaction of the effects on the individual sides will approach zero as $r_0 \rightarrow H$, and we would therefore expect to have $F \rightarrow F_2 - F_1$. It is in this area of H/r_0 (below about 3 to 5) that the assumptions originally made in Paragraph 4.2, approximating distances to the image line charges, became invalid. The dashed lines, Figure 4-12, indicate approximately the correct curves for F and $F/(F_2 - F_1)$ at low values for H/r_0 .*

*These are lower values of H/r_0 than were of interest in the objective of this analysis.

4.5.2 Maximum Force

A practical question which might be asked is, "If the voltage of the cylinder and one plate are fixed, what is the voltage on the other plate which will give maximum force?" The form obtained in Equation 4-48 is useful here, because if V_f and V_B , for example, are fixed, it is clear enough that maximum force is obtained when $V_A = V_f$.

On the other hand, we may ask, "If the voltage on the two plates are fixed, what fibre voltage will give maximum force?" Here it is easier to use Equation 4-45. $V_p = V_B - V_A$ is fixed. Then $v_s = V_s - 1/2 V_p = V_f - 1/2 (V_A + V_B)$. Thus, force is zero when the fibre voltage equals the average of the plate voltages (no charge) and increases linearly above and below that point, giving no "optimum."

4.5.3 Increase of Force Due to Second Plate

Having established that, for given potentials on one plate and the fibre, maximum force is obtained with the other plate at fibre potential, we now ask, "How much is the force increased by using this extra plate at fibre potential, over having just the fibre and one plate?" Figure 4-12 gives this directly; for

$$V_A = V_f = 0 (F_1 = 0), \frac{F}{F_2 - F_1} = \frac{F}{F_2}$$

is the ratio of the force on the fibre when it is between a pair of plates with one plate at fibre potential (optimum), to the force between the fibre and a single plate. We see that for H/r_0 of 15 to 20 the force increase obtained by the second plate is a factor of x 2, while the increase is x 2.5 for H/r_0 between 40 and 50.

4.5.4 Maximum "Drive"—Minimum Pickup

In certain sinusoidal drive applications, the steady "d-c" force is not significant, but only the "a-c" component, at the desired drive frequency. In this case, a d-c voltage component, called the d-c "bias" voltage, is applied to the electrodes, while incremental voltage changes, called the a-c "drive" voltages, are added (usually through capacitative coupling). It may then be desirable to reduce stray

coupling of this drive voltage to other circuits; in this case, it is desirable to maximize dF for given voltage changes. Defining

$$V_a = V_A - V_f \quad (4-53)$$

$$V_b = V_B - V_f \quad (4-54)$$

the basic force equation with the string centered ($\alpha = 0$) becomes from Equation 4-48

$$F = \frac{C_{wo}}{4H} (V_b^2 - V_a^2) \quad (4-55)$$

Then

$$dF = \frac{\partial F}{\partial V_a} dV_a + \frac{\partial F}{\partial V_b} dV_b \quad (4-56)$$

$$dF = \frac{C_{wo}}{2H} [V_b dV_b - V_a dV_a] \quad (4-57)$$

There are two cases of particular interest. The first is when one plate only is driving, that is with, say, $dV_a = 0$. This may be required, for example if the other plate is being used as a pickoff (sensor). The second case is $dV_a = -dV_b$; here, with both plates driving, opposite polarity of the "a-c" driving voltage is chosen to reduce stray pickup-producing electrostatic fields.

One Plate Driving.

For $dV_a = 0$,

$$dF = \frac{C_{wo}}{2H} V_b dV_b \quad (4-58)$$

Thus, to maximize dF for a given drive voltage, dV_b , it is desirable to have the d-c bias, V_b , as large as practical. It is interesting that, although the "d-c" force, F , depends on both V_a and V_b , dF , in this case, is independent of V_a , the d-c bias on plate A. Thus,

for a given V_b and dV_b , the bias, V_a , may be chosen equal to V_b , so as to keep the bias force $F_b = 0$, while not affecting dF/dV_b .

Likewise, in this case ($dV_a = 0$), if the plate A were not present, from Equation 4-50

$$dF_2 = 2K V_b dV_b \quad (4-59)$$

and, using Equation 4-58

$$\frac{dF}{dF_2} = \frac{C_{wo}}{4HK} \quad (4-60)$$

which, referring to Equation 4-52 is the "Ratio" plot of Figure 4-12. Thus we have the seeming anomaly that while the fixed potential of plate A does not affect the value of incremental force, its presence does.

Both Plates Driving and $dV_a = -dV_b$. Opposing voltage changes are selected to minimize electrical "stray" pickup and also because this permits the two force components in Equation 4-57 to add directly. This gives

$$dF \Big|_{dV_a = -dV_b} = \frac{C_{wo}}{2H} (V_b + V_a) dV_b \quad (4-61)$$

In this case, dF is maximized, for a given $dV_b = -dV_a$, by maximizing the sum $(V_b + V_a)$, in which case we would likely choose $V_a = V_b$ and pick as large a d-c value as practical.

5. GENERAL N^{TH} MODE STRING EQUATIONS

A parametrically-driven vibrating string, operating in the n^{th} mode, as in Figure 5-1, has characteristics which can be deduced, directly, by applying, to one (or each) loop of the multi-mode operation, the single-mode results as given in Reference 1.

To accomplish this, the symbols l , X_0 , X_d , ξ , ω_0 , u , τ , and η_1 , used in Reference 1, are first replaced with the same symbols primed, l' , X_0' , X_d' , ξ' , ω_0' , u' , τ' and η_1' in the equations in Reference 1. The primes indicate that the symbols apply to one loop of the string, Figure 5-1, and thus differentiate these symbols from the unprimed symbols which are used here to apply to the entire string. (For first-mode operation, this one loop is, of course, identical to the entire string.) This set of equations, for equilibrium, self-start, etc, with the primes added, thus applies to any one loop of the entire string. To obtain the expressions for multiloop operation, it is thus necessary only to relate these loop parameters to the entire-string parameters, and, using these relations, eliminate the loop parameters from the equations.

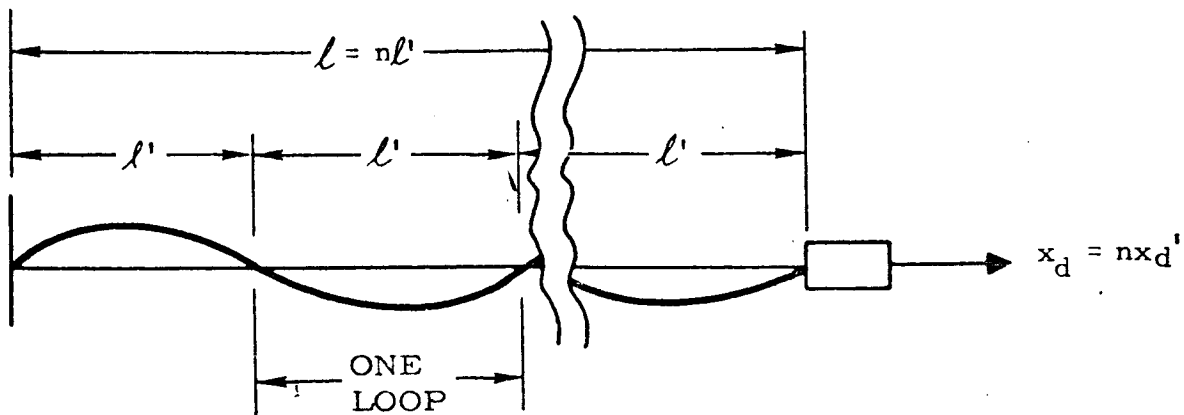


Figure 5-1. Vibrating String, n^{th} Mode

To begin, the length of one loop, ℓ' , is related to the length of the entire string by

$$\ell = n\ell' \quad (5-1)$$

and the initial elongation and the end drive amplitude must be the sum of the initial elongation and drive amplitude for all loops,

$$X_o = nX_o' \quad (5-2)$$

$$X_d = nX_d' \quad (5-3)$$

Here we assume that the added axial motion of loops near the drive does not significantly affect string operation, just as axial motion was neglected in the basic derivation, on the basis that longitudinal natural frequency is much greater than lateral natural frequencies. Numerous values remain the same, including

$$Y_1 = \text{maximum lateral deflection at string antinode} \quad (5-4)$$

$$\omega = \text{driven string frequency, or half the end-drive frequency} \quad (5-5)$$

$$\rho = \text{string mass density} \quad (5-6)$$

$$E = \text{Young's modulus of string material} \quad (5-7)$$

$$\begin{aligned} \xi &= \frac{X_d}{2X_o} \\ &= \frac{nX_d'}{2nX_o'} \\ &= \xi' \text{ dimensionless string drive} \end{aligned} \quad (5-8)$$

The frequency, ω_o , will now represent the lowest natural frequency of the entire length, ℓ_n , and is thus given by

$$\omega_o = \frac{\pi}{\ell} \left(\frac{X_o E}{\rho \ell} \right)^{\frac{1}{2}}$$

$$\begin{aligned}
 &= \frac{\pi}{n\ell'} \left(\frac{X_o' E}{\rho \ell'} \right)^{\frac{1}{2}} \\
 &= \frac{\omega_o'}{n}
 \end{aligned} \tag{5-9}$$

That is, the frequency of the lowest mode is $\frac{1}{n}$ times the frequency of any of n loops. Then the dimensionless frequency parameter becomes

$$\begin{aligned}
 u &= \frac{\omega}{\omega_o} = \frac{f}{f_o} \\
 &= nu'
 \end{aligned} \tag{5-10}$$

The string-amplitude nondimensionalizing factor, Υ' , will now become a parameter in terms of the entire string of length, ℓ , and the entire string elongation, X_o . We choose the definition

$$\begin{aligned}
 \Upsilon &= \frac{4\ell^2 \omega_o}{\pi^2} \left(\frac{\rho}{3E} \right)^{\frac{1}{2}} \\
 &= \frac{4}{\pi} \left(\frac{X_o \ell}{3} \right)^{\frac{1}{2}} \\
 &= n\Upsilon'
 \end{aligned} \tag{5-11}$$

This choice is desirable because, then, for first-mode operation ($n = 1$), Υ reduces to the previous definition. The dimensionless amplitude now becomes

$$\begin{aligned}
 \eta_1 &= \frac{Y}{\Upsilon} \\
 &= \frac{\eta_1'}{n}
 \end{aligned} \tag{5-12}$$

Using these changes, the various conditions given in Reference 1 can now be converted to the conditions for n^{th} mode operation in terms of entire-string parameters.

The equilibrium condition

$$\eta_1'^2 = \xi' + u'^2 - 1 \quad (5-13)$$

becomes

$$n^2 \eta_1'^2 = \xi + \frac{u^2}{n^2} - 1 \quad (5-14)$$

In terms of the drive amplitude and frequency, the conditions for self-start,

$$\begin{cases} \xi' > 1 - u'^2 & \text{for } u'^2 < 1 \\ \xi' > u'^2 - 1 & \text{for } u'^2 > 1 \end{cases} \quad (5-15)$$

become

$$\begin{cases} \xi > 1 - \frac{u^2}{n^2} & \text{for } u^2 < n^2 \\ \xi > \frac{u^2}{n^2} - 1 & \text{for } u^2 > n^2 \end{cases} \quad (5-16)$$

The "critical" condition (for no anisoelastic bias, no third harmonic, for constant tension and for linear operation), from Reference 1,

$$\begin{cases} \eta_1'^2 = \frac{3}{2} (u'^2 - 1) \\ \text{or } \xi' = \frac{1}{2} (u'^2 - 1) \\ \text{or } \eta_1'^2 = 3\xi' \end{cases} \quad (5-17)$$

becomes

$$\left\{ \begin{array}{l} n^2 \eta_1^2 = \frac{3}{2} \left(\frac{u^2}{n} - 1 \right) \\ \text{or } \xi = \frac{1}{2} \left(\frac{u^2}{n} - 1 \right) \\ \text{or } n^2 \eta_1^2 = 3\xi \end{array} \right. \quad (5-18)$$

The condition for no "drop-out" (i.e., oscillations continue if already started),

$$\left\{ \begin{array}{l} \eta_1'^2 > 0 \quad \text{for } u'^2 < 1 \\ \xi' > 0 \quad \text{for } u'^2 > 0 \end{array} \right. \quad (5-19)$$

becomes simply

$$\left\{ \begin{array}{l} \eta_1^2 > 0 \quad \text{for } u^2 < n \\ \xi > 0 \quad \text{for } u^2 > n \end{array} \right. \quad (5-20)$$

These values are now plotted in Figure 5-2 along with the pertinent equations and definitions of terms.

To consider which mode of vibration the string will break into, when sufficient drive level for self-start is attained, we note, in Figure 5-2 (plots and equations) that, for example, if $u^2 = 1.1$, the first mode will start at a drive amplitude of $\xi > 0.1$, while it would have taken a drive of $\xi > 0.725$ to start the second mode. On the other hand, at $u^2 = 2$, the first mode will not start until $\xi > 2$, while the second mode will start for $\xi > 0.5$. There is thus a frequency

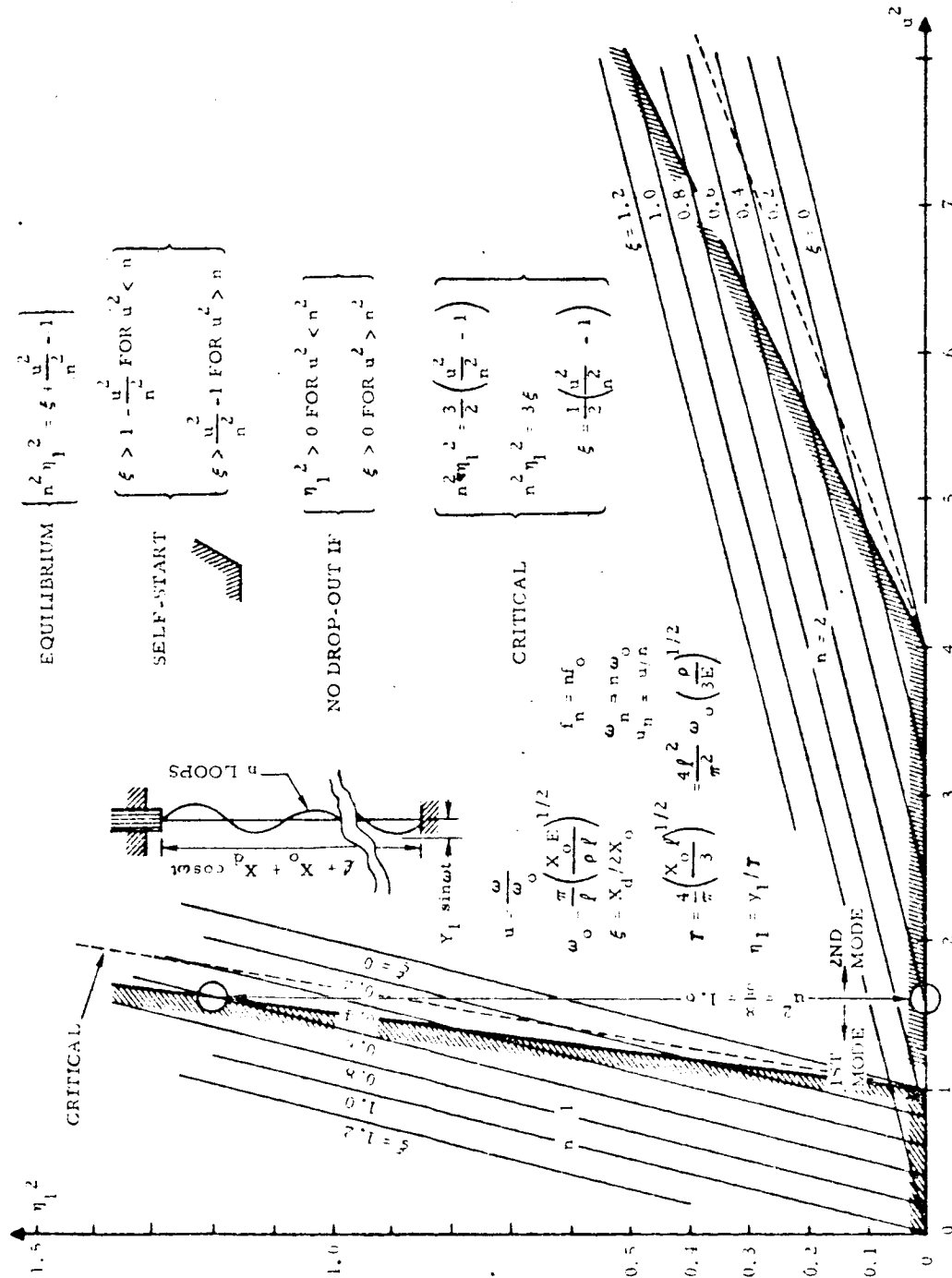


Figure 5-2. Parametrically-Driven Vibrating-String Characteristics for the n^{th} Mode

above which the string will first break into oscillation at the next higher mode, and below which, oscillation will commence in the next lower mode.

For the general case, between the n^{th} and the $(n + 1)^{\text{st}}$ mode, that is for $n^2 < u^2 < (n + 1)^2$, we can use Equation 5-16 and state that the $(n + 1)^{\text{st}}$ mode will start before the n^{th} mode if

$$\xi > 1 - \frac{u^2}{(n + 1)^2} \quad (5-21)$$

before

$$\xi > \frac{u^2}{n^2} - 1 \quad (5-22)$$

that is, if

$$1 - \frac{u^2}{(n + 1)^2} < \frac{u^2}{n^2} - 1 \quad (5-23)$$

$$u^2 > \frac{2}{\frac{1}{n^2} + \frac{1}{(n + 1)^2}} \quad (5-24)$$

For $n = 1$, the dividing frequency ratio between the first and second mode starting is found to be $u^2 = 8/5$. This value of u^2 is indicated in the plot, Figure 5-2. At this frequency ratio, first and second mode both require $\xi \geq 0.6$, to obtain self-start. (We note, however, that near $u^2 = 8/5$, the amplitude of the first mode, immediately after self-start is $\eta_1^2 = 1.2$, a large value, while the second mode starts at η_1^2 essentially zero. Therefore, in practice, it is expected that it would be necessary to have u^2 appreciably

greater than $8/5$ before the second mode would be clearly seen to be starting first. This is to say that it is not expected that the transition, between first and second mode at $u^2 = 8/5$, will be very sharp. Interaction between two modes existing simultaneously, and the effect of vibration in one mode on the possibility of another mode starting, have not been studied.)

In practice, dealing with a particular instrument, operating in the mode for which it was designed, one tends to think only in terms of the frequency of that mode. Hence it is convenient to define that frequency as f_n , as is done in Section 6, from Equations 6-16 to 6-20. As discussed there, we then use $u_n = u/n$, in more convenient association with experimental results.

Equation 5-2 is self-contained, with n^{th} -mode equations and term definitions, as well as first and second mode plots, so is generally more convenient for reference than the individual equations in the above development.

6. DETERMINATION OF DETAILED MODEL FOR STAR GYRO TORQUING

6.1 INTRODUCTION

In this section, the results of the previous three sections are applied in order to obtain the overall torquing response. The major result is expressed in Equation 6-15, with supplementary expressions, Equations 6-4, 6-21, and term definitions following Equation 6-21.

In obtaining this, additional analysis is done, including the effect of non-ideal plate geometry, and the effect of platform servo error. In addition a calculation of the theoretical value for string-amplitude pickoff sensitivity is made, using the results of Section 4.

Finally, the torquing sensitivity expression is expanded by partial differentiation to obtain a set of individual error terms. After presenting a partially specialized form of this equation, the terms of this set which are directly temperature sensitive are combined into a temperature-sensitive term. A typical error budget is presented and the nature of the errors is discussed.

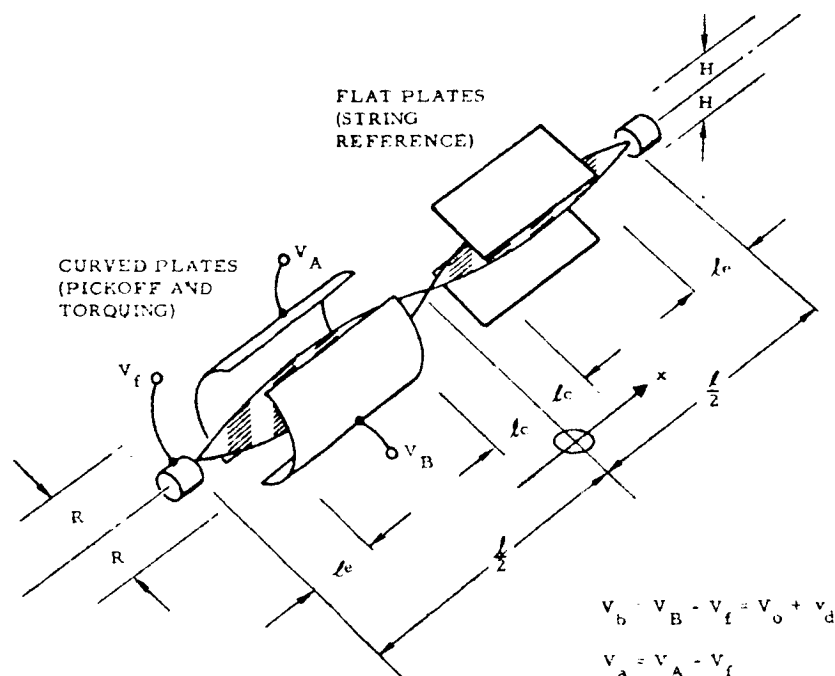


Figure 6-1. Electrostatic Plate Geometry. String is Vibrating In Second Mode in a Vertical Plane.

6.2 DEVELOPMENT

6.2.1 Combined Torquing Expressions

The fundamental torquing equation, from Section 3, is

$$\Delta\phi = K \left[\cos \theta_r - \frac{\theta_d}{k\pi} \cos \theta_r + \frac{1}{2k\pi} (\sin 2\theta_d) \cos(\theta_r + 2\theta_{sa}) \right] \quad (3-31)$$

repeated

where

$$K = \frac{2k\pi F_o S_n}{\rho a \omega^2 l_Y} \quad (3-32)$$

repeated

$$S_n = \int_{-l/2}^{l/2} S(x) \sin \frac{n\pi}{l} \left(x + \frac{l}{2}\right) dx \quad (3-14)$$

repeated

$S(x)$ is the space distribution function in the expression for force per unit length, $F_o S(x) T(t_I)$, Equation 3-8. ($S(x)$ and the time distribution function $T(t_I)$ are both unity at their maximum values.) Referring to Figure 6.1,

$$S(x) = \begin{cases} 1, & -\frac{l}{2} + l_e < x < -l_c \\ 0, & \text{elsewhere} \end{cases} \quad (6-1)$$

We are currently interested in the case of the string operating in the second mode ($n=2$). In this case, integration gives

$$S_2 = \frac{l}{\pi} \left[\frac{1}{2} \cos \frac{2\pi l_c}{l} + \frac{1}{2} \cos \frac{2\pi l_e}{l} \right] \quad (6-2)$$

To express the force in terms of instrument geometry and applied voltages, we use Equations 4-48 and 4-47, combined, for the force on a string centered between infinite parallel plates, Figure 4-11(b),

$$F = F^* \frac{L}{H} \left[V_b^2 - V_a^2 \right] \quad (6-3)$$

where

$$V_b = V_B - V_f$$

$$V_a = V_A - V_f$$

$$F^* = \frac{\pi \epsilon}{2 \ln(1.273 \frac{H}{r_o})} \quad (6-4)$$

F^* is a quantity which may be obtained from the plots in Figure 4-12.

Because normal string vibration is parallel to the plates, the use of the equations for the string centered is correct. The effect of the plates being curved and finite (Figure 6-1), rather than flat and infinite will be treated below (Paragraph 6.2.2). For the moment we may think of $H \approx R$.

In Paragraph 3.3.4, the conditions for obtaining maximum "drive" (the change in force resulting from voltage change), while preserving minimum stray "pickup" between torquing and low-level circuits, are considered. As discovered there, the preferred arrangement is to have the same "a-c" drive voltage, v_d , added and subtracted from identical bias voltages, V_o , on the two plates. Thus

$$\left. \begin{aligned} V_b &= V_o + v_d \\ V_a &= V_o - v_d \end{aligned} \right\} \begin{array}{l} \text{Balanced} \\ \text{drive} \end{array} \quad (6-5)$$

which can be conveniently mechanized with the string grounded ($V_f=0$; in current instruments the string is internally grounded). However, in tests currently being conducted, only two pairs of plates are available and it is necessary to use one plate of the pair parallel to the string plane for the string-angle pickoff. For this reason, only one plate parallel to the string plane is available for torquing. The voltages on these plates is therefore

$$\left. \begin{aligned} V_b &= V_{Bo} + v_d \\ V_a &= V_{Ao} \end{aligned} \right\} \begin{array}{l} \text{One-plate} \\ \text{drive} \end{array} \quad (6-6)$$

Substituting this in Equation 6-3, letting $V_{Bo} = V_o$, and, dropping the "d-c" terms, which have been shown previously to have no effect on torquing, we obtain "driving" force as

$$\Delta F = F^* \frac{L}{H} \left[2V_o v_d + v_d^2 \right] \quad (6-7)$$

(Had we used the driving voltages in Equation 6-5 rather than those of Equation 6-6, the drive would have simply been doubled, so there is no important loss in generality.)

This driving force, divided by the length, L , and multiplied by the space distribution function, $S(x)$, is the net force per unit length of Equation 3-8,

$$\frac{\Delta F}{L} S(x) = F_o S(x) T(t_I) \quad (6-8)$$

This gives an expression for the forcing time function in terms of the applied voltages and geometry

$$F_o T(t_I) = \frac{\Delta F}{L} \quad (6-9)$$

or

$$F_o T(t_I) = \frac{F^*}{H} \left[2V_o v_d + v_d^2 \right] \quad (6-10)$$

If the drive voltage is now given a sinusoidal form as in Figure 3-4, then Equation 3-14 may be integrated to obtain the response. Upon doing this, it is discovered that the v_d^2 term leads only to harmonics, which have no known effect on torquing. Hence, to shorten the derivation here, it is most convenient to neglect this term which produces only harmonics. This enables us to utilize the solution already obtained in Equations 3-31 and 3-32, repeated above. The drive voltage is now given the same time functions as the force, $T(t_I)$, depicted in Figure 3-4.

$$v_d = V_T T(t_I) \quad (6-11)$$

$$v_d = V_T \begin{cases} \cos(\omega t_I - \theta_r), \\ -\frac{\pi}{2} + \theta_r + \theta_{sa} + \theta_d < n\omega t_I < 2k\pi - \frac{\pi}{2} + \theta_r + \theta_{sa} - \theta_d \\ 0, \\ \text{elsewhere} \end{cases} \quad (6-12)$$

Then, combining Equations 6-10 and 6-11, neglecting the harmonic-producing v_d^2 term, as just stated,

$$F_o = \frac{2F^* V_o v_d}{H T(t_I)} \quad (6-13)$$

$$F_o = \frac{2F^* V_o V_T}{H} \quad (6-14)$$

Combining Equations 3-31, 3-32, 6-2, and 6-14, we have

$$\Delta \theta = \frac{kF^* V_o V_T \left[\frac{1}{2} \cos \frac{2\pi \ell_c}{\ell} + \frac{1}{2} \cos \frac{2\pi \ell_e}{\ell} \right]}{\pi^2 \rho a f^2 H Y_1} \left[\cos \theta_r - \frac{\theta_d}{\pi} \cos \theta_r + \frac{1}{2k\pi} \sin 2\theta_r \cos (\theta_r + 2\theta_{sa}) \right] \times \left[1 - \frac{D}{G_o \tau_*} \right] K_p \quad \text{for string in second mode } (n=2) \quad (6-15)$$

The factor K_p is an added term, used to account for the difference between the finite-width flat or curved plates actually used, and the infinite flat plates assumed in the solution (see Paragraph 6.2.2). The factor involving $D/G_o \tau_*$ comes from Equation 6-31 developed in Paragraph 6.2.3. It represents the effect of the gyro "error" signal which is required by the platform servo. This gyro torquing error is inversely proportional to the platform servo gain G_o , and is proportional to the damping D , on the platform, and to $1/\tau_*$, an inherent STAR gyro characteristic, discussed in detail in Reference 1.

The factor F^* , a function of H/r_o , may be obtained directly from the plot, Figure 4-12, or from Equation 6-4.

The torquing scale factor expression, in the form of Equation 6-15 is especially useful when the torquing-voltage amplitude, V_T , is being slaved to the measured string amplitude, because the relation between V_T and Y_1 is then obtained directly from this control system.

To obtain, theoretically, the absolute value of the torquing scale factor, it is desirable not to use the theoretical sensitivity of the capacity pickoff to measure Y_1 , directly, because a large proportion of any theoretical errors which would make Y_1 appear, say, large, would carry over to the capacity torquing theory and cause the sensitivity F^* also to appear large. Such errors thus would not be revealed in $\Delta \phi$, Equation 6-15, because these two effects would cancel. To measure Y_1 therefore, we prefer to use the basic string theory, as modified here in Section 5 for n^{th} mode operation. Using Equations 5-12, 5-11 and 5-18,

$$Y_1 = \eta_1 \Gamma$$

$$= \frac{2\sqrt{2}}{\pi^2} \frac{\omega_o l^2}{n} \left(\frac{\rho}{E} \right)^{1/2} \left(\frac{u^2}{n^2} - 1 \right)^{1/2} \quad (6-16)$$

The natural frequency, ω_o , here is the first-mode natural, and u is drive-frequency-to-first-mode-natural-frequency ratio. When dealing with higher-mode operation, it is more convenient to talk in terms of the natural frequency of that mode, which is the quantity normally measured experimentally. The n^{th} mode low-amplitude natural frequency is

$$\frac{\omega_n}{2\pi} = f_n = n f_o$$

$$= \frac{n\omega_o}{2\pi} \quad (6-17)$$

and the frequency ratio, in terms of f_{on} or ω_{on} , is

$$u_n = \frac{f}{f_n} = \frac{\omega}{\omega_n} \quad (6-18)$$

$$u_n = \frac{f}{nf_o} \quad (6-19)$$

$$u_n = \frac{u}{n} \quad (6-20)$$

This frequency ratio, u_n , is a number near unity and corresponds to the ratio which is familiar in experimental parlance. Equation 6-16 can then take on the more convenient form

$$Y_1 = \frac{4\sqrt{2}}{\pi} \frac{f_n \ell^2}{n^2} \left(\frac{\rho}{E} \right)^{1/2} \left(u_n^2 - 1 \right)^{1/2} \quad (6-21)$$

Equations 6-15, 6-2, and 6-21, thus give the total scale factor in rather convenient form. Term definitions are now repeated for convenience. Units are of any consistent set.

$\Delta\theta$ = "torqued" or precessed angle (radians) per pulse (sine-wave pulse, electrostatic on one plate) - second mode

k = number of full sine waves per pulse (1 in current experiment)

K_p = plate geometry factor -- see Paragraph 6.2.2

ϵ = dielectric constant = 0.0885 pf/cm = 1.99×10^{-12} lbf/volt²

H = the half-gap between electrostatic plates

r_o = fibre radius

V_o = torquing bias voltage

V_T = voltage amplitude (peak) of torquing sine pulse

ρ = mass density of string material

a = string cross section area = πr_o^2

f = frequency at which string is vibrating (second mode)

Y_1 = string amplitude of vibration (peak at anti-node).

l = total length of string.

l_e, l_c = electrostatic-plate dimensions (see Figure 6-1)

$\theta_r, \theta_d, \theta_{sa}$ = torquing pulse phase errors (Figure 3-4)

f_{on} = nf_o = low-amplitude natural frequency in n^{th} mode

n = mode number = 2

E = Young's modulus of fibre material

u_n^2 = "u-squared ratio" = $\left(\frac{\omega}{\omega_{on}}\right)^2$ = ratio of driven frequency to low-amplitude natural frequency squared

r_* = STAR gyro time constant expressing the anisoelastic drift effect.

G_o/D = platform servo "velocity-error coefficient"

The three foregoing boxed equations are convenient for obtaining such information as the absolute value of the torquing scale factor, and changes when the electronics are built to maintain V_T proportional to Y_1 . For direct temperature effects, for example, it is convenient to combine these, along with an expression for f_n from Equations 6-19, and 5-9

$$f_n = nf_o^{1/2} = \frac{\pi n}{l} \left(\frac{X_o E}{\rho l} \right)^{1/2} \quad (6-22)$$

and f , the vibrating frequency, which is controlled by the resonant drive, having the frequency

$$f = a \left(\frac{E_d h_d^2}{(1 - \nu_d^2) \rho_d L_d^4} \right)^{1/2} \quad (6-23)$$

where

α = dimensionless constant depending on the shape of the resonator

E_d = Young's modulus of drive resonator

h_d = thickness of drive resonator

ν_d = Poisson's ratio of drive resonator

ρ_d = drive resonator mass density

L_d = drive resonator characteristic length (diameter of a disk)

6.2.2 Effect of Plate Width and Curvature

The electrostatic torquing solutions presented up to here have been for flat, infinite plates. This is a good approximation for the plates actually used. However, the results can be refined a bit by the method of free-hand graphing of Laplace's equation.

First, we note that the force, although obtained above by differentiation of the energy expressions (Equation 4-21), can also be expressed as the charge on the fibre, multiplied by the electrostatic field at the fibre. For the string centered ($u=0$), the force (Equation 4-48), may be written as

$$F = C_{wo} \left[V_f - \frac{V_A + V_B}{2} \right] \frac{V_A - V_B}{2H} \quad (6-24)$$

From Equations 4-16 and 4-2 we see that the charge on the string is (for $u=0$)

$$Q_f \equiv Q_s = -\frac{1}{2} C_w V_p + C_w V_s \quad (6-25)$$

$$= C_{wo} \left[V_f - \frac{V_A + V_B}{2} \right] \quad (6-26)$$

and $(V_A - V_B)/2H$ is clearly the gradient due to the plates at the fibre. Thus the force on the string is given by charge times gradient, the familiar expression for force on a particle with a small charge. The somewhat surprising point here is that the expression is not restricted to small charges as it is in the general case (for example, even for the parallel wire and two plates, considered here, if the wire is not centered, the force is no longer proportional to charge times field, except at small charge). We note that the linearity of force vs voltage is a concomitant of force being proportional to charge times field.

To make these free-hand sketches to conform approximately to Laplace's field equation, it is necessary to make and modify the sketches until all areas enclosed by the flux and potential lines are approximately square, and boundary conditions are satisfied. In Figure 6-2(a), this has been done for a pair of finite flat plates of the proportions used in the tests made here. It is estimated from this plot that the field at the center is about 0.9 of the average uniform field for infinite flat plates. *

Figure 6-2(c) shows this field for curved plates, as used. Here it is estimated that the field at the center is $(6.3/5)$ or $1.26 \times$ the average uniform field over that diameter.

Capacity, wire to plate, may be obtained as follows.

$$C = \epsilon \frac{\text{area}}{\text{gap}} \quad (6-27)$$

$$= \epsilon L \frac{(\text{number of gaps between flux lines})}{(\text{number of gaps between potential lines})} \quad (6-28)$$

However, the difference here is too small to be indicated by these plots. In this case, for example, Figure 6-2(b) gives a higher value for C by 10 percent than Equation 4-47 for $H/r_0 = 8$, indicating that they are the same within the accuracy of the plot. For smaller radii, the shape of the outer electrode has even less effect. For $R/r_0 = H/r_0 = 100$, for example, the exact solution for the capacity of two concentric cylinders, $2\pi\epsilon L/\ln(R/r_0)$, gives a value only 5 percent higher than Equation 4-47 for infinite parallel plates, with the half-gap H equal to the outer radius R . (As $R/r_0 = H/r_0 \rightarrow \infty$, the ratio of the two capacities $\rightarrow 1.0$.) It is reasonable to consider that the gap in the cylinder (Figure 6-2(c)) offsets this 5 percent and to call the two capacities the same.

*Reproductions deviate slightly from original sketch, making scaling more difficult.

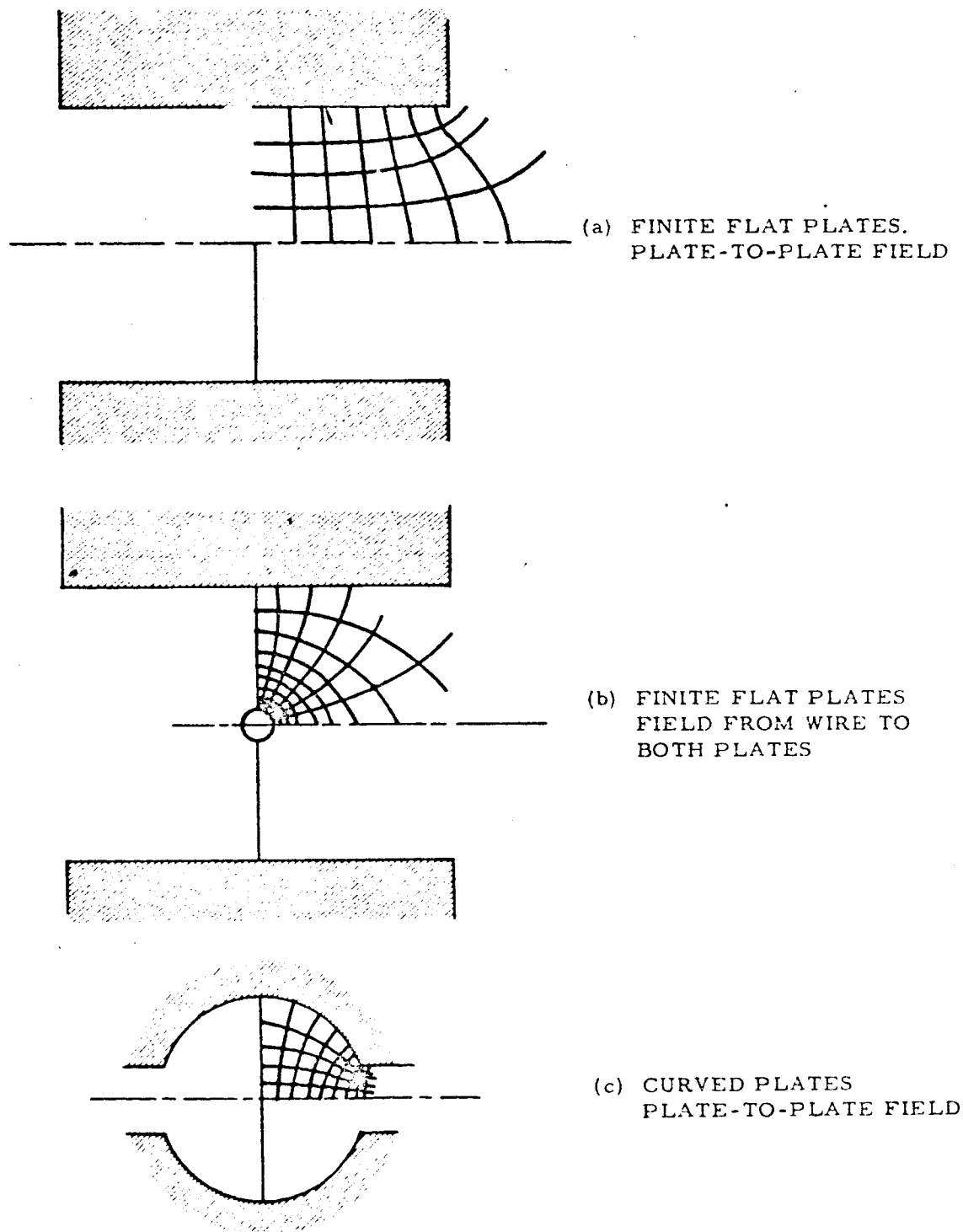


Figure 6-2. Free-Hand Plots of Fields.
(Field Shown in First Quadrants Only)

Thus we can approximate that the curved plates will have forces and torquing rates larger than those given by the equations for infinite parallel plates by a factor of

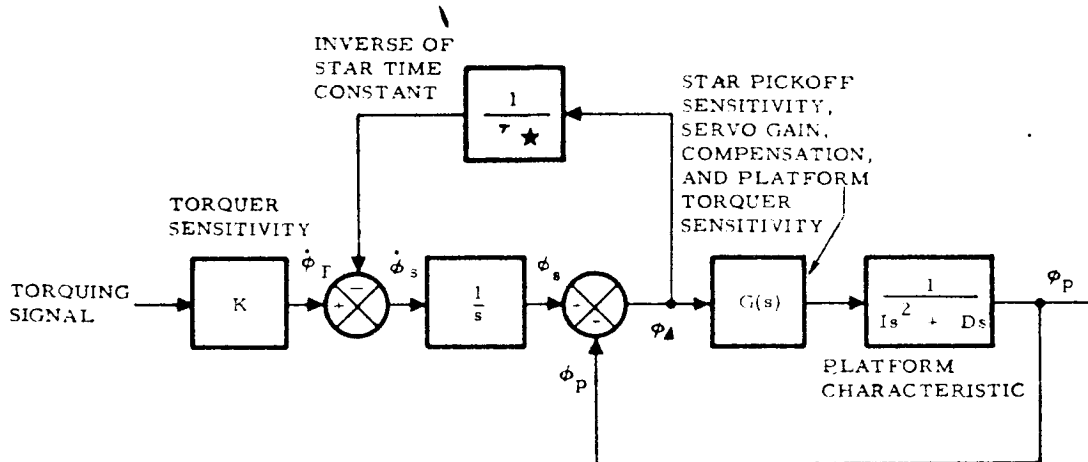
$$K_{p \text{ curved}} = 1.26 \quad (6-29)$$

and that the finite flat plates will have torquing rates related to those of the infinite parallel-plate solution by the factor

$$K_{p \text{ flat}} = 0.9 \quad (6-30)$$

6.2.3 Platform Servo-Error Effect

This error is not so much a torquing error per se, but more a gyro error, resulting from gyro and platform characteristic response to torquing. A platform controlled by a vibrating-string STAR gyro has a response as shown in the servo block diagram of Figure 6-3.



$\dot{\phi}_s$ = STRING-PLANE ANGLE

$\dot{\phi}_T$ = RATE AT WHICH STRING PLANE IS BEING TORQUED

ϕ_A = DIFFERENCE ANGLE, BETWEEN STRING PLANE AND PLATFORM

Figure 6-3. Vibrating String (STAR) Gyro and Platform Response to Torquing

The STAR time constant effect is a result of anisoelastic bias, described in detail in Reference 1. As a result of this effect, the string plane precesses at a rate of $(1/r_*)$ arc sec/sec for each arc sec the string plane deviates from critical. The torquing response may, by standard techniques, be obtained (in terms of the Laplace s) from Figure 6-3.

$$\frac{\dot{\phi}_p}{\phi_T} = \frac{(Is^2 + Ds)r_*}{\left[Is^2 + Ds + KG(s) \right] r_* + Is + D} \frac{G(s)}{Is^2 + Ds} \quad (6-29)$$

To obtain the error during steady-state torquing, we let $s \rightarrow 0$. The STAR gyro pickoff sensitivity is a constant, independent of frequency, from dc to all frequencies of interest, and the servo and servo torquer gain normally approaches a constant value at zero frequency; hence, letting $G(0) = G_o$, we may write

$$\left. \frac{\dot{\phi}_p}{\phi_T} \right|_{\text{steady state}} = \frac{1}{1 + \frac{D}{G_o r_*}} \quad (6-30)$$

$$\cong \left[1 - \frac{D}{G_o r_*} \right] \quad (6-31)$$

for small $\frac{D}{G_o r_*}$, as is necessary for reasonable response. The term,

$\frac{D}{G_o r_*}$, is the fractional change in torquing scale factor due to servo

response to gyro torquing. G_o/D , known as the "velocity-error constant" of the servo, must be kept large, consistent with the minimum expected value of r_* , and the required system accuracy.

This ratio of torquing rate with finite servo gain to what the torqued rate would have been with an ideal, infinitely stiff servo (Equation 6-31) has been added as a multiplier to the total torquing expression, Equation 6-15. Any effect of the difference between the servo error for steady-state torquing, and the servo error for a single pulse has not been computed, only the steady-state value being used here.

6.2.4 String Amplitude Pickoff Sensitivity

When the torquing pulse amplitude is controlled by the measured string amplitude, the sensitivity of this pickoff becomes an important factor. The capacity solutions in Section 3 make it possible to calculate the string-amplitude pickoff sensitivity on a direct theoretical basis. Figure 6-4 shows the pickoff circuit used. The use of a transformer allows an improvement in the signal-to-noise ratio to be gained by tuning the primary of the transformer to the string frequency.

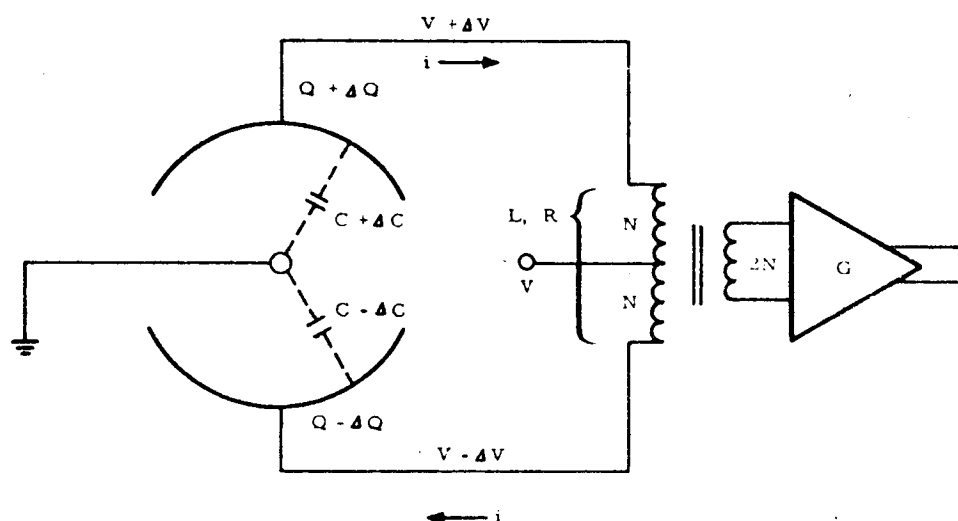


Figure 6-4. String Amplitude Pick-off Circuit

It is assumed here that the capacities CC include these tuning capacitors.

Although the excitation in this circuit is actually parametric, the attendant difficulties can be avoided by dealing only with small perturbations of the values. We assume symmetry so that ΔC , ΔV , Δq , and i are negative images in the bottom half of the circuit. Then taking the total primary inductance to be L (end to end), we have

$$2\Delta V = L \frac{di}{dt} + iR \quad (6-32)$$

The charge on each capacitor is $q \pm \Delta q$, and the change in charge is

$$\Delta q = C \Delta V - V \Delta C \quad (6-33)$$

for values sufficiently small that the $\Delta V \Delta C$ term may be neglected. The charge and current are related by

$$i = - \frac{d}{dt} \Delta q \quad (6-34)$$

Then combining, and using the Laplace s ,

$$i = -Cs \Delta V - Vs \Delta C \quad (6-35)$$

$$\frac{2 \Delta V}{Ls + R} = -Cs \Delta V - Vs \Delta C \quad (6-36)$$

from which

$$\frac{\Delta V}{V} = - \frac{s(Ls + R)}{LCs^2 + CRs + 2} \Delta C \quad (6-37)$$

Defining

$$\omega_r^2 = \frac{1}{L(C/2)} \quad (6-38)$$

$$Q_r = \frac{1}{R(C/2)\omega_r} = \frac{L\omega_r}{R} \quad (6-39)$$

we have

$$\frac{\Delta V}{V} = - \frac{\frac{s}{\omega_r Q_r} \left(\frac{Q_r}{\omega_r} s - 1 \right)}{\frac{s^2}{\omega_r^2} + \frac{s}{Q_r \omega_r} + 1} \frac{\Delta C}{C} \quad (6-40)$$

When the circuit is tuned for resonance, $s \rightarrow j\omega_r$ and

$$\frac{\Delta V}{V} \rightarrow - (jQ_r - 1) \frac{\Delta C}{C} \quad (6-41)$$

or the magnitude is

$$\left| \frac{\Delta V}{V} \right| = \left| \frac{\Delta C}{C} \right| \sqrt{Q_r^2 + 1} \quad (6-42)$$

$$\boxed{\left| \frac{\Delta V}{V} \right| \approx Q_r \left| \frac{\Delta C}{C} \right|} \quad (6-43)$$

and lags by 90 degrees, showing that the voltage signal, at resonance, is in phase with string velocity.

From Figure 4-4 and Equation 4-47 we see that the change in capacity (using the expression for the string centered, a good approximation) is

$$\Delta C = \frac{\pi C_w}{2} \quad (6-44)$$

$$\frac{d(\Delta C)}{dx} = \frac{\pi \epsilon y}{H \ln \left(1.273 \frac{H}{r_o} \right)} \quad (6-45)$$

Integrating over the length of the plates, as depicted in Figure 6.1, we obtain

$$\Delta C = \frac{\pi \epsilon Y_1}{H \ln \left(1.273 \frac{H}{r_o} \right)} \int_{l_c}^{\frac{l}{2} - l_e} \sin \frac{2\pi x}{l} dx \quad (6-46)$$

$$\boxed{\Delta C = \frac{l \epsilon Y_1}{H \ln \left(1.273 \frac{H}{r_o} \right)} \left[\frac{1}{2} \cos \frac{2\pi l_e}{l} + \frac{1}{2} \cos \frac{2\pi l_c}{l} \right]} \quad (6-47)$$

The capacity C is not C_w , but as stated, the total capacity in the circuit including that used to tune the transformer.

6.3 TORQUING ERRORS

Writing an expression for explicit error terms is somewhat trivial now that detailed theoretical expressions have been obtained for torquing scale factor in Equations such as 6-15, 6-4, 6-21, 6-23, and 6-31. Having these explicit expressions, the worst-case error expression is simply

$$\frac{d(\Delta\phi)}{\Delta\phi} = \sum_i \frac{\partial(\Delta\phi)}{\partial \alpha_i} \frac{d\alpha_i}{\Delta\phi} \quad (6-48)$$

This may now be worked out, but it is to be emphasized that in a particular case, the information desired may be more easily obtained by referring directly to the expressions in Paragraph 6.2.

For example, let us suppose that the torquing voltage is being set by an electronic gain, $V_T = G_T Y_1$, and that we wish the errors due to the terms in Equation 6-15, using Equation 4-51, namely $G_T = (V_T/Y_1)$, $\rho a = \frac{m}{l}$ (the fibre mass, m , is constant), V_o , H , r_o , f , l_c , l_e , θ_r , θ_d , and θ_{sa} . Differentiating with Equations 6-48, 6-15 and 4-51 (for small θ 's),

$$\begin{aligned} \frac{d(\Delta\phi)}{\Delta\phi} = & \frac{dG_T}{G_T} + \frac{dV_o}{V_o} + \frac{dl}{l} - \frac{2df}{f} \\ & - \frac{2\pi l_c}{l} \left(\tan \frac{2\pi l_c}{l} \right) \frac{dl_c}{l_c} - \frac{2\pi l_e}{l} \left(\tan \frac{2\pi l_e}{l} \right) \frac{dl_e}{l_e} \\ & - \left(1 + \frac{1}{\ln \frac{1.273H}{r_o}} \right) \frac{dH}{H} + \frac{1}{\ln \frac{1.273H}{r_o}} \frac{dr_o}{r_o} \\ & - \left(\theta_r + \frac{2\theta_d \theta_{sa}}{k\pi} \right) d\theta_r \\ & - \frac{2}{k\pi} \left(\theta_d^2 + \theta_{sa} [\theta_r + \theta_d] \right) d\theta_d \\ & - \frac{2}{k\pi} \theta_d \left(\theta_r + 2\theta_{sa} \right) d\theta_{sa} - d \left(\frac{D}{G_{r_o^*}} \right) \end{aligned} \quad (6-49)$$

The last term comes from Equation 6-31, which was derived for a string of pulses (steady state). Any difference which might occur between a string of pulses and an individual pulse has not been investigated.

If it is assumed that the θ 's are nominally zero, then the $d\theta$'s may be replaced by the values of θ , and the last three terms above should be replaced by $(\frac{\Delta\phi}{K} - 1)$, from Equation 3-34, which is

$$-\frac{1}{2}\theta_r^2 - \frac{2}{k\pi}\left(\theta_d\theta_{sa}\theta_r + \theta_d\theta_{sa}^2 + \frac{1}{3}\theta_d^3\right)$$

In any case, we see that, because of the optimum choice for nominal values of the θ 's, the sensitivity to change of these phase angles is not great. The reference phase, θ_r , is the most important. If all phases change from 0 degree to 1 degree the contribution of the expression above is

$$- (1.5 + 0.05 + 0.05 + 0.02)/10^4 \quad (\text{for } k = 1)$$

showing that θ_r is normally dominant.

For values applicable to the present instrument under test, we may evaluate some of the coefficients.

$$l = 1.74 \text{ in}$$

$$l_c = 0.188 \quad (6-50)$$

$$l_e = 0.120$$

$$H/r_o = 115$$

$$r_* \text{ changes from } \infty \text{ to } r_*'$$

$$\theta's = \text{deviations from zero}$$

These give the fractional change in scale factor,

$$\begin{aligned}
 \frac{d(\Delta \phi)}{\Delta \phi} = & \frac{dG_T}{G_T} + \frac{dV_o}{V_o} + \frac{d\ell}{e} - \frac{2df}{f} \\
 & - 0.545 \frac{d\ell_c}{\ell_c} - 0.182 \frac{d\ell_e}{\ell_e} \\
 & - 1.20 \frac{dH}{H} + 0.20 \frac{dr_o}{r_o} \\
 & - \frac{1}{2} \theta_r^2 - \frac{2}{k\pi d} \left[\theta_{sa} (\theta_r + \theta_{sa}) + \frac{1}{3} \theta_d^2 \right] \\
 & - \frac{D}{G_o \tau_*}
 \end{aligned} \tag{6-51}$$

The worst case change is the sum of the absolute values of the individual terms. The rss (root-sum-square) error is more often used, because it is the most probable error. However, before doing the rss, correlation of errors must first be accounted for. The most important source through which correlated errors will occur is temperature. The terms $d\ell$, df , $d\ell_c$, $d\ell_e$, dH and dr_o will depend on temperature in a correlated manner.

We may assume that the drive frequency, f , is determined by the natural frequency of a resonant driver

$$f = \beta_i \left(\frac{Eh^3}{(1-\nu^2) mL^2} \right)^{1/2} \tag{6-52}$$

where β_i depends on the geometry of the resonator, h is its thickness, L is a characteristic length in its plane, m is its mass, and E and ν are Young's modulus and Poisson's ratio.

If then

$$\frac{E}{1-\nu^2} = \frac{E_o}{1-\nu_o^2} (1 + \alpha_{Ed} \Delta T) \tag{6-53}$$

$$L = L_o (1 + \alpha_d \Delta T) \quad (6-54)$$

$$\begin{aligned} \frac{df}{f} &= \frac{1}{2} \frac{d|E/(1-\nu^2)|}{E/(1-\nu^2)} + \frac{1}{2} \frac{dL}{L} \\ &= \frac{1}{2} \alpha_{Ed} \Delta T + \frac{1}{2} \alpha_d \Delta T \end{aligned} \quad (6-55)$$

Assuming that the case and resonator are of the same material, then

$$\begin{aligned} \alpha_d \Delta T &= \frac{d\ell}{\ell} \\ &= \frac{d\ell_c}{\ell_c} \\ &= \frac{d\ell_e}{\ell_e} \\ &= \frac{dH}{H} \end{aligned} \quad (6-56)$$

The fibre will, in general, be made of a different material than the case, so that

$$\frac{dr_o}{r_o} = \alpha_f \Delta T \quad (6-57)$$

We may take sample numerical values, corresponding to the tests being made. For an Invar resonator and case and a fused silica fibre

$$\begin{aligned} \alpha_f &\cong 0.3 \times 10^{-6} / ^\circ F \\ \alpha_{Ed} &\cong 280 \times 10^{-6} \text{ psi/psi/} ^\circ F \\ &\quad (\text{or } -33 \text{ to } 280) \end{aligned} \quad (6-58)$$

$$\alpha_d \cong 0.35 \times 10^{-6} \text{ to } 1 \times 10^{-6} \text{ in./in./} ^\circ F$$

Anomalies of nickel-iron alloys of the Invar, Nilvar, Elinvar, etc, type show so much variation with small changes in constituents and heat treatment, that it is difficult to pick absolute values from the tables for a given sample. The measured frequency change corresponds to α_{Ed} of $210 \times 10^{-6} / ^\circ\text{F}$, with α_d too small to have much effect. This is quite within the range of reasonable values, so is used here (the effect of Poisson's ratio may also account for part of the difference from 280 to 210). We will use 0.9×10^{-6} for α_d . Then

$$\begin{aligned} \frac{d(\Delta\phi)}{\Delta\phi} = & \frac{dG_T}{G_T} + \frac{dV_o}{V_o} + (103.8 \times 10^{-6} / ^\circ\text{F}) \Delta T \\ & - \frac{1}{2} \theta_r^2 - \frac{2}{k\pi} \theta_d \left[\theta_{sa} (\theta_r + \theta_{sa}) + \frac{1}{3} \theta_d^2 \right] \quad (6-59) \\ & - \frac{D}{G_o (100 \text{ sec})} \end{aligned}$$

We see here that the temperature term in this equation is completely dominated by the thermoelastic coefficient of the drive resonator, α_{Ed} . If this term proved to be a problem, it could be reduced by a factor approaching 100 through use of a constant-modulus alloy such as Elinvar.

If we were to select one part in 10,000 as the desired stability of $\Delta\phi$, an error budget might be selected along these lines;

$$\theta_r = \pm 0.5^\circ (0.00872 \text{ rad})$$

$$\theta_{sa} = \pm 2^\circ (0.0349)$$

$$\theta_d = \pm 2^\circ$$

$$\frac{dG_T}{G_T} = \pm 3/100,000$$

$$\frac{dV_o}{V_o} = \pm 3/100,000 \quad (6-60)$$

$$\Delta T = \pm 0.3^\circ\text{F}$$

$$G_o/D = \pm 1000$$

The terms, in the order of Equation (6-59), would then be $\pm 3 \times 10^{-5}$, $\pm 3.1 \times 10^{-5}$, $\pm 3.8 \times 10^{-5}$, $\pm 4.3 \times 10^{-5}$, $\pm 1 \times 10^{-5}$. The rss of these terms is about 8/100,000, or slightly less than one part in 10,000. The fact that the algebraic sum adds up to a low value is simply a coincidence in the choice of the sign of changes, which cannot be predicted in advance except where known correlation exists, as in the case of the terms combined in the ΔT term. The root-sum-square, thus, is the proper method of combining these terms.

In connection with item (1) (iv) of the contract, the phase errors (A) are covered by the three θ terms in Equation 6-49, the pulse magnitude (B), and string amplitude term (C) have been combined in the first term, Equation 6-49, the torquing gain term, although they can be left separate when expanding Equation 6-15 according to Equation 6-48, if desired. The effect of string amplitude pickoff nonlinearity (D) is, first, to produce harmonics in the signal which, when amplified, is used for torquing. The string, as torqued here, has been shown to be insensitive to these harmonics by the integration of Equation 3-15 with harmonics in $T(t_1)$. The effect of the nonlinearity, secondly, on amplitude of the fundamental appears as an amplitude sensitivity of the gain term error, dG_T / G_T , and may be obtained from Equations 6-43, 6-44 and 4-28. The angle-off (F) produces trajectory ellipticity (E), which, through a mechanism discussed in detail in Reference (1), causes string-plane drift; this effect is described by τ_* ; the resulting error is the last term in Equation 6-49.

The effect of electronics errors (G) is expressed in the first term of Equation 6-49, gain stability, and the second term, bias stability. In the form, Equation 6-59 the effect of temperature stability (H) is shown. The dominant effect in this temperature term is the thermoelastic temperature coefficient of the disk resonator. The use of a material with a more constant Young's modulus for the drive resonator, or the use of other methods for controlling drive frequency, would reduce this term greatly.

7. LABORATORY MECHANIZATION FOR PROVIDING STAR TORQUING DATA

7.1 INTRODUCTION

This section describes the mechanization used to yield STAR Gyro torquing data. The data obtained is described in Section 8 of this report.

The operation of this implementation can best be described by reference to Figure 7-1 which is a block diagram of the torquing loop.

The instrument used during the tests is an Invar STAR gyro operating in the second mode. This instrument contains two pairs of capacitive plates to sense motion of the vibrating string. One pair, referred to here as the reference plates, is essentially perpendicular to the plane described by the string vibrating motion; it provides a signal proportional to the amplitude of the string oscillation. The second set of plates is approximately parallel to the plane described by string motion. One of these, called the pickoff plate, is used to sense the angle between the string plane and a reference plane defined by a null output from the pickoff plate. The other plate is used to provide torquing pulses to force the string plane to change orientation in a controlled manner.

The string in the test instrument vibrates at a frequency of approximately 6,225 cps. The disc driving the string into this motion thus operates at twice string frequency — approximately 12,450 cps.

The general operation of the mechanization is as follows:

Neglecting for the moment the flow of torquing pulses, the basic platform servo is straightforward. The pickoff plate (Plate 4) is used to sense any changes in the string plane angle from the servo nulling position. Signals obtained from this plate are buffered by the pickoff buffer amplifier, amplified, filtered, and applied to a phase sensitive demodulator. The reference for the demodulator is obtained following suitable amplification from the reference plates (Plates 6 and 7). Following demodulation, a d-c signal proportional to string plane angle deviation from the servo null is available. This signal is compensated, amplified, and applied to a d-c platform torquer. This drives the platform mounting the STAR gyro in a direction towards servo null, thereby providing a stable platform.

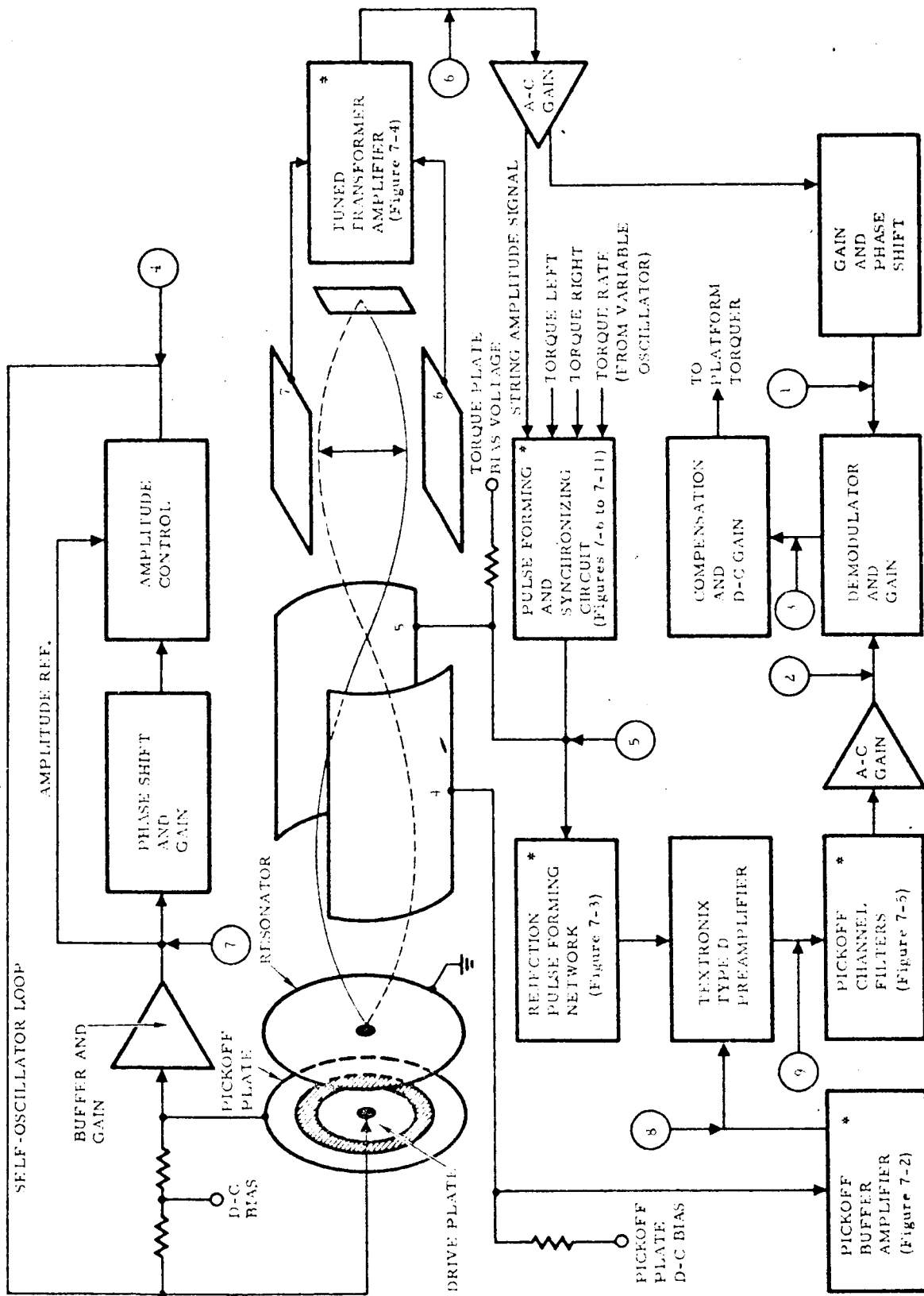


Figure 7-1. Star Gyro Electrostatic Torquing Loop

Torquing of the STAR gyro which subsequently controls this platform is accomplished by providing voltage pulses of proper phase and amplitude to the torquing plate (Plate 5). In this mechanization the pulses take the form of integral sine wave pulses although other pulse wave forms could be used. Formation and control of the torquing pulses is accomplished using circuitry designated as pulse forming and synchronization circuitry. A continuous sine wave at string frequency and proportional to string oscillation amplitude is obtained from the reference plates. Using digital techniques, this sine wave is broken into integral sine wave pulses either in-phase or out-of-phase with the string velocity. The phase of the pulses along with torque plate bias polarity determines torquing direction. The pulses are applied to the torquing plate at a rate controlled by an external variable oscillator. The logic limits the maximum torquing rate to one-half string frequency. (This is not a necessity but somewhat simplifies the logic mechanization.) The pulses applied to the torquing plate cause the string plane to change orientation in a controlled manner. This change is sensed in the normal servo channel and the servo action will cause the stable platform to rotate accordingly.

As evidenced by Figure 7-1, an electrical cross-talk of torquing pulses from plate No. 5 to plate No. 4 occurs during torquing. This cross-talk can be considered as introducing an excessively large noise input into the servo channel and if allowed to continue will disrupt the servo. The method of bypassing this difficulty in this mechanization is to provide a cancelling pulse into the servo to null out the cross-coupled pulses. The cancelling pulse is obtained by applying the torquing pulse to the rejection pulse forming network at the same time it is applied to the torquing plate. This network closely approximates the transfer characteristic seen by the torquing pulse from the torquing plate to the point where cancellation is to be done. The actual cancellation is accomplished by summing the output from the network with the cross-coupled pulse in a commercial differential amplifier (Tektronix Type D).

7.2 DETAILED CONSIDERATION

Certain elements of this mechanization deserve elaboration. Some of the circuits involved are unique to the implementation presently being used and thus fundamentally determine satisfactory operation. In addition, the manner in which data is accumulated and the factors which control its relevancy are important. A number of figures are included which may or may not be discussed in detail. Also

oscillograms are shown when pertinent to illustrate operation of the mechanization. These also serve to show critical settings which must be maintained in order to provide stable operation during data accumulation.

7.2.1 Circuit Consideration

Figure 7-1 depicts the circuitry used in this STAR gyro torquing mechanization in block form. The self-oscillator loop (disk drive oscillator) shown at the top is required to drive the string into stable vibratory motion. It is required for operation of any STAR gyro but it is not directly pertinent to the discussion of STAR torquing. It is pictured in Figure 7-1 since certain critical signals in the oscillator loop are used for reference in the torquing mechanization (i.e., disc drive voltage at test point No. 4 and the disc pickoff voltage at test point No. 7). Five blocks of circuitry are unique to the gyro torquing mechanization and are indicated by asterisks in Figure 7-1. These will be discussed below. The rest of the circuitry is essentially conventional (a-c gain, phase shifters, switching demodulator, etc) and will not be considered further.

Pickoff Buffer Amplifier. Figure 7-2 depicts the pickoff buffer amplifier. This circuit incorporates low noise transistors (2N930's), boot strapping to pick up the input impedance, and guard shielding on the pickoff signal input line. The utilization of guard shielding allows use of reasonably long cables without excessive shunting of pickoff signal due to line capacity. No voltage gain is incorporated in the amplifier as a highly stable voltage transfer function is required if adequate cross-coupled pulse rejection is to be feasible. The input impedance of the amplifier is approximately 6 megohms at signal frequency. (The source impedance of the pickoff signal including shunt capacities is about 560 kohms at signal frequency.) An approximate measurement of amplifier output voltage versus string plane angle was made using the test STAR gyro. This scale factor is approximately 0.2 uv/sec with a pickoff plate excitation of 100 volts. For purposes of designing the rejection network required for cross-coupled pulse rejection, the torquing plate to pickoff amplifier output transfer function was determined. With the test instrument described previously and the amplifier of Figure 7-2, this transfer function is given by

$$\text{Pickoff Amplifier Output} \approx \frac{Ks(\tau_2 s + 1)}{(\tau_1 s + 1)(\tau_3 s + 1)} \frac{v}{v} \cdot$$

Torque Pulse Voltage

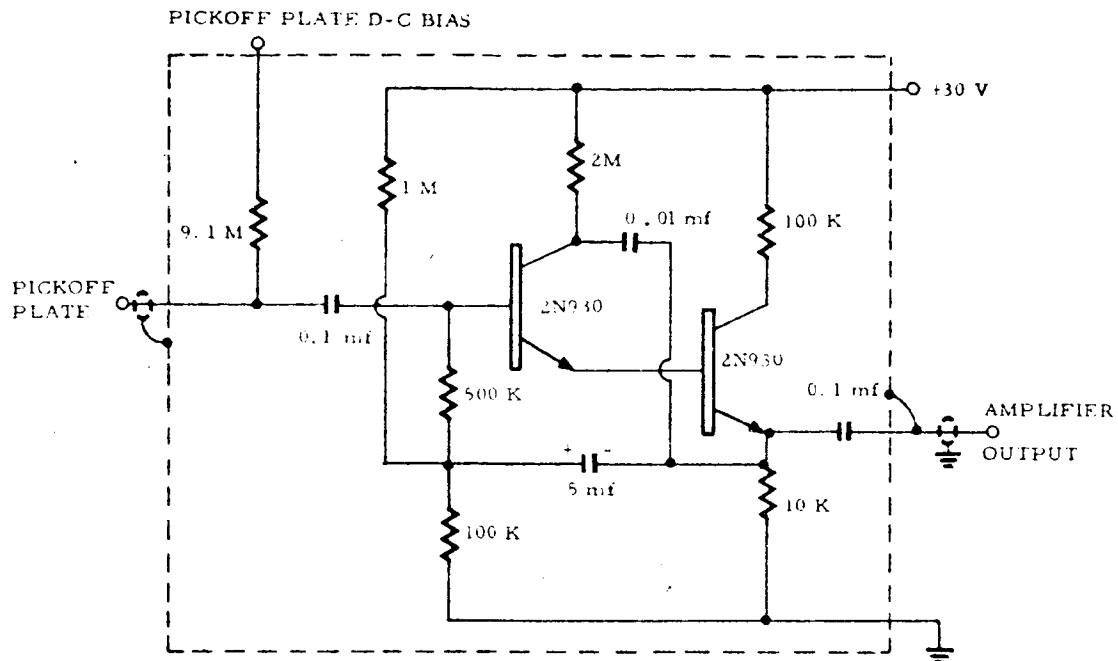


Figure 7-2. Pick-off Buffer Amplifier

where

$$K \approx 0.2 \times 10^{-5} \text{ sec.}$$

$$\tau_1 \approx 0.94 \times 10^{-4}$$

$$\tau_2 \approx 4.5 \times 10^{-8}$$

$$\tau_3 \approx 1.0 \times 10^{-6}$$

Rejection Pulse Forming Network. Inspection of the transfer function determined above as well as experimental data indicates that the zero at $\omega_2 = 1/\tau_2$ can be neglected. The lead introduced is

sufficiently outside of the frequencies of interest as to have negligible effect. Thus a network to synthesize

$$\frac{\text{Pickoff Amplifier Output}}{\text{Torque Pulse Voltage}} \approx \frac{Ks}{(\tau_1 s + 1)(\tau_3 s + 1)} \quad \frac{v}{v}$$

where

$$K \approx 0.2 \times 10^{-5} \text{ sec}$$

$$\tau_1 \approx 0.94 \times 10^{-4}$$

$$\tau_3 \approx 1 \times 10^{-6}$$

was determined. This network is shown schematically in Figure 7-3.

Tuned Transformer Amplifier. Figure 7-4 is a schematic of the amplifier used to derive the signal from the reference plates (Plates 6 and 7). This amplifier incorporates a high Q ($Q \approx 60$) transformer which is capacitively tuned to provide anti-resonance at string frequency. Use of tuning in this manner provides a fairly large signal proportional to string amplitude with a minimum of active gain

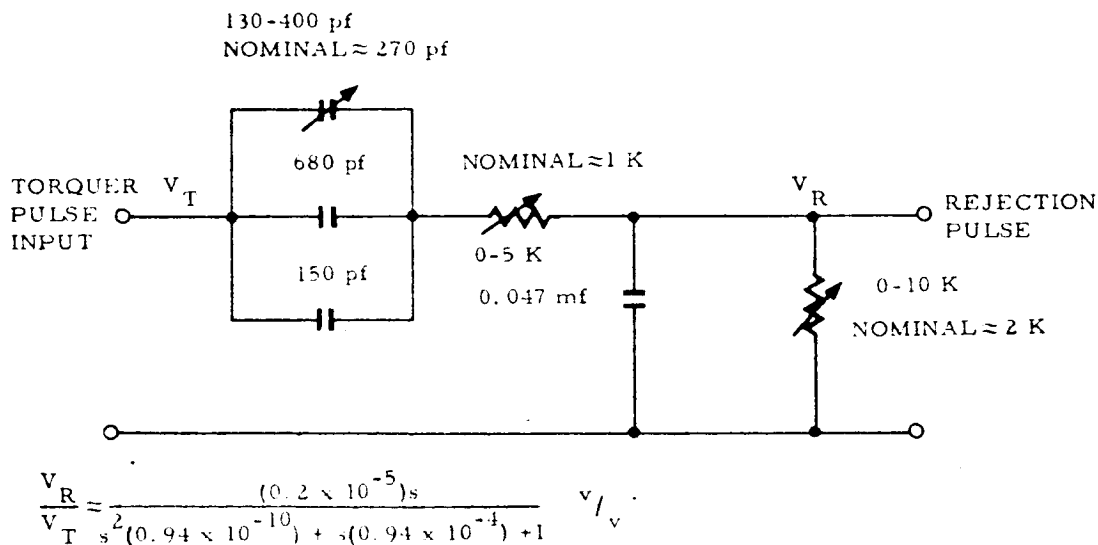


Figure 7-3. Rejection Pulse Forming Network

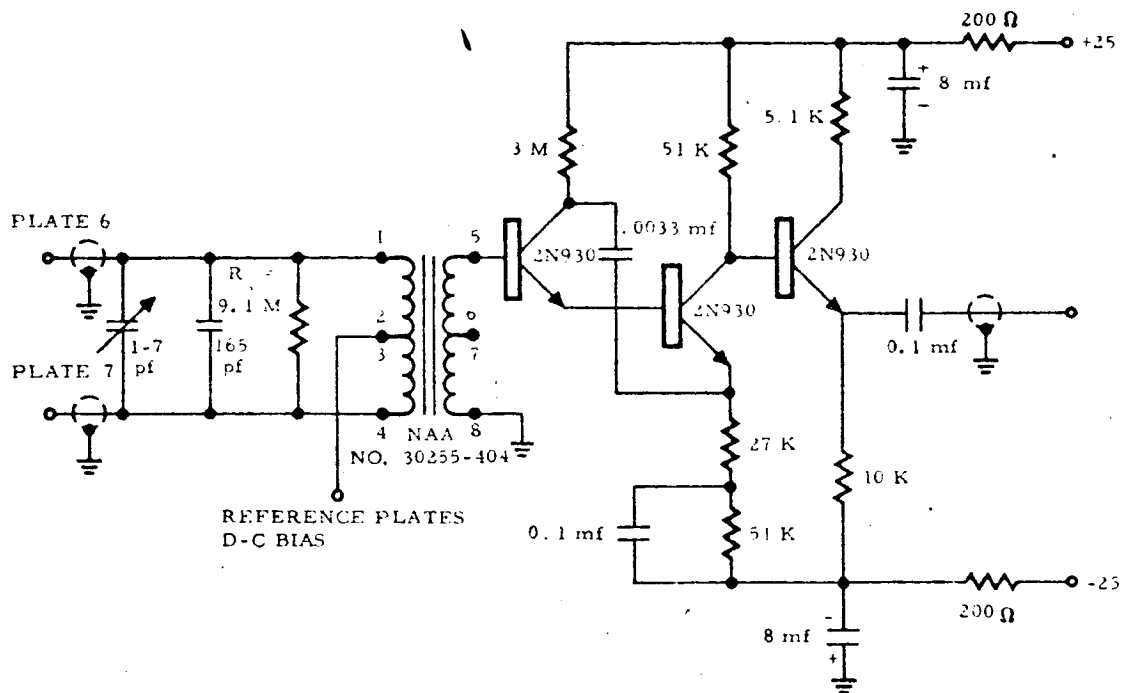


Figure 7-4. Tuned Transformer Amplifier

(gain ≈ 20). Experimentally, it has been found that the circuit Q was too high. De-tuning due to slight ambient changes was causing unreasonable phase shifts in the output signal. A shunt resistor, R_s , was connected across the transformer for stabilization. The circuit is now adequately stable. With the test instrument and the amplifier as shown, output voltage at nominal test temperature is about 400 mv.

Pickoff Channel Filters. Figure 7-5 depicts the filtering which has been incorporated into the servo channel. The input to the filters contains noise predominantly generated in the input stage of the pickoff buffer amplifier. In addition noise components due to imperfect cross-coupled pulse rejection are possible. This latter noise source, potentially periodic in nature, if not filtered out will undesirably affect servo operation. For this reason the action of the filters can have a substantial effect on the performance of the

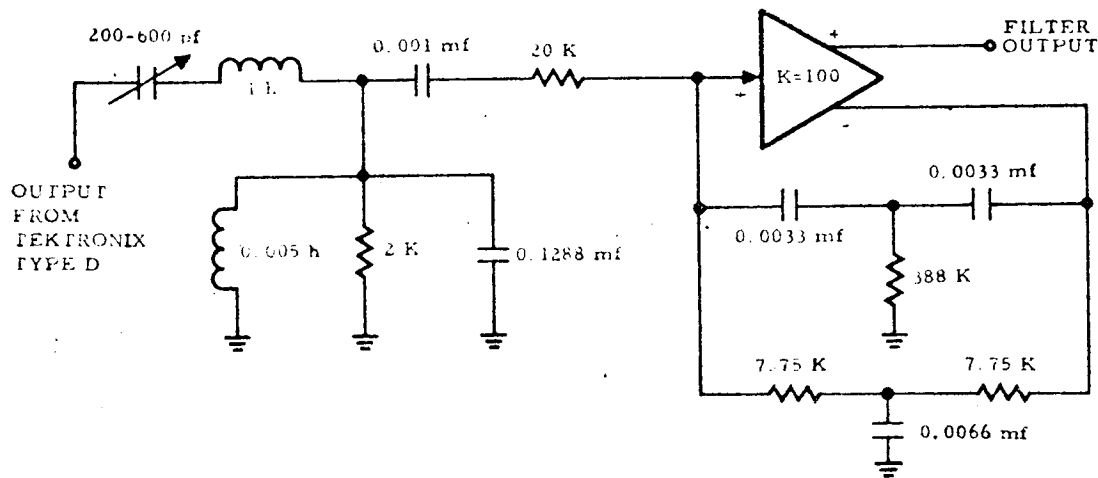


Figure 7-5. Pick-off Channel Filters

mechanization. The filtering used consists of one active filter using twin-T feedback preceded by a conventional series-parallel LC band-pass filter.

Pulse Forming and Synchronization Circuitry. Figures 7-6 through 7-11 provide detailed schematic information as well as descriptions of the logic performed by the circuitry. They are included here as reference only since the details of this circuitry do not directly affect the operation of this mechanization. The only requirement for this circuitry is that it faithfully reproduces an integral sine wave from a continuous sine wave and controls the necessary phase relationships.

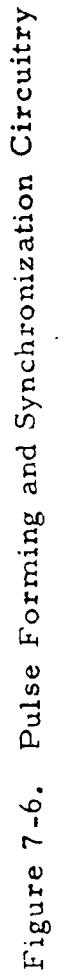


Figure 7-6. Pulse Forming and Synchronization Circuitry

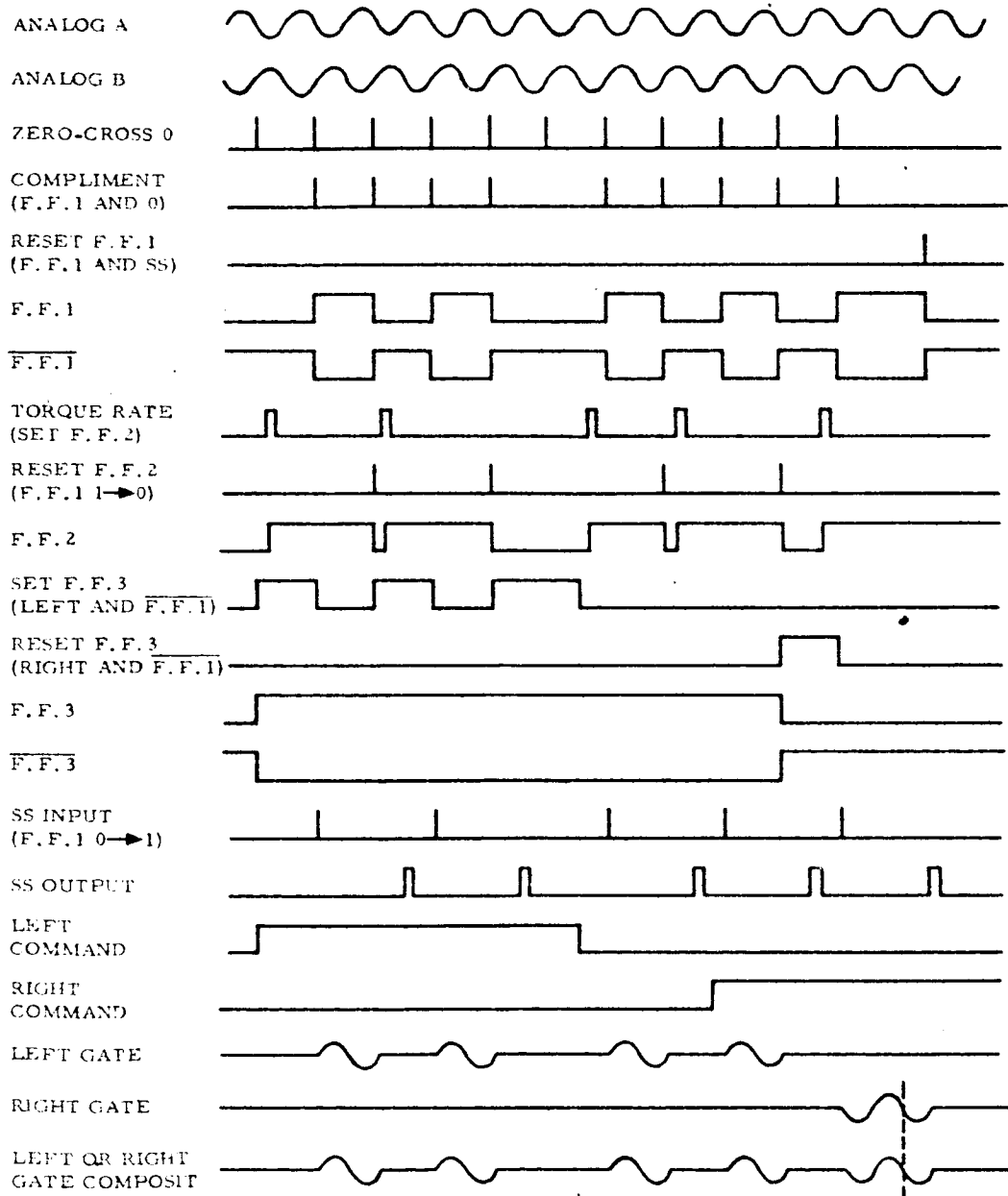


Figure 7-7. Timing Diagram Depicting Logic Being Performed by Pulse Forming and Synchronization Circuitry

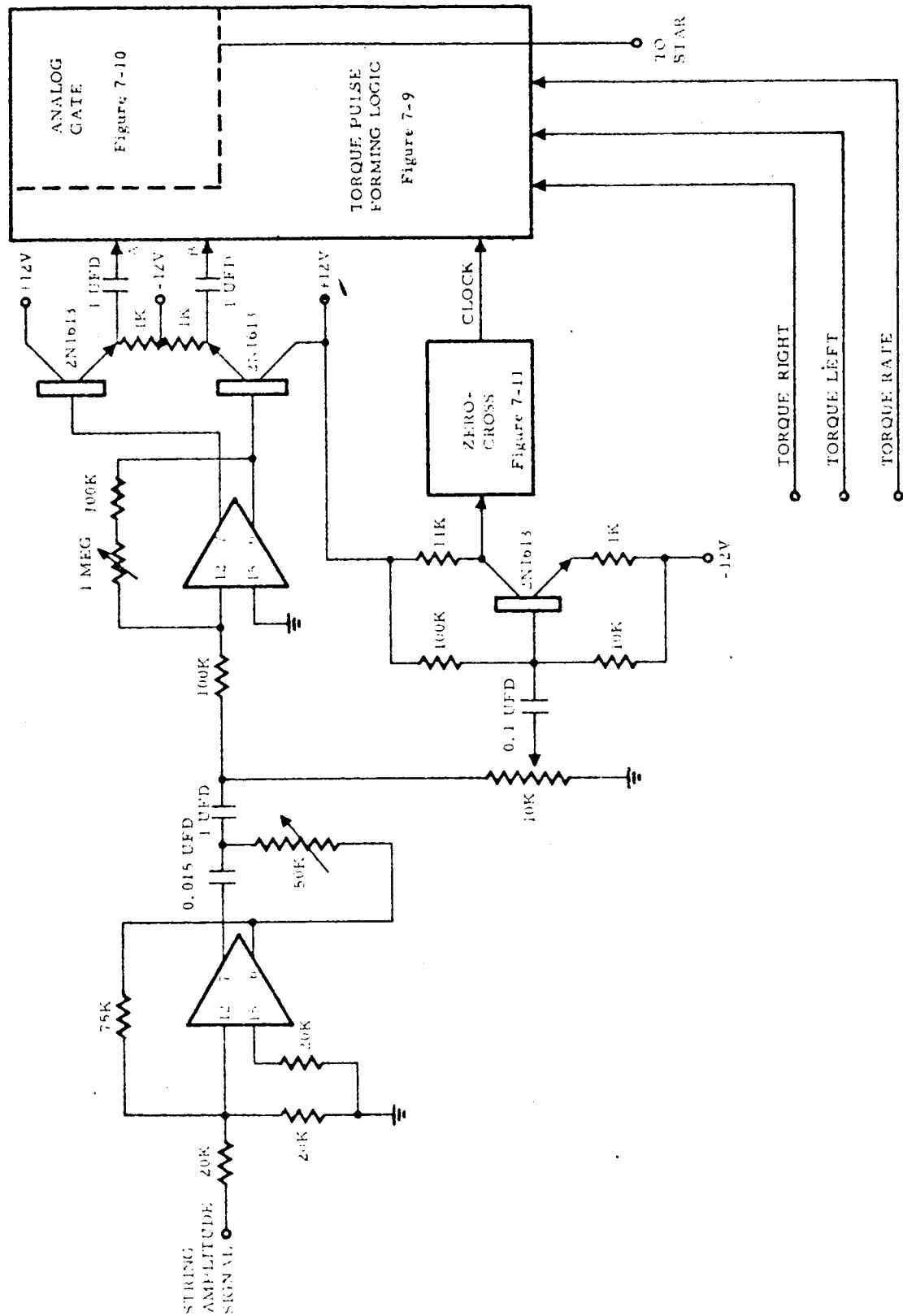
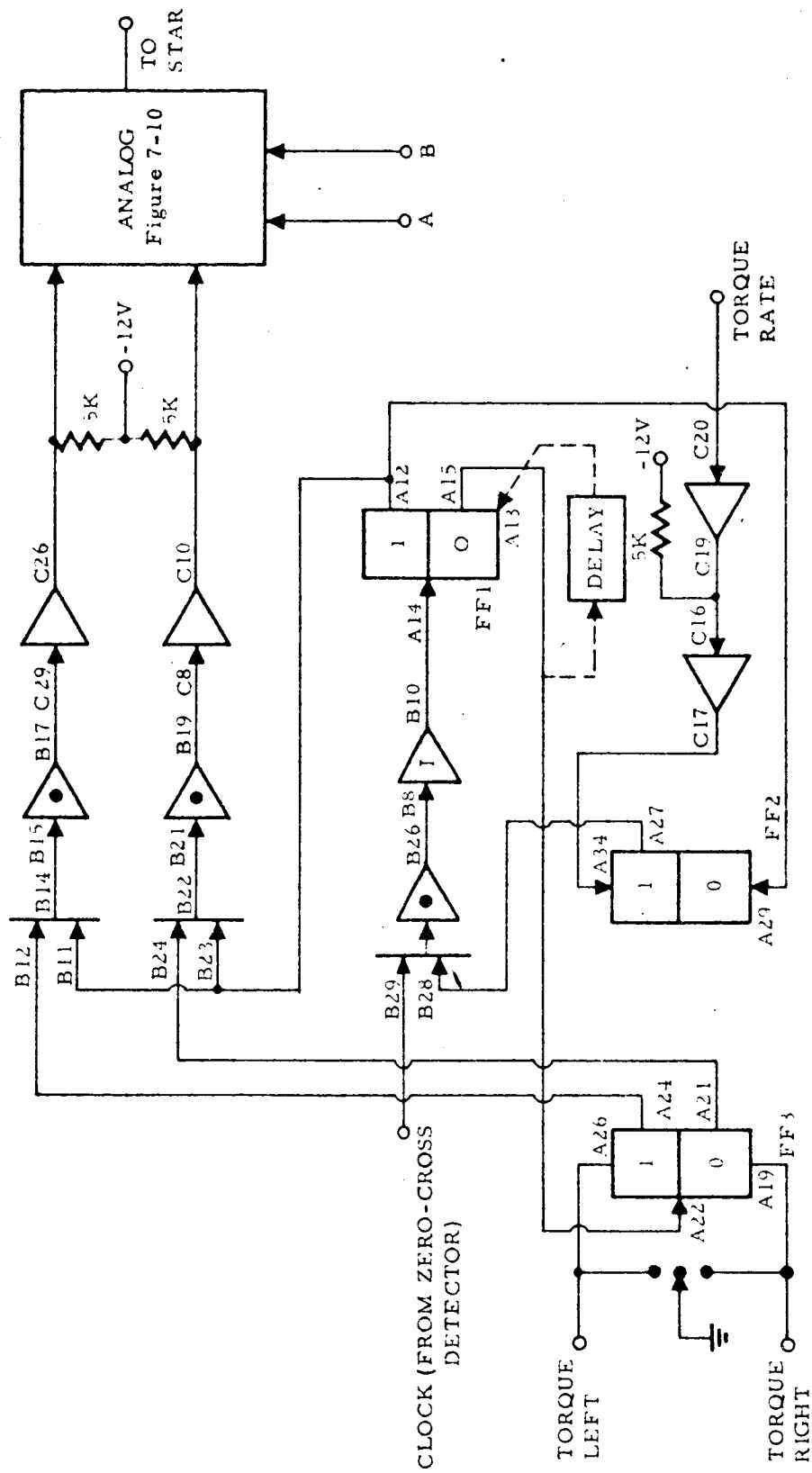
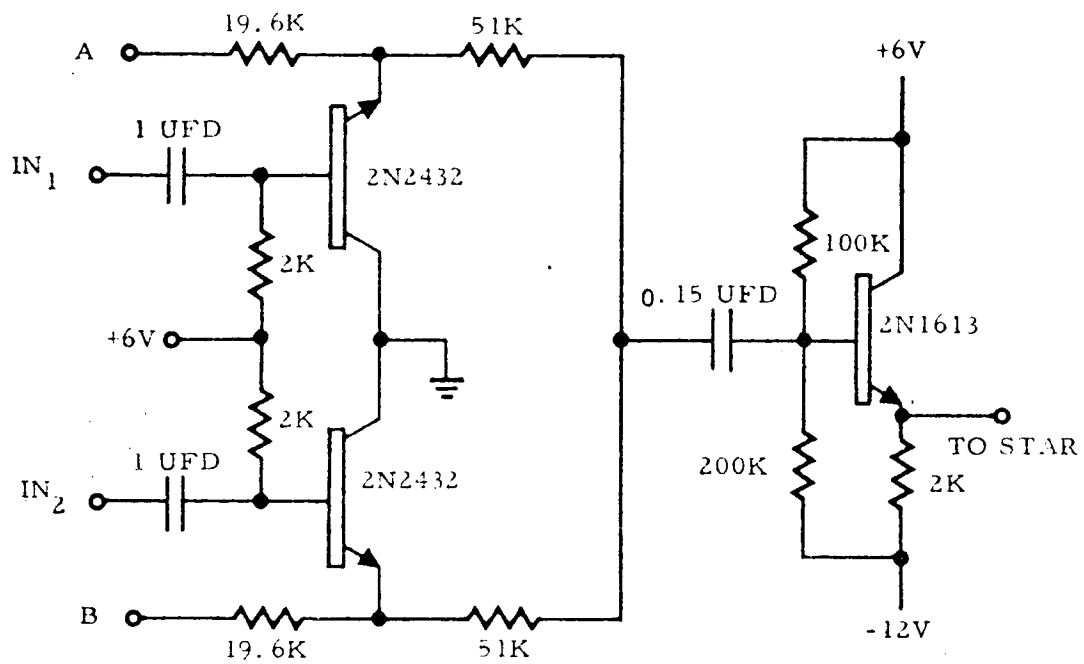


Figure 7-8. Master Signal Flow Schematic for Pulse Forming and Synchronization Circuitry

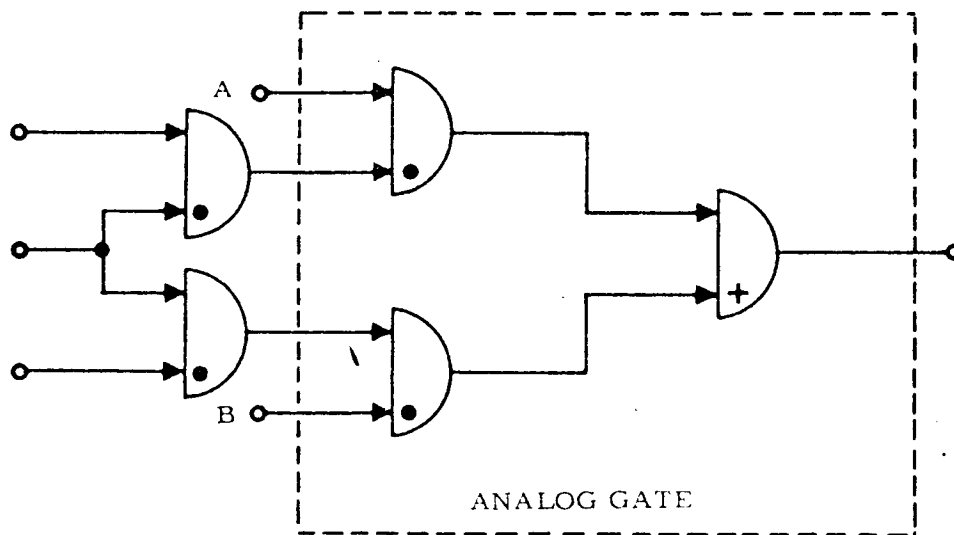


BOARD A - COMPUTER LOGIC CORP QF-2 (4 FLIP FLOPS)
 BOARD B - COMPUTER LOGIC CORP DN-1 (LOGIC CARD)
 BOARD C - COMPUTER LOGIC CORP CD-1 (CLOCK DRIVER)

Figure 7-9. Torque Pulse Forming Logic - Signal Wiring Schematic



ANALOG GATE



ANALOG GATE

Figure 7-10. Analog Gate Schematic

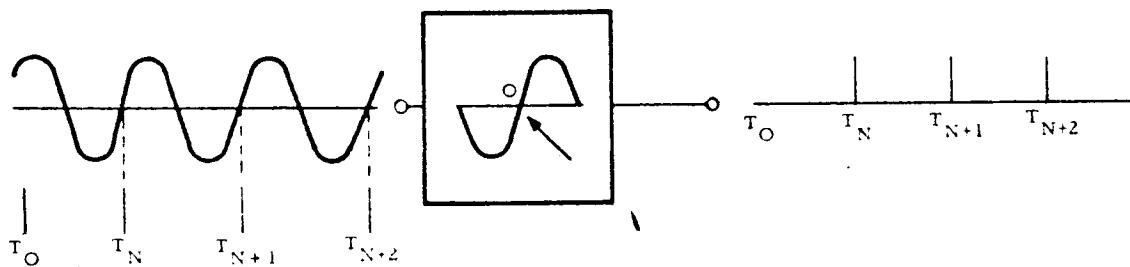
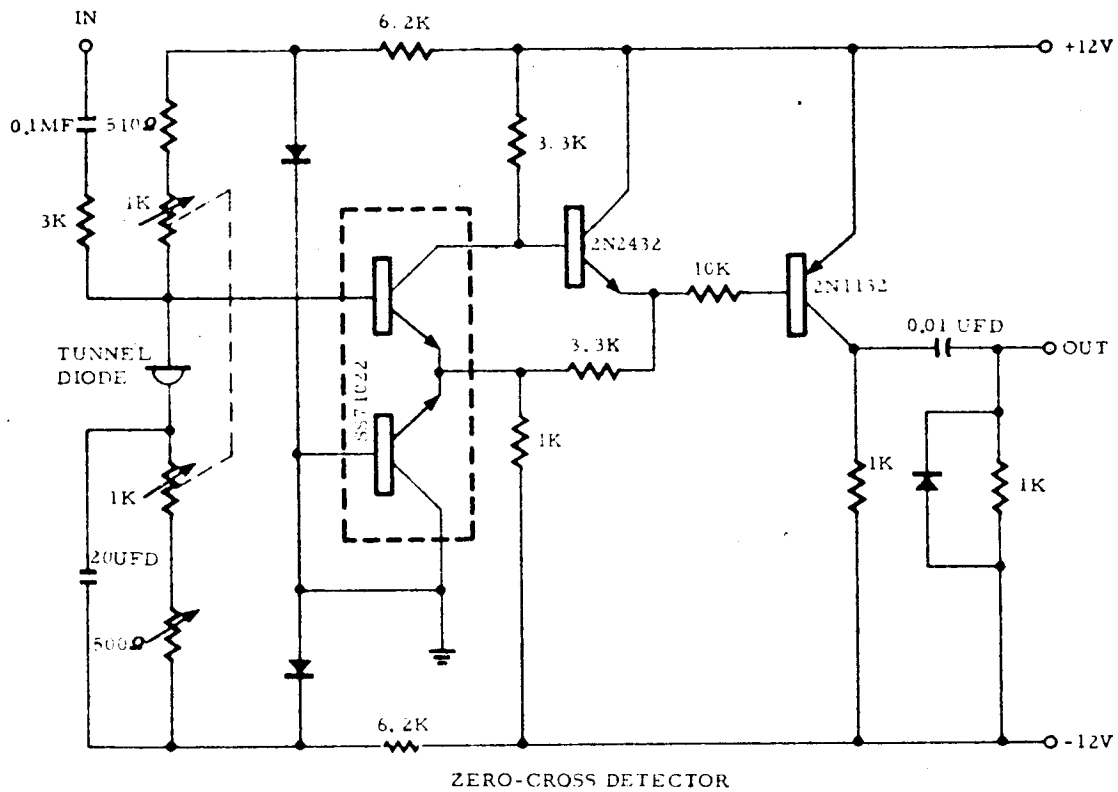


Figure 7-11. Zero-Cross Detector Wiring Schematic

7.2.2 Laboratory Setup Operation

To illustrate the operation of this mechanization and to provide background for the procedures involved in data accumulation, a number of oscillograms have been taken. These are photographs of the signals appearing at various points in the laboratory setup as observed on an oscilloscope. In all cases the signals shown refer to test points 1-9 in Figure 7-1. For convenience these test points are defined as:

TP1 - Demodulator Reference

TP2 - Pickoff Error Signal (after filtering and amplification)

TP3 - Demodulator Output

TP4 - Disc Drive Voltage

TP5 - Torque Pulses

TP6 - String Amplitude Reference

TP7 - Disc Pickoff Voltage

TP8 - Pickoff Buffer Amplifier Output

TP9 - Tektronic Type D Preamplifier Output

Oscillogram 7.1 (Figure 7-12) is a representative picture of the normally monitored signals throughout the mechanization. Achievement of this set of wave forms indicates that the mechanization is working satisfactorily. The servo loop is closed and the instrument is being alternately torqued left and right with no net torquing rate.

Oscillogram 7.2 (Figure 7-13) provides a reference for the gain settings throughout the loop. This picture is used when it is desired to check or return the loop gains to a nominal set of values. This picture is important when it is desired to make runs to check data repeatability and serves as a monitor of gain stability.

Oscillogram 7.3 (Figure 7-14) is used as a reference for phasing the demodulator reference. Monitoring of the demodulator reference phasing and comparing it to this photograph indicates phase stability of this quantity. In addition, the picture is used as a basis to allow returning the demodulator reference to its initial set point in the event of any phase shift. This is vital for coherent data accumulation.

Oscillogram 7.4 (Figure 7-15) is used as a reference for phasing the pickoff error signal. Monitoring of the pickoff error signal and comparing it to the photograph indicates phase stability of this quantity.

Oscillogram 7.5 (Figure 7-16) is used as a reference for phasing the string amplitude reference signal. Monitoring of the string amplitude reference phasing and comparing it to the photograph indicates phase stability of this quantity. It should be noted that any shift of this quantity affects both the modulator reference phasing and the torque pulse phasing.

Oscillogram 7.6 (Figure 7-17) is used as a reference for phasing the torque pulses. Monitoring of this quantity and comparison to the reference photograph indicates the phase stability of the torque pulses. In addition, when it is desired for data accumulation to intentionally shift phase from the photograph reference position, use of this reference is necessary to set the desired phase shift.

Oscillogram 7.7 (Figure 7-18) shows the normally monitored quantities while the instrument is being torqued at maximum rate. The top set of traces is for one torquing direction while the lower set is for the other torquing direction. Note the phase relations of the torquing pulses and the polarity of the demodulator outputs.

Oscillogram 7.8 (Figure 7-19) is similar to Oscillogram 7.7 except a rate of one-half maximum is used.

Oscillogram 7.9 (Figure 7-20) is used to show the string actually precessing while being torqued. The servo loop is open and torque rates are applied in both directions. Monitoring of the string plane angle (T.P. 2) and use of a slow scope sweep on this trace shows the pickoff angle buildup. The demodulator output (T.P. 3) is also shown on a slow sweep and clearly shows the d-c output buildup as a function of pickoff angle.

Oscillogram 7.10 (Figure 7-21) is used to show the waveform of the torquing pulse when the turn-off and turn-on times of the pulse are varied. This figure shows pulses one full string cycle and one-half string cycle wide with different turn-on times.

Oscillogram 7.11 (Figure 7-22) is used to show the waveform of the torquing pulses when the turn-on and turn-off times are varied. This figure shows pulses one and one-half string cycle and one-quarter string cycle wide with different turn-on times.

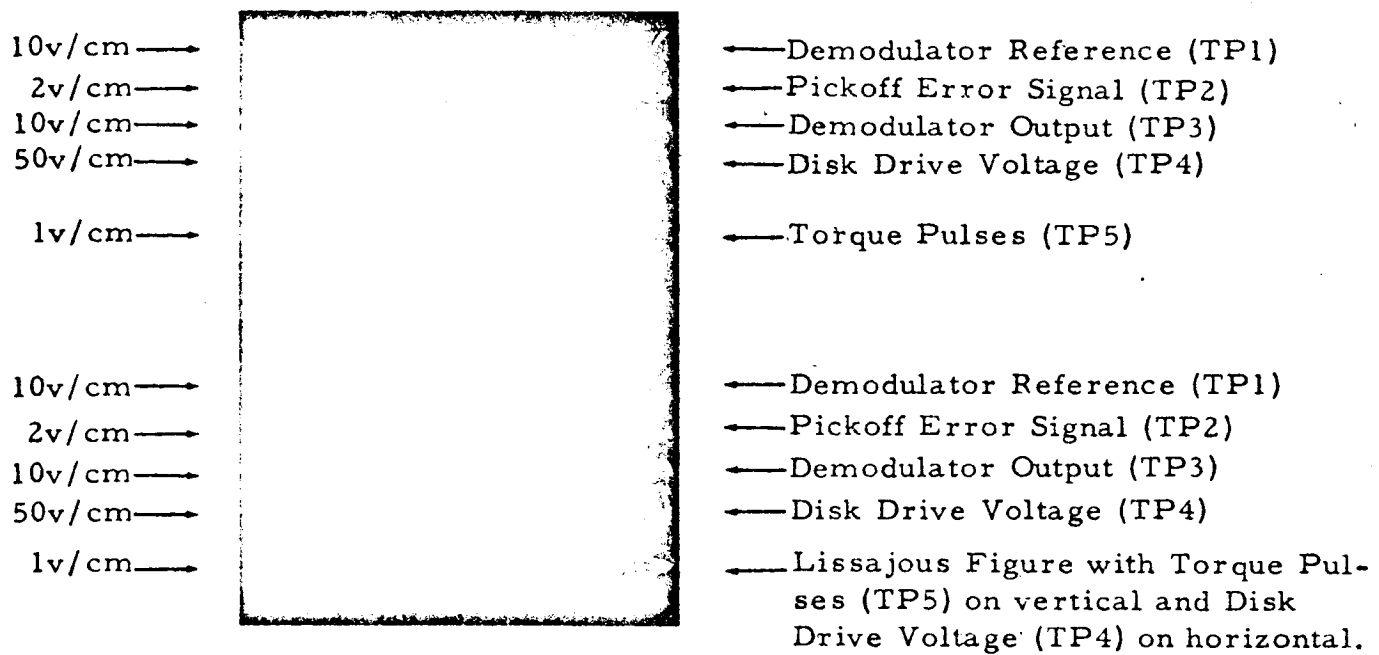


Figure 7-12. Oscillogram 7.1: Normally Monitored Signals Throughout the STAR Gyro Electrostatic Torquing Mechanization

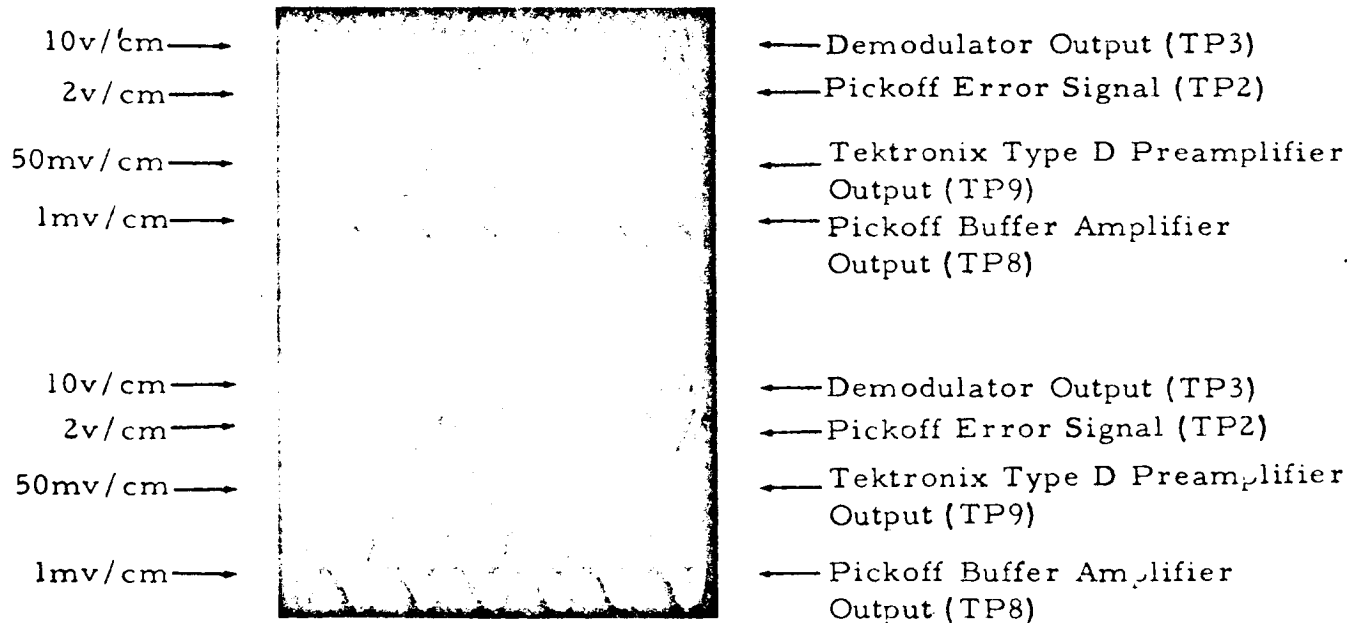


Figure 7-13. Oscillogram 7.2: Pickoff Error Signals at Various TP's in the Servo Channel. Used to Verify Loop Gains. (Note phase reversal between top and bottom traces)

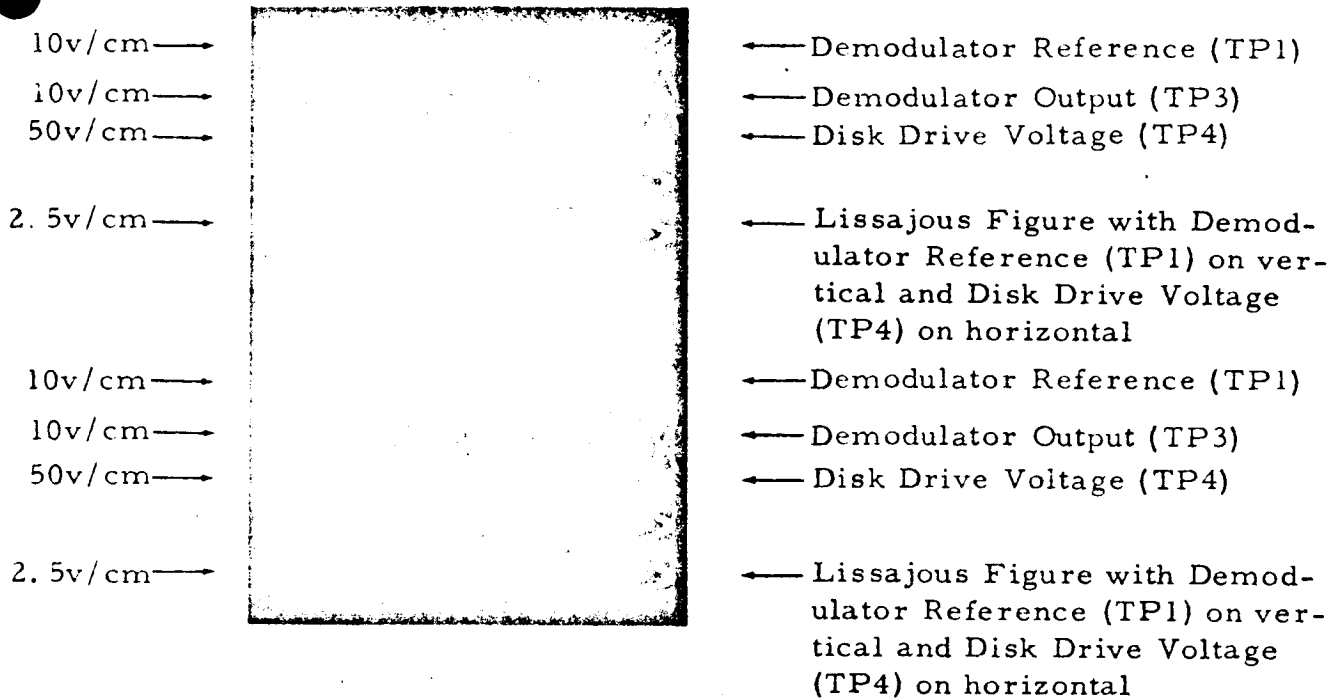


Figure 7-14. Oscilloscope 7.3: Demodulator Phasing With Respect to Disk Drive Voltage. Normally Used for Demodulator Phasing Checks.

(Note that the error signal phase has been reversed between the top and bottom traces)

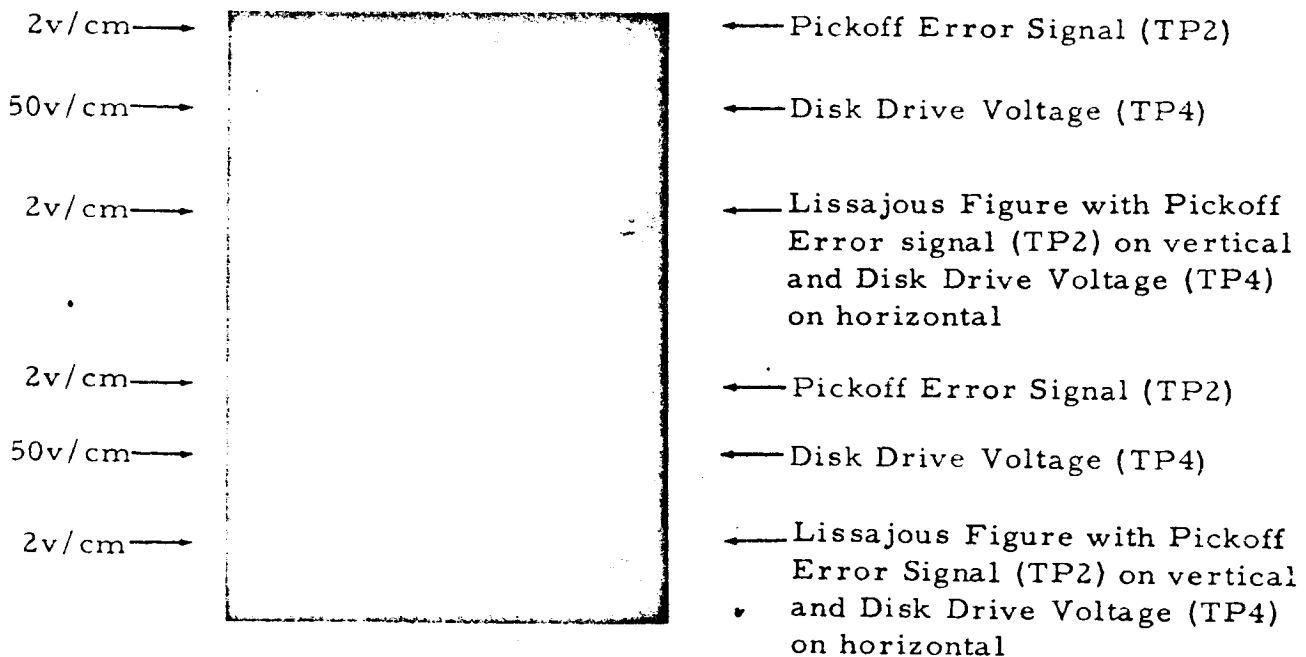


Figure 7-15. Oscilloscope 7.4: Pickoff Error Signal Phasing With Respect to Disk Drive Voltage. Normally Used for Error Channel Phasing Checks. (Note that the error signal has been reversed between the top and bottom traces)

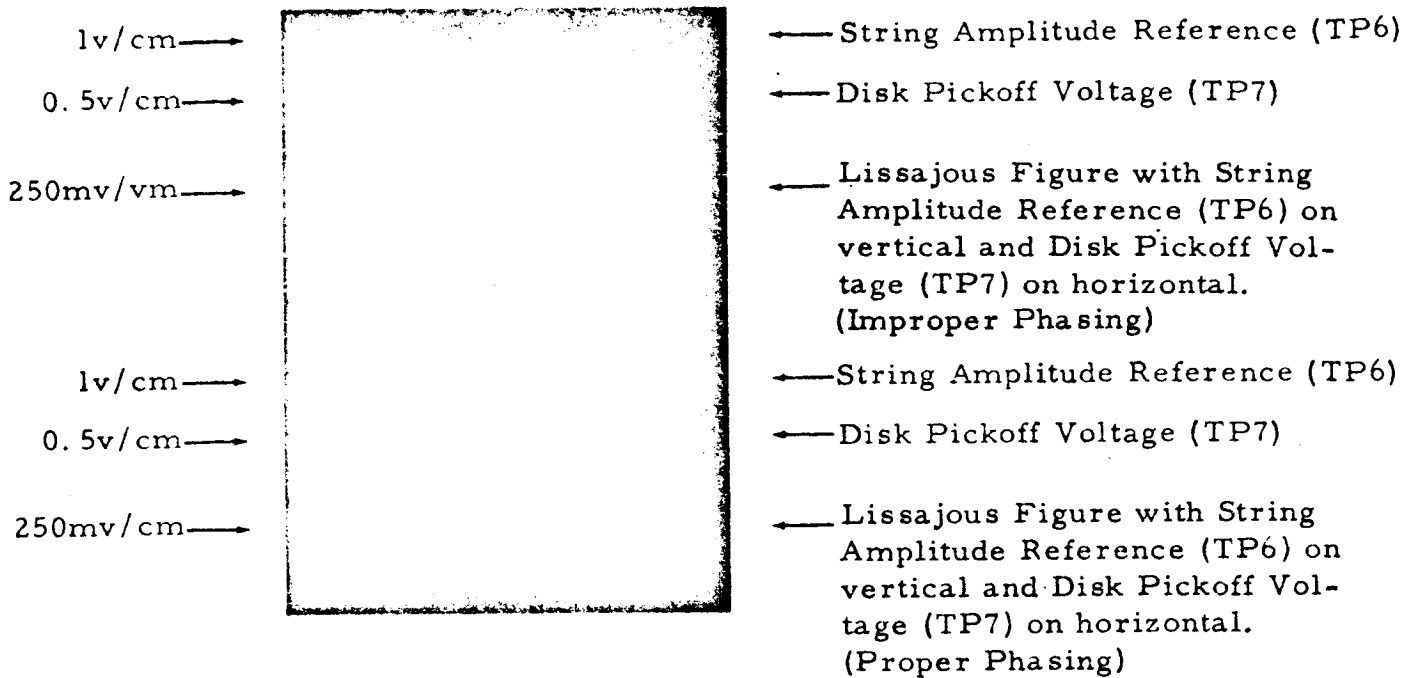


Figure 7-16. Oscillogram 7.5: String Amplitude Reference Phasing With Respect to the Disk Pickoff Voltage

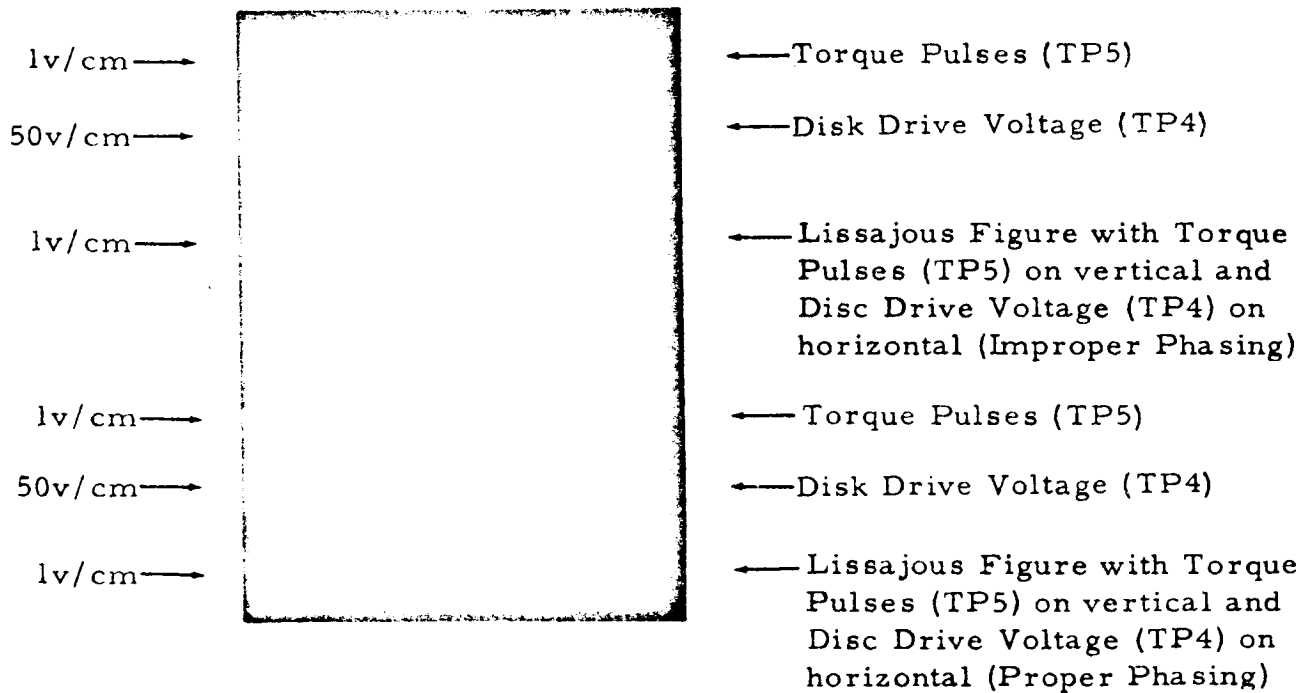


Figure 7-17. Oscillogram 7.6: Torque Pulse Phasing With Respect to the Disk Drive Voltage

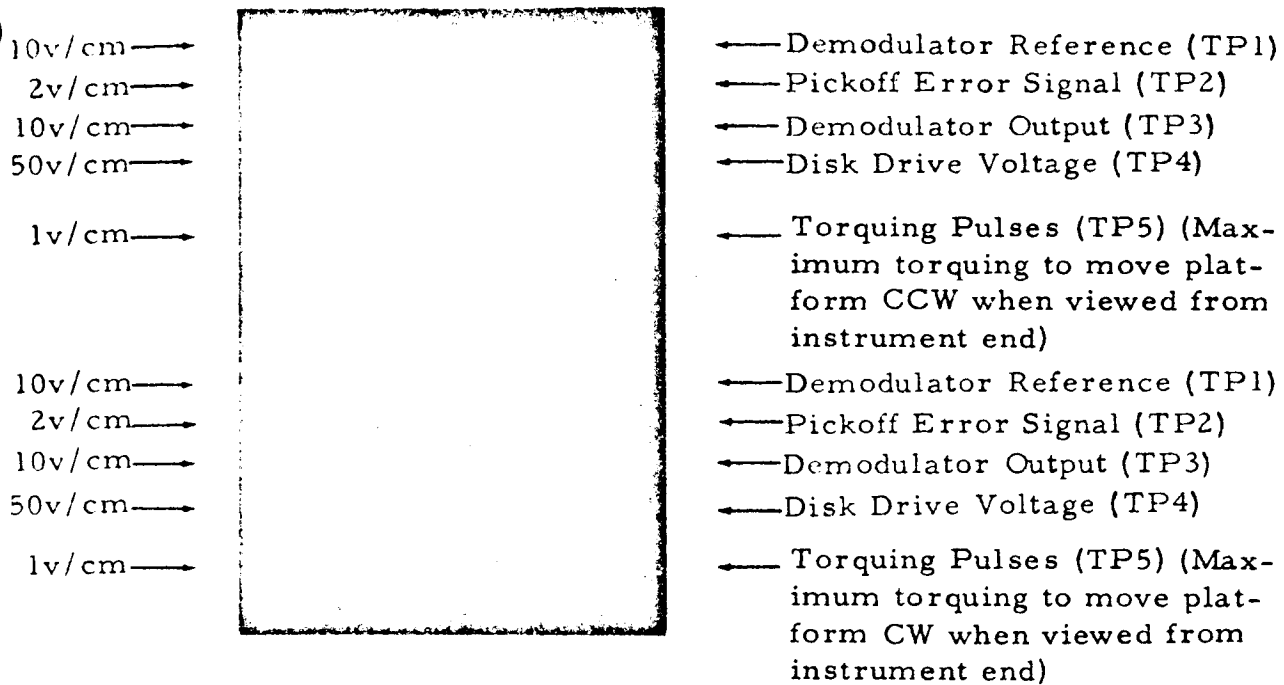


Figure 7-18. Oscillogram 7.7: Representative Signals When Torquing at Maximum Rate in Both Directions

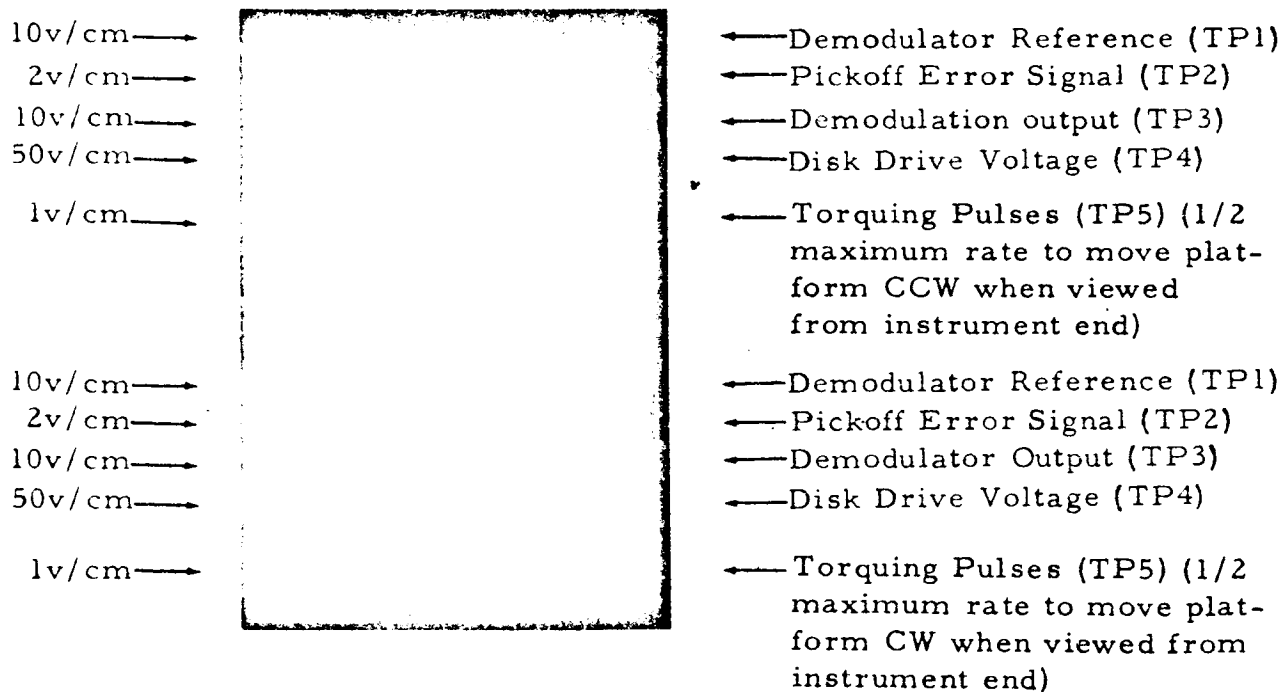


Figure 7-19. Oscillogram 7.8: Representative Signals When Torquing at One-Half of Maximum Torquing Rate in Both Directions

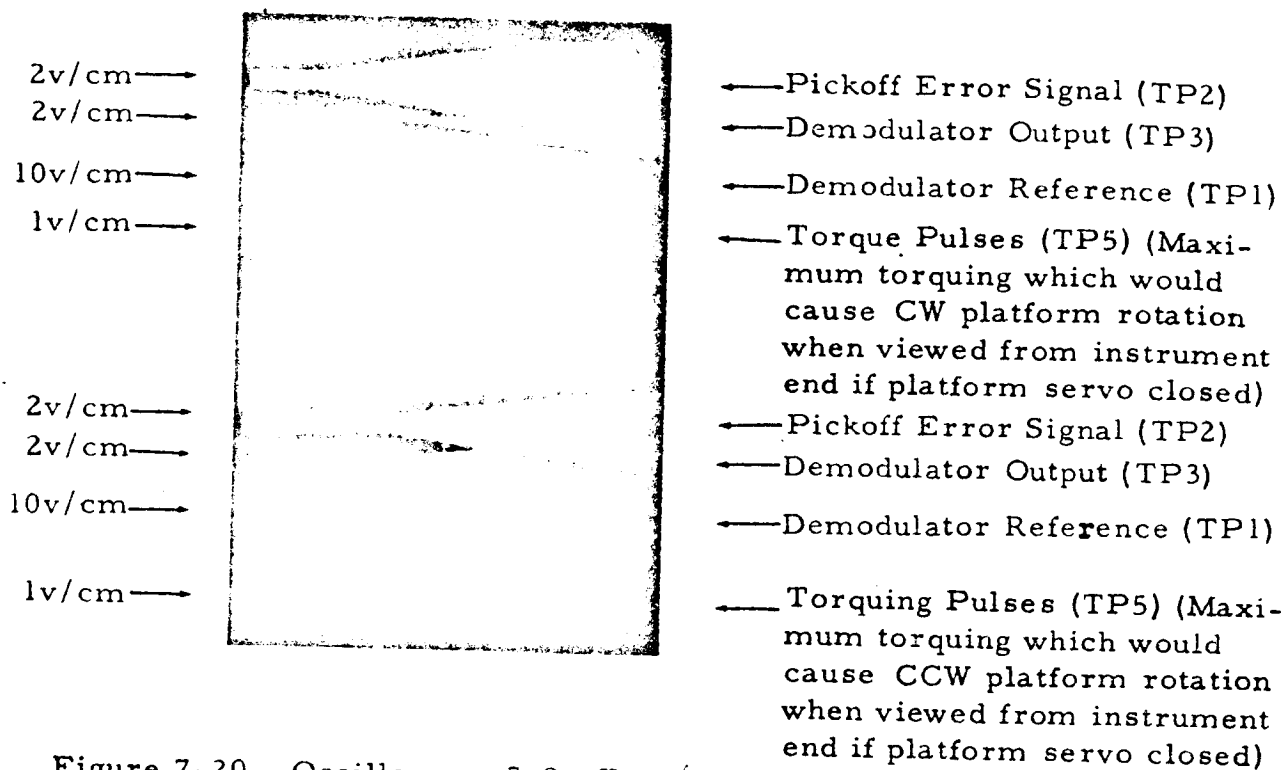


Figure 7-20. Oscillogram 7.9: Error Angle Buildup During Torquing With Platform Servo Loop Opened.

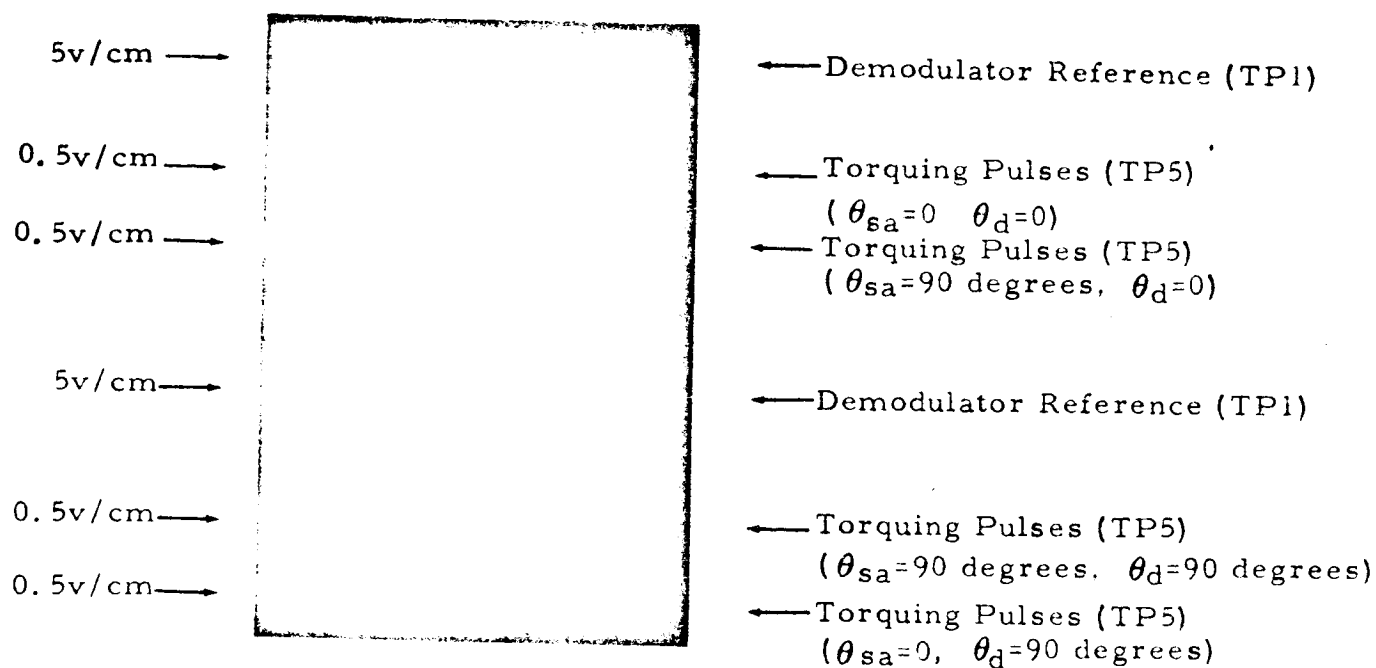


Figure 7-21. Oscillogram 7.10: Representative Torquing Pulse With Various Turn-on and Turn-off Times ($\theta_d = 0$, $\theta_d = 90$ Degrees)

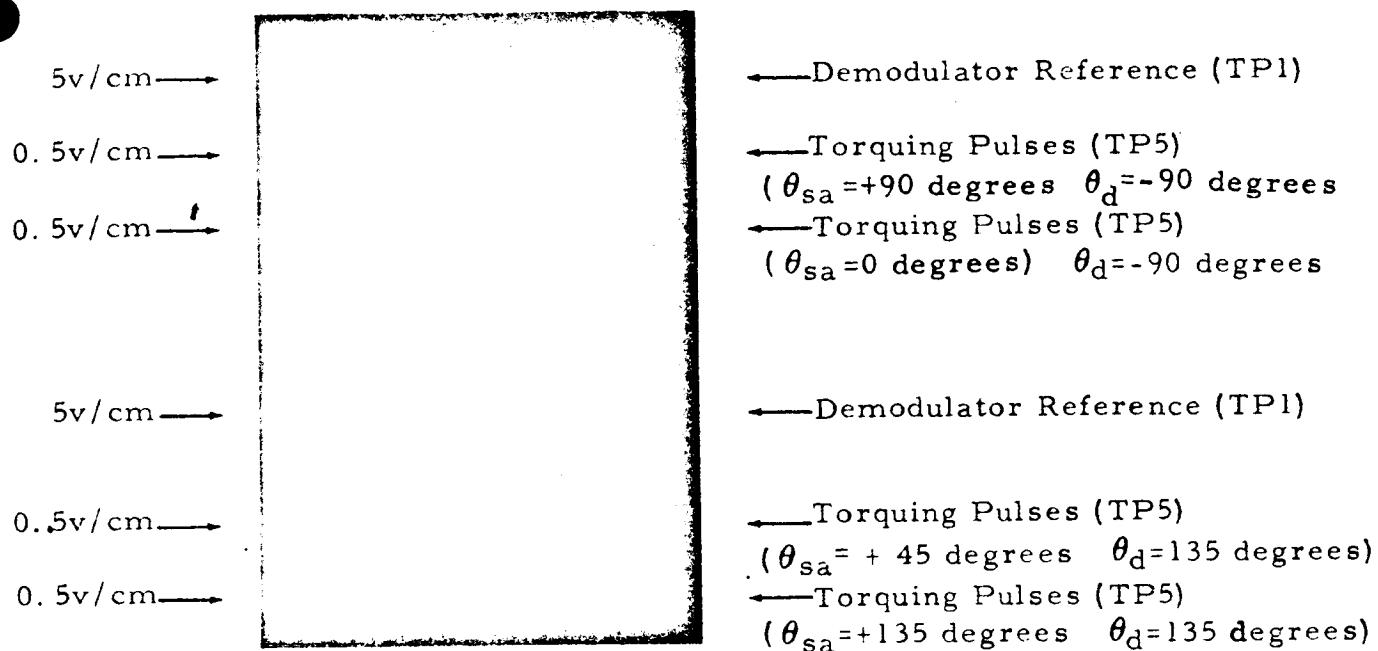


Figure 7-22. Oscillogram 7.11: Representative Torquing Pulses With Various Turn-on and Turn-off Times ($\theta_d = -90$ degrees, $\theta_d = +135$ degrees)

7.2.3 Data Accumulation Technique

In order to obtain torquing data using the mechanization described, a procedure has been evolved which will be outlined here. Such a procedure is vital if repeatable and correlated data is to be obtained and is included here to indicate the capability of this mechanization to yield useful data. Provision is made in this procedure to monitor both electronic stability as well as instrument stability. No attempt is made to detail the accuracies of measurements as these will be recorded in the actual determined data.

The test procedure follows:

General - For convenience a set of definitions is included here to facilitate writing this outline.

1. Test Period - Total test program from start of first data acquisition until all data is accumulated.
2. Test Session - A grouping of several data runs. Typically a test session will occur each working day of the test period.
3. Test Run - The actual taking of one set of test data. Typically this means changing one parameter and measuring torquing capability.

During the entire test period all elements of the mechanization will be left energized. The disc drive will only be turned off when measuring the low amplitude natural frequency of the string (this will be described later). Instrumentation may be turned off provided adequate warmup time prior to data acquisition is allowed for instruments to reach specified operating tolerances. All test data will be accumulated while holding the STAR at one test temperature. Following the test period, selected data runs will be made at different set temperatures. Measurement of the low-amplitude natural frequency of the string will indicate the stability of the temperature control. All test data will be taken while holding the instrument pressure at 30 ± 10 microns. The type of instrumentation used to acquire data will be included with the data. Where a special procedure is used to determine a quantity, a description of this procedure shall be available.

Pre-Test Session Check List - Prior to the start of a test session the following check list will be performed:

1. Energize all required test instrumentation. Allow adequate time for stabilization.

2. Measure the low-amplitude natural frequency of the string. This is obtained by connecting one pair of instrument plates in one leg of a balanced bridge. By driving one plate with a stable external oscillator and sweeping frequency, resonance of the string can be observed on an oscilloscope. Monitoring the external oscillator frequency at the resonance on a counter yields low-amplitude natural frequency. This parameter is sensitive to instrument temperature and appears in the equations of the STAR gyro.
3. Measure the disc drive oscillator frequency.
4. Set an approximate saddle point with no torquing pulses applied. The saddle point for the STAR gyro can be defined as a setting of both critical drive voltage (controls string oscillation amplitude) and of string plane angle at a point where changes in either have least effect on the instruments' self bias drift. This point is achieved by an iterative process of holding one quantity constant and varying the other. Disc drive voltage is varied by adjusting an amplitude control potentiometer in the disc drive oscillator. String plane angle is adjusted by biasing the servo to force the string plane angle to change in order to satisfy servo null requirements.
5. Check loop phasing and readjust if necessary. This check is accomplished by returning phasing to the reference phasing defined in Oscillograms 7.3, 7.4, 7.5, and 7.6. If any phase shifts have occurred, these will be recorded in the data as they indicate electronic stability.
6. Check loop gain and readjust if necessary. This check is accomplished by returning gain to the reference gain defined in Oscillograph 7.2. If gain changes occur these shall be recorded in the data to indicate electronic gain stability.
7. Tune the rejection pulse forming network for best rejection of cross-coupled torquing pulses. This is accomplished by opening the servo loop, removing the d-c bias from the torquing plate, and applying torquing pulses to the torquing plate. The pickoff angle error signal is monitored as well as the demodulator output. The network is tuned for minimum change in these quantities from a no-torque to torque switching. Any tuning required shall be recorded in the data.

Test Run Procedure - The following procedure will be used to perform each of the test runs:

1. Set plate bias voltages at values for the anticipated test run.
2. Set an approximate saddle point with no torquing pulses applied.*
3. Check out loop phasing, readjust if necessary, and record any readjustment.*
4. Set an accurate saddle point with no torque pulses applied.*
5. Check adequacy of rejection of cross-coupled torquing pulses.*
6. Adjust phase relationship of torquing pulses with respect to disc drive voltage to the value desired for the anticipated test run. (See Oscilloscope 7.6)
7. Set the amplitude of the torquing pulses to the value desired for the anticipated test run.
8. Torque the instrument and adjust the torquing rate to hold the platform steady (i.e., balance fixed instrument rates and sensed component of earth rate).
9. Torque the instrument at the approximate desired torque rate and direction for the test run. Measure and record the rate and direction.
10. Measure and record the time required for platform to sweep through a fixed angle and the angle traversed.
11. Torque the platform back to the original start position. Adjust the torque rate to hold the platform steady (as in Step 8). This latter measurement is used to indicate stability of the instrument during the test run.

Post-test Session Check List - Repeat steps 2, 3, 4, 5, and 6 of the "Pre-test Session Check List" procedure.

*For elaboration see previous section on "Pre-test Session Check List".

C5-1277/32

8. EXPERIMENTAL RESULTS AND COMPARISONS TO THEORETICAL RESULTS

8.1 INTRODUCTION

Using the Laboratory mechanization described in Section 7, considerable experimental data relating to STAR torquing was obtained. Numerous torquing runs were performed with various parameter configurations to provide support to the theoretical developments in this report.

It is worth mentioning that no effort was expended towards precision torquing of the test instrument, and no attempt towards improving the mechanization beyond that required to obtain usable data was made. Therefore, these data should not be assumed to reflect how well the STAR gyro can be torqued.

Consideration of the accuracy of these data as well as pertinent discussion are included with the test results presented later in this section. However, some generalizations and descriptions that are applicable to all the tests can be made here.

The readout of torquing rate was made by using a resolver to measure platform angle. The output of the resolver was demodulated and used to drive a Sanborn recorder. The angle swept on the recorder chart and the time required to sweep this angle (obtained from the chart speed and timing marks) were used to provide angular rate. Calibration of the chart angle readout to platform angle was accomplished using a micrometer mounted to the platform. Use of this micrometer to calibrate the chart allowed a convenient means of repeating platform angle scaling. Measurements in the Laboratory indicated an ability to repeat an incremental angle to one part in a hundred. It should be noted that this does not give absolute accuracy. No attempt was made to bring in a precision angular reference because the nature of the experimental work did not require this. Measurements in the Laboratory, however, did show an absolute accuracy within two percent. This was more than adequate for the experimental requirements.

The largest limiting factor to the data obtained in these experiments was the method of measuring and holding torquing pulse amplitude to desired values. Setting of pulse values was accomplished using a Tektronix Type 555 Oscilloscope with a Z-Preamplifier. The method used was to set

the peak of the pulse to the desired amplitude using the vertical magnification available with the Z-unit. However, as pointed out later in this section, waveform distortion was evident in the torquing pulse. Since this distortion varied as a function of the electronics configuration, it tended to lead to incorrect settings of pulse amplitude. That is, since torquing is only accomplished by the fundamental component of the torquing pulse waveshape, any distortion which changes the apparent fundamental peak will lead to an incorrect setting of the pulse amplitude. The contribution to inaccuracy caused by this difficulty is extremely difficult to measure. Were the torquing waveform analog the amount and type of distortion could easily be determined but with the integral sine wave pulses the determination is not so evident. (At this writing no reasonable measurement technique has been found.)

Inspection of the general data trend obtained during this test program does yield an estimate of data accuracy. Indications are that the mechanization is capable of providing three percent relative data. Improvement of the pulse forming electronics would substantially improve this figure.

The method of data accumulation closely follows the procedures outlined in Paragraph 7.2.3. The mechanization configuration was set to a desired set of parameters. The instrument was alternately torqued from right to left and the platform angle was plotted on a chart recorder. The chart provided angular rate. The data from the chart plus appropriate parameter values were recorded on data sheets. The final pertinent values appear in the remainder of this section.

8.2 TORQUING RESULTS AND COMPARISONS

8.2.1 Absolute Value of Torquing Scale Factor — Experimental vs Theoretical

To check the theoretical scale-factor expression, Equation 6-15, this Equation was used to determine the scale factor for the test instrument. The string amplitude term in Equation 6-15 was calculated from Equation 6-21, an expression which gives the best check on the theory because it does not depend on any of the same expressions as those being checked (electrostatic force and string-to-plate capacity). This latter comment is elaborated upon in Section 6 immediately preceeding Equation 6-16.

The values corresponding to the test instrument are:

$$l = 1.74 \text{ in.}$$

$$E = 10.4 \times 10^6 \text{ psi (fused silica)}$$

$$\rho = 2.2 \text{ gm/cc}$$

$$= 2.06 \times 10^{-6} (\text{lb} - \text{sec}^2)/\text{in.}^4 \text{ (fused silica)}$$

$$n = 2$$

$$2H = 0.126 \text{ in.}$$

$$2r_o = 0.0011 \text{ in.}$$

$$H/r_o = 115$$

(8-1)

$$a = .95 \times 10^{-6} \text{ in.}^2$$

$$l_c = 0.188 \text{ in.}$$

$$l_e = 0.120 \text{ in.}$$

and the pertinent values measured during test are:

$$f_n = 6198 \pm \frac{8}{3} \text{ cps}$$

$$(u_n^2 - 1) = 0.00864 \pm \frac{0.00005}{0.00003}$$

(8-2)

$$V_o = 100 \text{ volts}$$

$$V_T = 0.5 \text{ volts}$$

$$k = 1$$

Equation 6-21 then gives

$$Y_1 = 0.00348 \text{ in.}$$

(8-3)

and Equation 6-4, or Figure 4-12 gives

$$F^* = 0.62 \times 10^{-12} \text{ lb/volt}^2 \quad (8-4)$$

Using $\theta_r, \theta_d, \theta_{sa}$ and $1/\tau_*$ at nominal values of zero, Equation 6-15 gives

$$\Delta\phi = 0.332 \text{ sec/pulse for infinite flat plates.} \quad (8-5)$$

Using the equivalent correction for the finite, curved plates used during the tests, from Paragraph 6.2.2

$$\begin{aligned} \Delta\phi \text{ curved plates} &\cong 1.26 \times 0.332 \\ &\cong 0.418 \text{ sec/pulse} \end{aligned} \quad (8-6)$$

The experimental value which corresponds to the above set of parameters and conditions, is given by the average of the $\theta_r = 0^\circ$ runs of Table 8-4.

$$\Delta\phi \text{ experimental} = 0.345 \text{ sec/pulse} \quad (8-7)$$

This value is 17 to 18 percent lower than the theoretical value. There are a number of factors which affect this difference, and the accuracy is perhaps somewhat better than expected. For example, the string is not uniform in diameter and for the particular string under test, only the center diameter is known. Even if the diameter were known along the entire length it would not be known how to average this effect. The string diameter used in calculation is 9 percent larger than the center diameter recorded.

Strings are rejected which have diameters more than 0.00017 in. larger than the center diameter at points 0.30 in. from the center i. e., which increase more than 17 percent in diameter from the center to a point 17 percent of the length from the center. Thus, if we take the 25 percent point (antinodes of a uniform string) at which to measure our diameter, it is clear that the entire difference between theory and experiment could be accounted for by this taper ($\Delta\phi$ is proportional to $1/r_o^2$).

Other factors contributing to this difference between measured and theoretical scale factor could include the theoretical expression for torquing force directly, the effect of string taper on other equations, as

well as possible experimental error sources. In general, it is felt that the experimental data well substantiates the string torquing equation.

8.2.2 String Amplitude Pickoff Sensitivity — Experimental vs Theoretical

To check the theoretical string amplitude pickoff sensitivity given in Paragraph 6.2.4, these equations were used to determine the sensitivity for the test instrument. Test parameters measured at the experimental setup are

$$\begin{aligned} Q_r &= 52 \text{ to } 62 \\ C &= 500 \text{ pf} \\ V &= 27.3 \text{ volts} \end{aligned} \tag{8-8}$$

Using these values with the parameters given in Equations 8-1 and 8-2 we obtain from Equations 6-43 and 6-47

$$\begin{aligned} \Delta C &= 0.00364 \text{ pf peak} \\ \Delta V &= 10.35 \text{ to } 12.3 \text{ mv peak} \end{aligned} \tag{8-9}$$

as the change in voltage (all values in this section are peak) and change in capacity for a pair of infinitely-long parallel flat plates. These values correspond to the string oscillation amplitude obtained at the nominal test parameter settings specified.

Because pickoff sensitivity is directly proportional to gradient, applying the estimate of Paragraph 6.2.2, we obtain

$$\begin{aligned} V \text{ finite flat plates} &\cong 0.9 (10.35 \text{ to } 12.3) \\ &\cong 9.3 \text{ to } 11.1 \text{ mv} \end{aligned} \tag{8-10}$$

and

$$\begin{aligned} V \text{ curved plates} &\cong 1.26 (10.35 \text{ to } 12.3) \\ &\cong 13 \text{ to } 15.5 \text{ mv} \end{aligned} \tag{8-11}$$

By comparison, the experimental voltages corresponding to the same test conditions are:

$$\Delta V \text{ finite flate plates (experimental)} = 10.5 \text{ mv} \quad (8-12)$$

and

$$\Delta V \text{ curved plates (experimental)} = 20.4 \text{ mv} \quad (8-13)$$

These values all refer back to the peak voltages across one-half of the transformer primary. (See Figure 6-4)

As seen by the above results, the experimental value for the finite flat plates lies in the theoretically predicted range. The results obtained for the curved plates were not as good. The theoretical value was from 32 to 48 percent lower than the actual experimental value. However, effects such as string diameter nonuniformity could contribute substantially to the difference obtained. A discussion similiar to that given at the end of Paragraph 8.2.1 is applicable here and in this light the results obtained appear satisfactory.

8.2.3 Torquing Pulse Scale Factor vs. Torquing Pulse Rate

Data were taken to determine any variation in the torquing pulse scale factor as a function of the rate at which the pulses are applied. An integral sine wave pulse with a peak-to-peak amplitude of 2 volts was used. The torquing plate d-c excitation was -100 volts. The pulse rate was varied from 154.4 pulses/second to 3112.8 pulses/second (half of string frequency). The results are tabulated in Table 8-1.

Table 8-1. Torquing Pulse Scale Factor
vs Torquing Pulse Rate

| Data RUN | Pulse Rate (Pulse/second) | Scale Factor | |
|-------------|------------------------------|-------------------|--------------------|
| | | LEFT sec/pulse | RIGHT sec/pulse |
| #1-3/26/65 | 3112.8 | -0.678 | +0.680 |
| #2-3/26/65 | 1608.4 | -0.670 | +0.672 |
| #3-3/26/65 | 751.1 | -0.666 | +0.673 |
| #4-3/26/65 | 353.6 | -0.663 | +0.677 |
| #5-3/26/65 | 154.4 | -0.688 | +0.663 |
| #1a-3/26/65 | 3112.8 | -0.670 | +0.680 |

Using these data, the average scale factor calculates to be:

Average Left Torquing Scale Factor = $-0.672 \text{ } \widehat{\text{sec}}/\text{pulse}$

Average Right Torquing Scale Factor = $+0.674 \text{ } \widehat{\text{sec}}/\text{pulse}$

These scale factors will provide a torquing rate of approximately $2090^\circ/\text{hr}$ when a pulse rate of 3112.8 pulses/second (half of string frequency) is provided.

The greatest deviations from the averages obtained from these data are +2.4 percent and -1.6 percent for left and right scale factors respectively. This is considered to be within experimental error. It should be noted that the largest deviation occurs at the lowest torquing rate. Mention must be made of a residual torquing effect caused by the electronics in the Laboratory mechanization. With a zero torquing rate, because of imperfect switching at the gates which control the torquing pulses, small noise remnants appear on the torquing plate. Depending upon the phasing of these remnants with respect to string velocity, small torquing rates will be introduced into these data which vary with pulse rate. The largest effect occurs at the lowest pulse rate. A residual torquing rate of $-2^\circ/\text{hr}$ was observed during these runs with a zero pulse rate.

8.2.4 Effect of Torque Pulse Magnitude Change on Torquing Pulse Scale Factor

Data were taken to show that torque pulse scaling changed linearly with the amplitude of the torquing pulse. An integral sine wave pulse with a peak-to-peak amplitude variation from 2 volts to 0.25 volts was used. The torquing plate d-c excitation was held constant at +100 volts. In all cases the instrument was torqued at maximum rate (3113 pps). The results are tabulated in Table 8-2. The final column in this table shows the expected scale factor using the scale factor for the 2-volt peak-to-peak pulse as a reference.

Table 8-2. Torque Pulse Scale Factor vs. Torque Pulse Amplitude

| Data Run | Pulse Amplitude (volts peak-to-peak) | Scale Factor Measured (sec/pulse) | | Scale Factor Calculated (sec/pulse) | |
|------------|-----------------------------------------|--------------------------------------|--------|----------------------------------------|-------|
| | | Left | Right | Left | Right |
| #2-4/2/65 | 2.00 | -.672 | +.675 | -.672 | +.675 |
| #3-4/2/65 | 1.00 | -.326 | +.329 | -.336 | +.337 |
| #4-4/2/65 | .50 | -.167 | +.167 | -.168 | +.168 |
| #5-4/2/65 | .25 | -.0823 | +.0837 | -.084 | +.084 |
| #3a-4/2/65 | 1.00 | -.333 | +.331 | -.336 | +.337 |

Inspection of these data indicates a peak deviation from expected results of less than 3 percent. This is considered to be within experimental accuracy. Pulse waveform distortion as described in Paragraph 8.1 was evident when the pulses were closely viewed on an oscilloscope.

8.2.5 Effect of Torque Pulse Phase Shift Due to Shifts in the String Reference Signal (2-volt peak-to-peak pulses)

Data were taken to determine the variation in the torquing pulse scale factor with phasing of the torquing pulse. An integral sine wave pulse with a peak-to-peak amplitude of 2 volts was used. The torquing plate d-c excitation was +100 volts. Variation in phasing with respect to a zero reference between -39 degrees and +32 degrees was performed. All runs were performed at the maximum pulse rate of this mechanization, specifically, one-half string frequency. The results of these runs are given in Table 8-3. Figure 8-1 is a plot of data for both the right and left torquing pulses.

It is evident in Figure 8-1 that data points do not perform a particularly good job of tracing a smooth curve. Theoretically, these data should track a cosine curve and the solid curves in the Figure are cosine curves drawn for reference. With data as shown, both the left and the right torquing pulse scale factors deviated as much as 8 percent from the theoretical drawn curves. These deviations, being quite large, require discussion.

The method of shifting the phase of the torquing pulses in the Laboratory was to shift the phase of the string reference signal prior to switching. An oscilloscope was used to monitor the amount of phase shift. This was accomplished by triggering the scope from a stable reference (Disc Drive Pickoff Signal) and using the calibrated time sweep of the scope to measure phase angle. Between oscilloscope accuracy and operator capability, it is estimated that the phase angle setting could be off as much as ± 3 degrees. It is difficult to express this uncertainty as a percentage error in the scale factor data because of the cosine relationship. At the point where the largest deviation occurred ($\theta_r = +24^\circ$) a -3 degree error in setting θ_r would cause a 3.5 percent error in scale factor. Because this uncertainty did not entirely explain the roughness of these data, further Laboratory investigation was done. Observation of the 2-volt peak-to-peak pulses on the oscilloscope showed quite substantial distortion of the pulse waveform. Obvious flattening of the pulse peak due to lack of sufficient amplifier linear range was evident. Because the distortion was so noticeable, it was decided to redo the phasing runs at a lower amplitude. These data are presented in Paragraph 8.2.6.

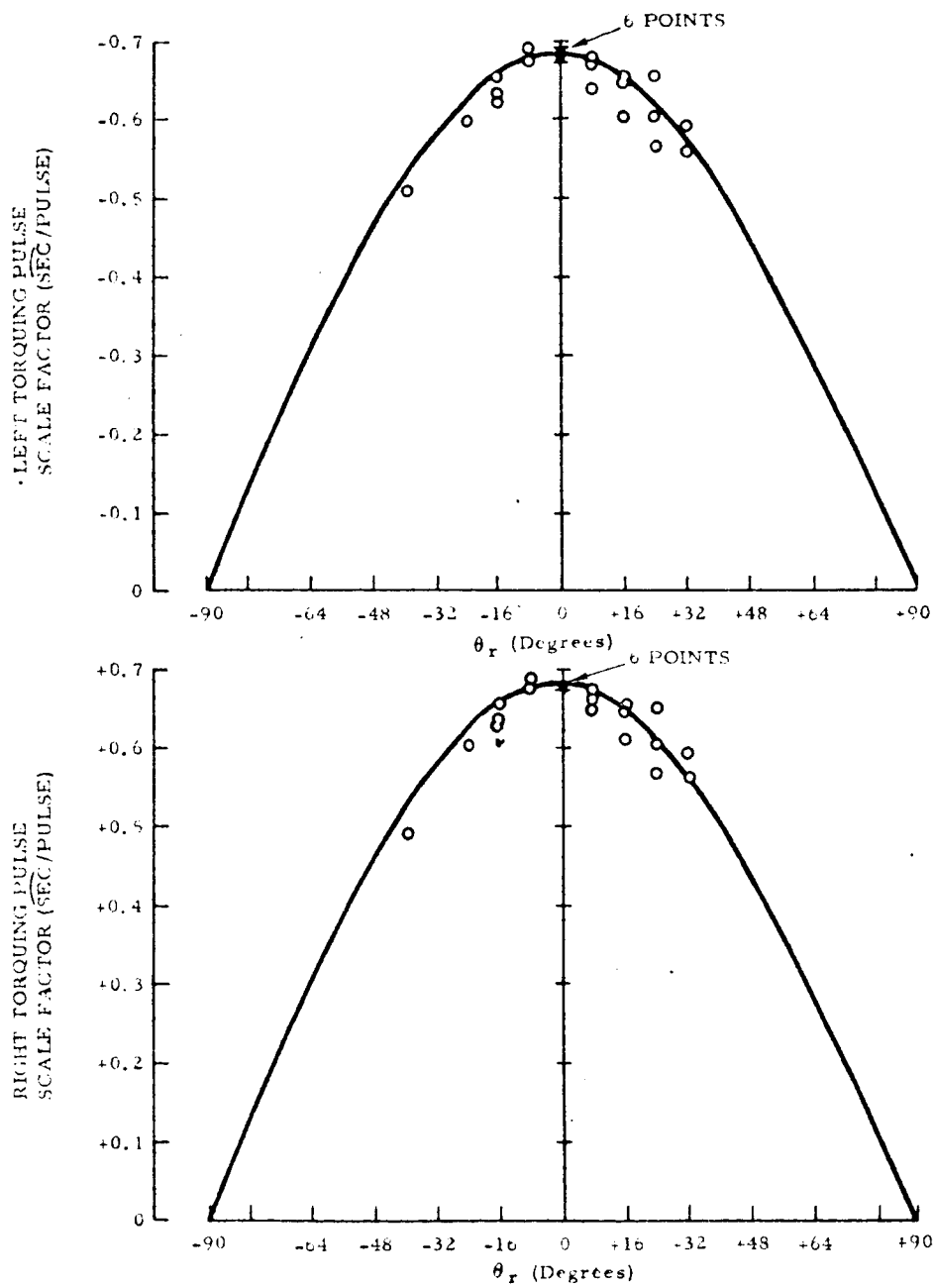


Figure 8-1. Torquing Pulse Scale Factor vs. Pulse Phasing (2-Volt Peak-to-Peak Pulses)

Table 8.3. Torquing Pulse Scale Factor vs Pulse Phasing
(2 volt p-p pulses)

| Data Run | Pulse Phasing Angle (θ_r) (Deg) | Scale Factor | |
|------------|------------------------------------------|------------------------------------|-------------------------------------|
| | | Left $\overline{\text{sec/pulse}}$ | Right $\overline{\text{sec/pulse}}$ |
| #1-3/30/65 | 0 | -0.672 | +0.680 |
| #2-3/30/65 | +8 | -0.638 | +0.648 |
| #3-3/30/65 | +16 | -0.603 | +0.613 |
| #4-3/30/65 | +24 | -0.562 | +0.567 |
| #1-3/31/65 | 0 | -0.675 | +0.675 |
| #2-3/31/65 | +8 | -0.666 | +0.669 |
| #3-3/31/65 | +16 | -0.646 | +0.644 |
| #4-3/31/65 | +24 | -0.603 | +0.602 |
| #5-3/31/65 | +32 | -0.559 | +0.558 |
| #6-3/31/65 | 0 | -0.672 | +0.668 |
| #1-4/1/65 | 0 | -0.675 | +0.682 |
| #2-4/1/65 | -8 | -0.672 | +0.677 |
| #3-4/1/65 | -16 | -0.622 | +0.631 |
| #3a-4/1/65 | -16 | -0.631 | +0.635 |
| #4-4/1/65 | -24 | -0.597 | +0.602 |
| #1-4/2/65 | -39 | -0.507 | +0.493 |
| #1-4/28/65 | 0 | -0.678 | +0.682 |
| #2-4/28/65 | -8 | -0.688 | +0.690 |
| #3-4/28/65 | -16 | -0.654 | +0.658 |

Table 8.3. (Cont)

| Data Run | Pulse Phasing Angle (θ_r) (Deg) | Scale Factor | |
|------------|------------------------------------------|-----------------------------------|------------------------------------|
| | | Left $\widehat{\text{sec/pulse}}$ | Right $\widehat{\text{sec/pulse}}$ |
| #1-4/29/65 | 0 | -0.683 | +0.684 |
| #2-4/29/65 | +8 | -0.678 | +0.677 |
| #3-4/29/65 | +16 | -0.649 | +0.657 |
| #4-4/29/65 | +24 | -0.658 | +0.657 |
| #5-4/29/65 | +32 | -0.590 | +0.593 |

8.2.6 Effect of Torquing Pulse Phase Shift due to Shifts in the String Reference Signal (1-volt peak-to-peak pulses)

Because of difficulties outlined in Paragraph 8.2.5, substantial data were taken to determine torque pulse scale factor vs phasing for 1-volt peak-to-peak pulses. As before, the torquing plate d-c excitation was +100 volts. Variation in phasing between +40 degrees and -40 degrees from the zero reference position was done. All runs were performed at a pulse rate of one-half string frequency. The results are given in Table 8-4. Figure 8-2 is a plot of the data for both left and right torquing pulses.

As evidenced by Figure 8-2, the data shows a reasonably good correspondence to the theoretically expected cosine curve. A substantial improvement over data obtained using the 2-volt peak-to-peak pulses of Paragraph 8.2.5 was obtained. Check of the data points showed them to be within 4 percent of the theoretical values. As mentioned in Paragraph 8.2.5 this range of data accuracy approaches the uncertainty of setting the phasing of the torquing pulses. Also, some small change in distortion as a function of shifting phase could be observed. This, as discussed in Paragraph 8.1, would cause error in setting pulse amplitude. These error terms, plus the uncertainty in angular rate read out, indicate these data to be well within explainable experimental uncertainty.

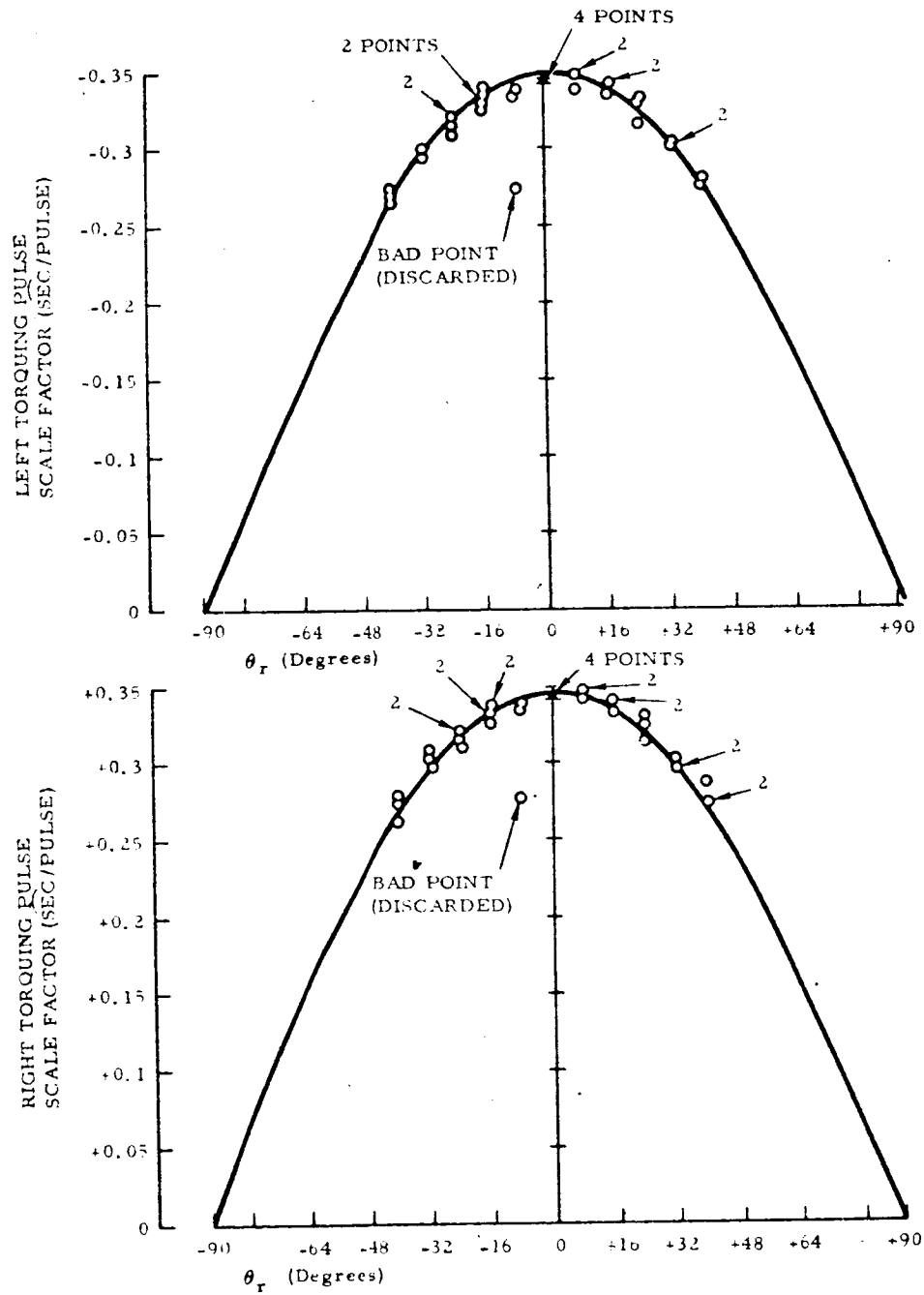


Figure 8-2. Torquing Pulse Scale Factor vs. Pulse Phasing (1-Volt Peak-to-Peak Pulses)

Table 8-4. Torquing Pulse Scale Factor vs Pulse Phasing
(1-volt p-p pulses)

| Data Run | Pulse Phasing Angle (θ_r) (Deg) | Scale Factor | |
|------------|------------------------------------------|-----------------------------------|------------------------------------|
| | | Left $\widehat{\text{sec/pulse}}$ | Right $\widehat{\text{sec/pulse}}$ |
| #1-5/3/65 | 0 | -0.344 | +0.347 |
| #2-5/3/65 | -8 | -0.338 | +0.341 |
| #3-5/3/65 | +16 | -0.333 | +0.333 |
| #4-5/3/65 | +24 | -0.314 | +0.312 |
| #5-5/3/65 | +32 | -0.303 | +0.303 |
| #6-5/3/65 | +40 | -0.283 | +0.288 |
| #1-5/4/65 | 0 | -0.346 | +0.347 |
| #2-5/4/65 | -8 | -0.273 | +0.277 |
| #3-5/4/65 | -16 | -0.325 | +0.332 |
| #4-5/4/65 | -24 | -0.307 | +0.311 |
| #5-5/4/65 | -32 | -0.294 | +0.302 |
| #6-5/4/65 | -40 | -0.272 | +0.278 |
| #5a-5/4/65 | -32 | -0.297 | +0.304 |
| #6a-5/4/65 | -40 | -0.269 | +0.275 |
| #1-5/10/65 | 0 | -0.346 | +0.341 |
| #2-5/10/65 | -8 | -0.336 | +0.333 |
| #3-5/10/65 | -16 | -0.335 | +0.336 |
| #4-5/10/65 | -24 | -0.314 | +0.314 |
| #1-5/11/65 | -16 | -0.337 | +0.335 |

Table 8-4. (Cont)

| Data Run | Pulse Phasing Angle (θ_r) (Deg) | Scale Factor | |
|-------------|------------------------------------------|-----------------------------------|------------------------------------|
| | | Left $\widehat{\text{sec/pulse}}$ | Right $\widehat{\text{sec/pulse}}$ |
| #2-5/11/65 | -16 | -0.328 | +0.323 |
| #3-5/11/65 | -16 | -0.329 | +0.331 |
| #4-5/11/65 | -24 | -0.320 | +0.317 |
| #5-5/11/65 | -32 | -0.300 | +0.300 |
| #6-5/11/65 | -40 | -0.264 | +0.261 |
| #7-5/11/65 | -24 | -0.318 | +0.315 |
| #8-5/11/65 | -8 | -0.337 | +0.336 |
| #1-5/12/65 | +8 | -0.347 | +0.344 |
| #2-5/12/65 | +16 | -0.341 | +0.338 |
| #3-5/12/65 | +24 | -0.333 | +0.329 |
| #4-5/12/65 | +32 | -0.300 | +0.295 |
| #5-5/12/65 | +40 | -0.279 | +0.271 |
| #6-5/12/65 | +40 | -0.275 | +0.270 |
| #7-5/12/65 | -32 | -0.300 | +0.296 |
| #8-5/12/65 | +24 | -0.328 | +0.323 |
| #9-5/12/65 | +16 | -0.341 | +0.338 |
| #10-5/12/65 | +8 | -0.346 | +0.343 |
| #11-5/12/65 | 0 | -0.347 | +0.343 |

8.2.7 Effect of Temperature Variations on Torquing Pulse Scale Factor

As shown in the theory, any temperature changes of the STAR will cause both first and second order effects. The first order effect will be to change the amplitude of the string oscillation because of change in string tension due to instrument contractions and expansions. This change in amplitude would directly change torque pulse scale factor should the amplitude of the pulse be held constant. Second order temperature effects will cause additional small changes in instrument geometry thereby affecting pickoff sensitivities. The mechanization accuracy was such that only the first order effect on scale factor could be observed.

The mechanization used in the Laboratory derives the torquing pulses from the string reference pickoff. This causes the pulse amplitude to directly vary with string amplitude and hence in normal operation holds the torquing scale factor constant. Because of lack of stability in the electronics (see Paragraph 8.2.10), check of scale factor consistency as a function of temperature variations could not be accomplished. Instead, for test purposes, it was decided to change instrument temperature and reset the torque pulse back to the nominal pulse amplitude. From theoretical expectations a changed scale factor could be determined and compared to the experimental scale factor.

The manner in which these data were taken follows: Temperature was changed from day-to-day. At each new temperature set point the torquing pulse amplitude was set to 1-volt peak-to-peak. Also, at each set point, the u^{2*} of the instrument was accurately measured (see Paragraph 7.2.3, Step 2 of the Pre-test Session Check List). This quantity provides a direct determination of string oscillation amplitude and allows prediction of torquing pulse scale factor at the set temperature. It can be shown (for example, see Equations 6-15 and 6-21) that the torquing pulse scale factor varies inversely as the square root of the quantity $(u^2 - 1)$. Using this relationship, predictions as to expected torquing scale factor were made.

The expected results and data obtained from these temperature runs are given in Table 8-5. It should be noted that the calculated scale factors are determined using the average scale factor at the normal operating temperature as a reference. Hence, each scale factor is obtained from the square root of the ratio of $(u^2 - 1)$ at the reference temperature to $(u^2 - 1)$ at the changed temperature. For reference purposes, the

*The ratio u^2 , strictly speaking, is u_2^2 / u_n^2 (u_n^2 at $n=2$) of Sections 5 and 6.

Table 8-5. Comparison of Torquing Data Scale Factor to Predicted Scale Factor
with Temperature Change

| Data Run | u^2 RATIO $\left(\frac{1/2 \text{ drive frequency}}{\text{low-amplitude string}} \right)^2$ natural frequency | Approx Temp (°F) | Scale Factor | | Average Predicted Scale Factor sec/pulse |
|------------|------------------------------------------------------------------------------------------------------------------------|---------------------|-------------------|--------------------|---------------------------------------------|
| | | | Left sec/pulse | Right sec/pulse | |
| #1-5/17/65 | 1.00677 | 85 | -0.383 | +0.393 | ±0.391 |
| #2-5/17/65 | 1.00677 | 85 | -0.395 | +0.395 | ±0.391 |
| #1-5/19/65 | 1.00231 | 96.5 | -0.685 | +0.685 | ±0.670 |
| #1-5/21/65 | 1.00361 | 89.5 | -0.532 | +0.532 | ±0.535 |
| #2-5/21/65 | 1.00361 | 89.5 | -0.548 | +0.548 | ±0.535 |
| #1-5/24/65 | 1.00856 | 80.0* | -0.347 | +0.349 | ±0.348** |
| #1-5/25/65 | 1.00938 | 78.0 | -0.331 | +0.333 | ±0.332 |

*indicates reference temperature

**indicates reference scale factor

approximate instrument case temperature is given in these data. It should be mentioned that the u^2 term is an easily measurable term from which string amplitude can be calculated directly on a theoretical basis. (String amplitude, on the other hand, can not so easily be obtained directly from case temperature).

As can be seen from these data, the correlation between the predicted and actual data were quite good. The largest deviation occurred with large temperature changes and these were less than 3 percent. As the u^2 term was decreased the string amplitude decreased and thus the signal available from the string reference pickoff became smaller. In order to hold torque pulse amplitude constant, it was necessary to make up this lost gain in the electronics. This had the effect of introducing variations in the torquing pulse waveform. It is felt that these variations were sufficient to cause these data to be no better than 3 percent without considering uncertainty in angular rate determination. It is worth mentioning that increasing instrument temperature more than 97°F (u^2 less than 1.00231) caused the string amplitude reference signal to decrease to a value less than a minimum for the electronics to hold the torque pulse constant.

8.2.8 Effects of Torque Pulse Phase Shifts in Pulse Turn-On Phase and Pulse Turn-Off Phase

Following suitable modification of the Laboratory mechanization, it was possible to change the relative turn-on and turn-off times for the torquing pulse. Paragraph 3.7, of this report presents the theory as to the effect such changes will have on the torquing scale factor. For convenience, the final result of the theory, specifically an equation giving normalized torquing scale factor as a function of pulse phases is repeated in Figure 8-3. Also included in the Figure is a sketch of the torque pulse waveform defining terms. Figure 8-4 is provided for information only to aid understanding of the effect of various pulse turn-on and turn-off times. It gives representative waveforms for a few different switching times.

To show the effect of pulse turn-on and turn-off times on scale factor more conveniently, a set of curves using the just-described equation is plotted in Figure 8-5. Using the Laboratory mechanization, it was attempted to experimentally come up with the same set of curves. As in previous data sets, a one-volt peak-to-peak pulse was used with a +100-volt d-c plate excitation. In all runs the instrument was torqued at pulse rates of one-half string frequency. Data points obtained are given in Table 8-6. Data points are plotted on Figure 8-5 next to the theoretical curve, to the same scale factor, to facilitate comparison.

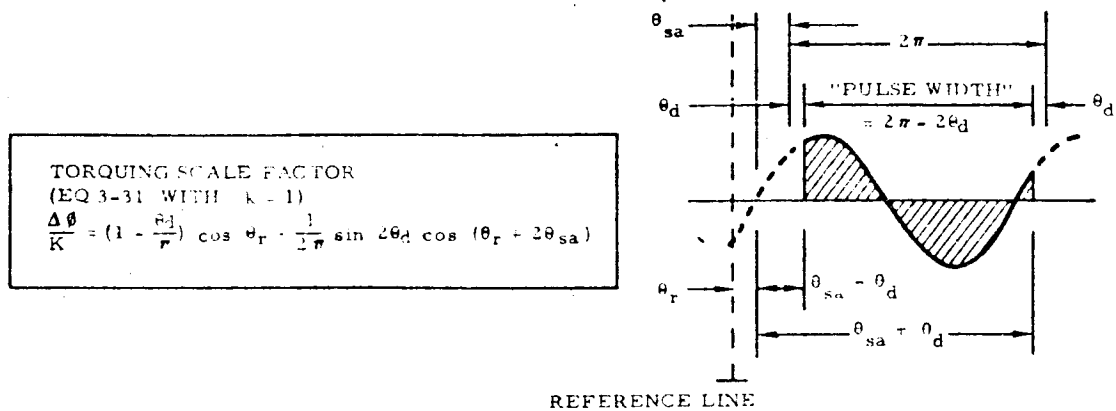


Figure 8-3. Equation of Torque Pulse Scale Factor as a Function of Torque Pulse Phasing With a Sketch of Waveform to Define Terms

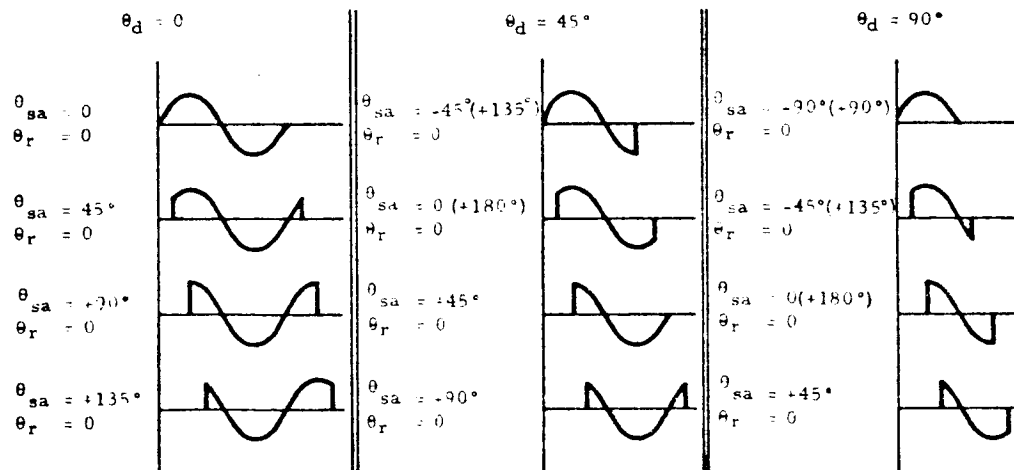


Figure 8-4. Representative Torque Pulse Waveform for Various Turn-on and Turn-off Times ($\theta_r=0$). Only the Left Torquing Pulse is Depicted

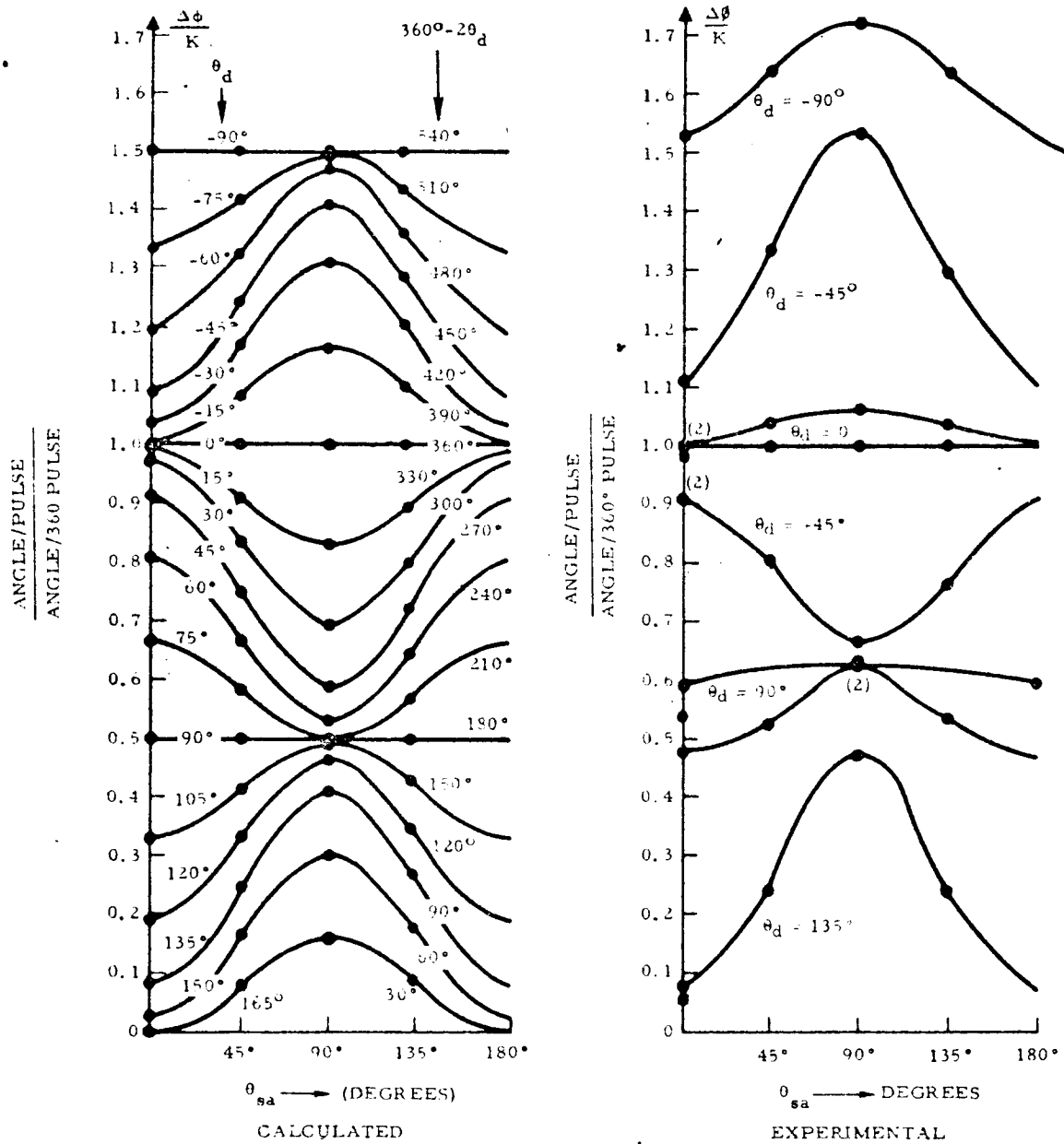


Figure 8-5. Torque Pulse Scale Factor as a Function of Turn-on and Turn-off Times ($\theta_r = 0$). Experimental Results are Normalized to Unity by the $\theta_d = \theta_{sa} = 0$ Pulse Scale Factor Value.

Table 8-6. Torque Pulse Scale Factor as a Function of Turn-on and Turn-off Times

| Data Run | θ_d (Deg) | θ_{sa} (Deg) | Scale Factor | | Average Left-Right Scale Factor Normalized to Pulse Value at $\theta_{sa}=0, \theta_d=0$ |
|------------|---------------------|------------------------|-------------------|--------------------|------------------------------------------------------------------------------------------|
| | | | Left sec/pulse | Right sec/pulse | |
| #1-6/8/65 | 0 | 0 | -0.352 | +0.358 | 1.00 $\left(\frac{.355}{.355}\right)$ |
| #2-6/8/65 | 0 | +45 | -0.352 | +0.355 | 0.997 |
| #3-6/8/65 | 0 | +90 | -0.354 | +0.354 | 0.998 |
| #4-6/8/65 | 0 | +135 | -0.355 | +0.358 | 1.003 |
| #5a-6/8/65 | 90 | +90 | -0.221 | +0.218 | 0.620 |
| #5b-6/8/65 | 90 | 0 | -0.211 | +0.213 | 0.597 |
| #5c-6/8/65 | 90 | +90 | -0.223 | +0.225 | 0.631 |
| #5d-6/8/65 | 90 | +180 | -0.215 | +0.207 | 0.594 |
| #1a-6/9/65 | 0 | 0 | -0.347 | +0.351 | 0.983 |
| #1b-6/9/65 | 45 | 0 | -0.322 | +0.325 | 0.911 |
| #1c-6/9/65 | 90 | 0 | -0.191 | +0.187 | 0.533 |
| #1d-6/9/65 | +135 | 0 | -0.0235 | +0.0235 | 0.0662 |
| #2a-6/9/65 | +135 | +45 | -0.0884 | +0.0848 | 0.244 |
| #2b-6/9/65 | +135 | +90 | -0.169 | +0.167 | 0.473 |
| #2c-6/9/65 | +135 | +135 | -0.0868 | +0.0853 | 0.242 |
| #2d-6/9/65 | +135 | 0 | -0.0271 | +0.0272 | 0.0765 |

Table 8-6. (Cont)

| Data Run | θ_d (Deg) | θ_{sa} (Deg) | Scale Factor | | Average Left-Right Scale Factor Normalized to Pulse Value at $\theta_{sa}=0$, $\theta_d=0$ |
|------------|---------------------|------------------------|-------------------|--------------------|---------------------------------------------------------------------------------------------|
| | | | Left sec/pulse | Right sec/pulse | |
| #3a-6/9/65 | + 90 | + 90 | -0.219 | +0.219 | 0.617 |
| #3b-6/9/65 | + 90 | +135 | -0.190 | +0.192 | 0.538 |
| #3c-6/9/65 | + 90 | 0 | -0.171 | +0.168 | 0.477 |
| #3d-6/9/65 | + 90 | 45 | -0.184 | +0.188 | 0.524 |
| #4a-6/9/65 | + 45 | +135 | -0.267 | +0.271 | 0.758 |
| #4b-6/9/65 | + 45 | 0 | -0.321 | +0.325 | 0.910 |
| #4c-6/9/65 | + 45 | + 45 | -0.385 | +0.286 | 0.804 |
| #4d-6/9/65 | + 45 | + 90 | -0.232 | +0.235 | 0.658 |
| #5a-6/9/65 | 0 | 0 | -0.349 | +0.360 | 1.00 |
| #5b-6/9/65 | 0 | + 45 | -0.368 | +0.368 | 1.037 |
| #5c-6/9/65 | 0 | + 90 | -0.376 | +0.376 | 1.059 |
| #5d-6/9/65 | 0 | +135 | -0.365 | +0.364 | 1.026 |
| #6a-6/9/65 | - 45 | + 45 | -0.472 | +0.472 | 1.328 |
| #6b-6/9/65 | - 45 | + 90 | -0.545 | +0.545 | 1.535 |
| #6c-6/9/65 | - 45 | +135 | -0.463 | +0.465 | 1.308 |
| #6d-6/9/65 | - 45 | 0 | -0.394 | +0.394 | 1.111 |
| #7a-6/9/65 | - 90 | + 90 | -0.608 | +0.613 | 1.720 |

Table 8-6. (Cont).

| Data Run | θ_d (Deg) | θ_{sa} (Deg) | Scale Factor | | Average Left-Right Scale Factor Normalized to Pulse Value at $\theta_{sa}=0, \theta_d=0$ |
|------------|---------------------|------------------------|-------------------|--------------------|------------------------------------------------------------------------------------------------|
| | | | Left sec/pulse | Right sec/pulse | |
| #7b-6/9/65 | - 90 | +135 | -0.572 | +0.588 | 1.635 |
| #7c-6/9/65 | - 90 | 0 | -0.546 | +0.553 | 1.550 |
| #7d-6/9/65 | - 90 | + 45 | -0.578 | +0.588 | 1.645 |

Comparison of the two sets of curves in Figure 8-5 yields some interesting observations. As evidenced by the sketches, the general shape of the experimental curves corresponds to the theoretical curve. The experimental curves were normalized to unity at the $\theta_d = \theta_{sa} = 0$ point. For a given θ_d , the experiment curves provide consistently higher scale factors than the theoretical curve except at the curve where $\theta_d = 0$ ($\Delta\phi/K = 1$). Descriptively, the family of curves obtained experimentally is not symmetrical about the curve of $\theta_d = 90^\circ$ as indicated by the theory. In addition, data are available (see Paragraph 8.2.9, Data Run #6a - 6/8/65) for the point $\theta_d = -180^\circ$ and $\theta_{sa} = 0^\circ$. At this point, $\Delta\phi/K = 2$ as predicted by the theory. Thus, the experimental family of curve from $\theta_d = 180^\circ$ to 0° appears to repeat the shape of the family of curves from $\theta_d = 0^\circ$ to -180° .

At this time, it is not known why these experimental results differ, as they do, from theoretical. It is difficult to conceive of a reason for the lack of non-symmetry obtained experimentally. Consider the data for $\theta_d = 90^\circ$. According to the data $\Delta\phi/K = 0.6$, i. e., the scale factor is six-tenths of its nominal value for a full integral sine wave pulse. Since for $\theta_d = 90^\circ$ the pulse is exactly one-half of an integral sine wave, it is quite hard to see how $\Delta\phi/K$ can be anything but 0.5. Both theory and intuition dispute the experimental results. On the other hand, reasonable care was exercised when performing the experiment. Hence, the results cannot be ignored.

Thus, while the general shape of the theoretical curves has been duplicated, the numerical values have not checked within what is believed to be the accuracy of the test. If we could take the maximum deviation of 20 percent and assume the θ_d and θ_{sa} error terms remain within this deviation, this accuracy would be, certainly, satisfactory for an error expression; however, we have not proven the validity of such an extension, although it seems reasonable intuitively.

8.2.9 Effect of D-C Torquing Bias

To investigate for possible side effects, one torquing run was made with the torquing plate dc-excitation reduced from +100 to +50 volts. An integral sine wave pulse with 2 volts peak-to-peak amplitude was used and the pulse rate was maximum (3113 pps). The Data Run (#1-4/5/65) yielded -0.330 sec/pulse and $+0.330 \text{ sec/pulse}$ for the left and right scale factor, respectively. The average scale factor for a 2-volt peak-to-peak pulse from Paragraph 8.2.3 was:

Left Scale Factor = -0.672 sec/pulse
 Right Scale Factor = $+0.674 \text{ sec/pulse}$

Theory indicates that halving the d-c plate bias halves the scale factor for d-c excitations of this magnitude. Thus, the scale factors should be:

Left Scale Factor (Expected) = -0.336 sec/pulse
 Right Scale Factor (Expected) = $+0.337 \text{ sec/pulse}$

The results agree within 2.5 percent.

8.2.10 Effect of Harmonics

In an effort to detect any performance detriment due to the quite-considerable harmonics generated by the single integral sine wave pulse normally used, two additional data sets were taken. The existence of these harmonics and the lack of any known effects on string operation is discussed in Paragraph 3.4.









These two data sets consisted of first comparing the normal "single" pulse torquing pulse waveform to analog torquing and then comparing to the "optimum" torquing pulse waveform (Paragraph 3.5.2) for a string operating in the second mode, i. e., a double-integral sine wave pulse. Data obtained from these runs are given in Figure 8-6.

Comparison of the runs yielded no detectable difference in torquing scale factor due to torquing with "optimum" or "non-optimum" waveforms, within the accuracy of the mechanization. Thus, within the accuracy of the test, it still may be said that we know of no specific effect of harmonics on string motion.

It should be mentioned that no particular difficulty was encountered in achieving the double integral sine wave pulse.

8.2.11 Torque Pulse Phase and Amplitude Stability

Early in the experimental program attempts were made to measure the short-term and day-to-day stability of the STAR torquing pulses. The pulses were monitored on a Tektronix 555 Oscilloscope using a Type Z Preamplifier. Phasing was monitored using both Lissajous techniques and the calibrated time sweep of the scope. Amplitude was monitored using the vertical magnification of the Type Z Preamplifier. It quickly became evident that the available circuitry

| DATA RUN | TORQUE PULSE WAVEFORM | SCALE FACTOR |
|----------|-------------------------------------------------------------------------------------|--------------------------------------|
| No. 1a - |  | -0.351 (LEFT) |
| 5/26/65 |  | +0.352 (RIGHT) |
| No. 1b - |  | -0.347 (LEFT) |
| 5/26/65 |  | +0.351 (RIGHT) |
| No. 6a - |  | (1) -0.714 ($\times 1/2 = -0.357$) |
| 6/8/65 |  | (1) +0.720 ($\times 1/2 = +0.360$) |
| No. 6b - |  | (1) -0.359 |
| 6/8/65 |  | (1) +0.362 |

(1) IN THE SET OF RUNS, THE ANGULAR PLATFORM PICKOFF WAS NOT CALIBRATED SINCE RELATIVE DIFFERENCE BETWEEN RUN 6a - 6/8/65 AND 6b - 6/8/65 WAS ONLY POINT OF INTEREST. THIS EXPLAINS INCREASE IN SCALE FACTOR VALUE OVER NORMAL VALUE.

Figure 8-6. Runs to Determine Scale Factor as a Function of Various Torquing Pulse Waveforms

was not stable enough to allow taking any meaningful data on stability. Both amplitude and phasing were drifting quite rapidly. Phase for example showed short term (a few hours) drift of +3 degrees. It was felt that the available circuitry did not provide indication to either the ability to design or to obtain circuitry which would meet necessary performance specifications. Since the experimental program was set up primarily to substantiate theoretical results, no effort was made to improve the electronic stabilities. It should be noted that the stability was sufficient to allow the taking of torquing data, as the pulses were constantly monitored and corrected as necessary.

8.3 CONCLUSIONS

In general, the experimental work provided substantial verification of the theory relating to torquing the vibrating string gyro. But, more importantly, the Laboratory work did not show any fundamental problems in torquing the STAR which may have been missed or neglected. Some effects (Paragraph 8.2.8) did turn up which require additional investigation, but these do not appear to seriously impair either the precision or reliability to which the STAR gyro can be torqued.

Specifically, the experimental effort provided the following most noteworthy results:

1. The torquing pulse scale factor for a given physical instrument can be predicted satisfactorily from theory.
2. In a similar fashion, the pickoff amplitude sensitivity is predictable.
3. Within the mechanization accuracy, no effects due to harmonic components in the torquing waveform are evident.
4. Phase shifts of the torquing pulse with respect to the string velocity cause the scale factor to change according to the predicted cosine relationship.

C5-1277/32

REFERENCES

1. Quick, W. H., "Theory of the Vibrating String as an Angular Motion Sensor," Journal of Applied Mechanics, September 1964, Vol. 31, No. 3, p. 523-534.
2. Quick, W. H., "Precision Torquing of the String Gyro," (Section VIII, a continuation to Theory of the Vibrating String, Autonetics, March 1963.)
3. McGurn, J. F., Precision STAR Torquing Electronics, Technical Memorandum 32-242-2-3, Autonetics, 18 October 1963.
4. IL 64-242-2-ERG-29 from P. H. Ito/J. H. Kabaian to F. W. Hauf, "Test Data on a STAR Torquing Experiment," Autonetics, 26 March 1964.
5. Quick, W. H., "Response to Random Translational Vibration" (Section IX, a continuation of Theory of the Vibrating String, Autonetics, September 1962).
6. James, Hubert M., Nathaniel B. Nichols and Ralph S. Phillips, Theory of Servomechanisms, McGraw-Hill Book Company, Inc., New York, 1947.
7. Hildebrand, F. B., Advanced Calculus for Engineers, Prentice-Hall, Inc., New York, 1949.
8. Smythe, William R., Static and Dynamic Electricity, McGraw-Hill Book Co., New York, 1950.
9. Kaplan, Advanced Calculus, Addison-Wesley, 1952.

C5-1277/32